AECL-11516, PR-PHY-9

Progress Report
Physical and Environmental Sciences
Physics Division

1995 January 1 to December 31

May1996 mai

AECL

PHYSICS DIVISION

Progress Report

1995 January 1 - December 31

edited by M. Harvey

Chalk River, Ontario

1996 May

AECL-11516, PR-PHY-9

CONTENTS

AECL

PHYSICAL AND ENVIRONMENTAL SCIENCES
PHYSICS DIVISION

STAFF LIST

1995 JANUARY 1 - DECEMBER 31

Vice-President, Research and Product Development	D.F. Torgerson
General Manager, Physical and Environmental Sciences	C.J. Allan
Executive Administrative Assistant, Physical and Environmental Sciences	G. McAuley
Director, Physics Division	M. Harvey
Administrative Assistant, Physics Division	J. Vaudry
Office Assistant, Physics Division	D. Heideman

1.1 Neutron and Condensed Matter Science (NCMS) Branch

BRANCH MANAGER: B.M. Powell

Professional Staff

W.J.L. Buyers
A.P. Clarke (1)
M. Couture
E.D. Earle
J.D. Hepburn (2)
T.M. Holden
J. Katsaras (3)
S.M. Kim
G. Jonkmans (4)
M.A. Lone
F.J. Marsiglio
R.B. Rogge (3)
J.H. Root
V.F. Sears
B. Sur
E.C. Svensson
I.P. Swainson
Z. Tun

Technical Staff

J.J-P. Bolduc
R.J.E. Deal
D.A. Doering
R.L. Donaberger (5)
J.H. Fox
E.R. Gaudette
M.D. Gauthier
L.E. McEwan
M.W. Montaigne
P.A. Moss
M.M. Potter
J.A. Rollings
G.A. Sims (6)
H.C. Spenceley (7)
D.C. Tennant

Secretarial Staff

J.S. Hill

(1) Research Associate, jointly with Reactor Materials Research Branch, terminated 1995 November 1.
(2) On attachment to SNO Project at Laurentian University, Sudbury.
(3) Research Associate.
(4) Research Associate with Queen's University attached to NCMS Branch 1995 July 16.
(5) NSERC Technician with McMaster University attached to NCMS Branch.
(6) Retired, 1995 September 22.
(7) Retired, 1995 March 29.

Visiting Scientists

Z. Altounian	McGill University
C. Balog	Queen's University
O. Binbrek	University of Waterloo
J. Bouillot	Université de Savoie
J. Brown	Queen's University
J. Cadogan	University of New South Wales
L. Clapham	Queen's University
M. Collins	McMaster University
L. Cranswick	CSIRO, Melbourne
Z. Gamba	CNEA, Buenos Aires
B. Gaulin	McMaster University
A. Gonzalez	IVIC, Caracas
J. Greedan	McMaster University
E. Hallman	Laurentian University
R. Hammond	McMaster University
M. Harris	Oxford University
A. Harrison	Edinburgh University
K. Jeffrey	University of Guelph
R. Kiefl	University of British Columbia
K. Khulbe	University of Ottawa
A. Lamarche	University of Ottawa
G. Lamarche	University of Ottawa
E. Larson	Los Alamos National Laboratory
S. MacEwen	Alcan International, Kingston
T. Mason	University of Toronto
G. Modlen	Loughborough University
W. Montfrooij	ISIS Facility, Rutherford Appleton Laboratory
H. Nakotte	Los Alamos National Laboratory
J. Noel	AECL, Whiteshell
J. Porter	Defence Research Establishment Atlantic, Halifax
R. Robinson	Los Alamos National Laboratory
D. Ryan	McGill University
D. Shoesmith	AECL, Whiteshell
J. Szpunar	McGill University
D. Taylor	Queen's University
L. Taillefer	McGill University
Y. Teisseyre	Université de Savoie
D. Tindall	Dalhousie University
B. Torrie	University of Waterloo
P. Webster	Salford University
J. Woolley	University of Ottawa

Postdoctoral Fellows

A. Anderson	Ames Laboratory, Iowa
S. Clarke	Cornell University
T. Krause	Queen's University
M. Mao	McMaster University
S. Mentink	University of Toronto
G. Mills	Salford University
H. Nakotte	Los Alamos National Laboratory
R. Nandyala	McMaster University

O. Petrenko	McMaster University
S. Presser	University of California, San Diego
X. Wang	Salford University
A. Wills	Edinburgh University

Graduate Students

H. Abuluwefa	McGill University
C. Adams	University of Toronto
N. Bonner	Loughborough University
V. Colmart	Laboratoire Léon Brillouin, Saclay
A. Di Chiro	McGill University
P. Dubouchet	Université du Quebec à Chicoutimi
S. Dunsiger	University of British Columbia/TRIUMF
V. Gerardo	University of California, Santa Barbara
M.A. Gharghouri	McMaster University
E. Girt	McGill University
R. Hammond	McMaster University
R. Ham-Su	McMaster University
B. Hernandez-Morales	University of British Columbia
E. Kartini	McMaster University
S. Lee	University of Waterloo
M. Lumsden	McMaster University
B. Lussier	McGill University
O. Mao	McGill University
E. Martinelli	McGill University
D. Micke	Queen's University
W. Minor	McMaster University
S. Nguyen	McMaster University
J. Pang	University of Toronto
J. Pencer	University of Guelph
T. Petersen	Risø National Laboratory
A. Piant	Laboratoire Léon Brillouin, Saclay
A.Purwanto	Los Alamos National Laboratory
M. Quintero	University of Ottawa
R. Sabet-Sharghi	Queen's University
M. Small	Dalhousie University
K. Van Acker	Catholic University, Leuven
P. Wanjara	McGill University

NEUTRON SCATTERING SUMMER SCHOOL

Visiting Lecturers

J. Ankner	Missouri University Research Reactor
M. Collins	McMaster University
B. Gaulin	McMaster University
T. Mason	University of Toronto
A. Mayes	MIT
H. Nakotte	Los Alamos National Laboratory
R. Robinson	Los Alamos National Laboratory

Scientists

A. Gonzalez	IVIC, Caracas
K. Khulbe	University of Ottawa
P. Timbrell	Surface Science

Postdoctoral Fellow

M. Mao	McMaster University

Graduate Students

C. Adams	University of Toronto
E. Buiel	Simon Fraser University
S. Cormier	University of Guelph
S. Dunsiger	University of British Columbia
E. Girt	McGill University
X. He	University of Waterloo
R. Holly	University of Waterloo
H. Kimura	Tohoku University
S. Lee	University of Waterloo
J. Li	McGill University
M. Lumsden	St. Francis Xavier University
M. Lumsden	McMaster University
A. MacFarlane	University of British Columbia/TRIUMF
O. Mao	McGill University
V. Murashov	Dalhousie University
S. Nguyen	McMaster University
J. Pang	University of Toronto
J. Pencer	University of Guelph
M. Small	Dalhousie University
C. Tulk	Memorial University
G. Xu	Johns Hopkins University
L. Young	University of Waterloo
C. Zhu	University of Guelph

1.2 Accelerator Physics Branch

BRANCH MANAGER: J. Ungrin

Professional Staff

F.P. Adams
S. Baset (1)
R.J. Burton
S.T. Craig
M.S. de Jong (2)
S.R. Douglas (1)
N.A. Ebrahim
C.R.J. Hoffmann
R.M. Hutcheon
J.Y. Sheikh
T. Taylor
P.Y-K. Wong (1)

Technical Staff

S.B. Alexander
B.A. Brown (1)
A.D. Davidson
R.W. Davis
D.W. Dunford (1)
G. Frketich
I.L. McIntyre
W.L. Michel
J.F. Mouris
L.W. Shankland
B.H. Smith
D.L. Smyth
L.S. Yamazaki (1)

Mechanical Laboratory

R.J. Bakewell
R.J. Kelly
J.F. Weaver

Laboratory Services

K.T. McKee

Secretarial Staff

M.E. Carey

(1) Joined branch on 1995 June 15.
(2) Transferred to Instrument and Control Branch, 1995 September 1.

2. SUMMARIES

2.1 General

As this report shows, much has been accomplished on the research front during 1995. The condensed matter science group continued to operate a multi-faceted program involving collaborative basic and applied research with external scientists in the fields of materials science, physics, chemistry and biology. The Applied Neutron Diffraction for Industry (ANDI) program gained strength with ever wider applications for the nuclear, aerospace, manufacturing and energy industries. In addition to the research programs, steps continued towards making the neutron scattering facilities at NRU more user friendly for external researchers. Efforts were made to introduce more students to the technique and to expand its applications to other fields.

The neutrino physics group, as part of the Sudbury Neutrino Observatory (SNO) Institute, collaborating with scientists from Canada, USA and UK, saw the start of construction of the acrylic vessel in the Creighton mine site of INCO. This activity will continue for much of 1996 with water fill and first data taking anticipated in 1997.

The accelerator physics group has spent considerable effort working with materials and fuels scientists to show the value of accelerators as an out-reactor source of radiation. Specific research activities have included the demonstration of laser plasma deposition of diamond coating, which has potential application for high-wear components in reactors, and the study for a Free Electron Laser upgrade for the IMPELA accelerator.

Physics Division has seen many changes throughout this past year. The Physical Sciences Unit under the Vice-President, Gerald Dolling was disbanded in April and Physics Division was put into the new unit of Physical and Environmental Sciences under General Manager Colin Allan. In the same reorganization six mathematicians from a disbanded Mathematics and Computation Branch joined the Division within Accelerator Physics Branch with the whole Branch taking on even more of a technical service role.

Stop Press Item

At the time of writing (1996 April) the division has just heard of the results of the reduction in funding of the federal government to AECL by about 40%. This reduction was accompanied by the announcement of a review of AECL's programs, which concluded that the company should concentrate solely on CANDU technology. The result of this is that all programs in Physics Division are to be unfunded by AECL by 1997 March 31, and the Division is to be dissolved. The accelerator physics program is being disbanded immediately, and we shall cease to be a partner in the SNO collaboration as of 1996 June 30. The neutron scattering program has until 1997 March 31 to find funding outside the AECL envelope in order to continue.

These events may reflect the fiscal realities of our times but are hard to accept nevertheless. Physics Division has had a history of fifty years in Chalk River, and many of the foremost physicists in Canada and abroad have spent sometime in these laboratories honing their research skills. Notable among this group is 1994 Nobel Prize winner, Bertram Brockhouse. We can only hope that reason will prevail and the benefits of the legacy left by Professor Brockhouse, which has so much potential for industry and a broad range of research fields, will not be lost to all Canadians.

Over the past thirty years, the accelerator physics program has been a world leader in ion accelerators, ion injectors, electron linacs, and high-current electron linacs suitable for industrial applications. The group was invited twice to hold the International Linac Conference (1976, 1992) which is a testament of the respect they have had with their peers. Its termination is another sad loss for Canadian science and technology. Jim Ungrin has written a review of the branch programs over this period; it is available as an AECL publication (RC-1644).

The Sudbury Neutrino Observatory is in the final stages of construction with data collection expected in early 1997. We can only wish our colleagues in the collaboration well in trying to unravel the mysteries of the missing neutrinos from the sun.

2.2 Condensed Matter Science

Materials Science

The program in materials science has expanded in its range of applications and in the number of external collaborators. Experiments were done on steels; the formation of oxide scales on the surface during hot fabrication was investigated by real-time powder diffraction measurements, and plastic deformation was probed by measurements of linewidth. The use of an aluminum plug and ring as a standard sample to calibrate residual stress measurements was investigated. Experiments on diffusion-bonded SiC-Mo joints were done to evaluate the residual stress as a function of joining temperature and cooling rate. The volubility of hydrogen in zirconium alloys is important to the nuclear industry. The precipitation and dissolution of hydrides were tracked and the critical temperatures for complete dissolution were evaluated. Experiments on intermetallic binary alloys explored long-range order and vacancies in Fe_3Al alloys and the defect structure of NiAl alloys. Neutron reflectometry was used to measure the changes in a thin Ti film subjected to an *in situ* electrochemical reaction.

Physics

The physics program continues to have as a major component research on magnetism, but studies of amorphous systems are becoming more numerous and significant work continues on liquid helium. The properties of uranium compounds remain of great interest. Further efforts to understand the existence of magnetism and superconductivity in the heavy fermion compound UPt_3 were made. Low-energy excitations in the partially ordered antiferromagnet UNi_4B were studied and the structures of the magnetic phases of UNiGe in a magnetic field were investigated. The structures and excitations were measured for the frustrated magnetic system $KNiCl_3$ and meso-scale ordering in other frustrated systems has been studied by depolarization measurements. Elastic scattering measurements were made to study the spin kinetics in a random anisotropy system. The chemical and magnetic structure of synthetic multilayers of NiCo/Cu have been measured by neutron reflectometry. Studies of amorphous systems include the temperature dependence of the structures and of the excitations of the liquid, crystalline and glassy phases of $ZnCl_2$ and, in CKN, a test of the predictions of mode-coupling theories for glass-forming systems. Recent measurements on liquid helium have been made closer to the transition temperature than ever before. They suggest a continuous transition from the superfluid phase to the normal fluid phase. High-resolution measurements were made of the multiexcitation component of the dynamic structure factor and these are being analyzed.

Structural Science

Most of the program in structural science is based on the DUALSPEC powder diffractometer. Measurements were made on deuterated ice formed in high electric fields to investigate the effect of such growth on its structural parameters. The width of domain walls in deuterated KDP was measured. It is suggested that an anomalous column of diffuse scattering observed in calcite is the result of the presence of competing ordering schemes. A re-analysis of powder data from the scheelite structure ammonium perrhenate showed that a two-site orientation for the ND_4 ion gave an excellent description of the data and agreed well with a pseudo-spin theory of the compound. Several magnetic structures were investigated. Measurements of the structures of several RFe_7 compounds suggested that it is a disordered structure, contrary to previous views, with Fe dumb-bell pairs on some of the sites. The substitution of X elements on the Fe-sites in the hard magnets Nd_2Fe_{17} was found not to be random. It is suggested this occurs because the sites have different volumes and different nearest neighbour shells. The magnetic structures of three chalcopyrites were investigated and the Cu spins in $CuFeS_2$ were found to order antiferromagnetically. It was found that UCuSn forms in an orthorhombic structure, contrary to previous views and must be considered an ordered ternary compound.

Biological Science

On the basis of x-ray diffraction data, the $L_{\beta'} \rightarrow L_{\alpha}$ phase transition in DPPC is interpreted as a disorder-order transition in two dimensions. Using oriented films of DPPC, the structure of the subgel phase is characterized by a two-dimensional molecular lattice containing two lipid molecules. High-resolution, one-dimensional scattering profiles of the subgel and gel phases of DPPC were used to construct pressure-distance curves. The straight line nature of the curve lends support to the view of hydration pressure as the intermembrane repulsive force. High-resolution specular reflectivity measurements were made in an

effort to establish the structure of the $P_{\beta'}$ phase of lipid membranes.

Theory

The optical conductivity in a conventional electron-phonon superconductor was calculated to elucidate what the measurements indicate about the order parameter and the mechanism responsible for superconductivity. The transmutation of statistics for a Heisenberg spin chain was explored using newly developed mathematical techniques and the first steps were taken to obtain exact and useable expressions for the correlation functions. A complete and exact analytic solution of the Darwin equations has been obtained and it is found that Fankuchen gains greater than two are possible. This general solution now allows the reflecting properties of an absorbing crystal of finite thickness to be calculated. Several reflecting properties have been calculated for common monochromator crystals. A Lennard-Jones atom-atom intermolecular potential has been developed for the carboranes and applied in molecular dynamics simulations. Several structural and dynamical properties are reproduced quite well. A benchmark test of a method to extract the phonon density of states from incoherent scattering measurements was made with vanadium. The resulting distribution is believed to be the most accurate obtained to date. Modelling of the vacancies in NiAl alloys suggests that the bond energies are sensitive functions of atomic spacing and of electronic structure.

Instrumentation

The T3 Bioscience Diffractometer was commissioned. It is one of only two such instruments in North America dedicated to the study of soft condensed matter. Benchmark tests were made on the DUALSPEC powder diffractometer with a standard ZrO_2 sample supplied by the International Union of Crystallography. The performance of the spectrometer was found to compare well with that of other diffractometers worldwide. The technique of near-surface stress mapping was further developed during the year and several approaches were considered that could increase the neutron intensity for stress scanning with very high spatial resolution. The development of multiwire grounded-anode ^3He detectors was completed. Their performance exceeded expectations and two are now installed in the E3 and L3 spectrometers. New hardware was designed and fabricated for use in the ANDI program. Several major upgrades to the spectrometer control programs were installed.

The utilization of the spectrometers during 1995 is given in Table 1.

Table 1 NRU operated for 291 days with an average power of 117.5 MW during the period 1995 January 1 to December 31. Spectrometer use is given in Table 1, (efficiency is the fraction of available reactor operating time used for experiments). The apparent efficiency of T3 is low because the spectrometer was not declared fully operational until 1995 May 5.

Beam hole	No. of experiments	No. of participating CRL scientists	No. of participating non-CRL scientist	Efficiency
C2	39	11	23	98%
C5	18	6	18	98%
E3	20	10	13	96%
L3	25	7	18	95%
N5	14	9	12	93%
T3	4	1	7	58%

2.3 Neutrino Physics

Construction of the acrylic vessel for the Sudbury Neutrino Observatory (SNO) began in 1995, with AECL staff playing a major role. It will remain on the critical path for the project for much of 1996. A prototype fluidized-bed facility to produce acrylic beads coated with MnO_2 was developed. Following several modifications to the original procedure, the beads produced are now acceptable to the SNO water group. A system to produce and deliver short-lived radioactivities for calibrating the SNO detector has

been developed. Three calibration sources have been tested and a safety analysis of the proposed system was completed. A Monte Carlo analysis software is being developed for SNO. It will read the data from the detector and reconstruct the event data structure.

The feasibility of using high-loading bubble detectors to search for cold dark matter is under investigation. The proposed method will use technology and expertise developed for the SNO project.

2.4 Accelerator Physics

The first experiments were performed on the laser plasma deposition of hydrogen-free diamond-like carbon (DLC) films on Zr-2.5Nb CANDU pressure tube materials and silicon substrates, using the short-pulse, high-power, CO_2 laser. The thin films show Raman spectra characteristics of diamond-like carbon films, have Vickers hardness of the coated surface of approximately 7000 kg force mm^{-2} and show diamond-like crystals distributed throughout the film, with film thicknesses of up to 0.5 μm generated with 50 laser pulses. These experiments suggest that it should be possible to deposit hydrogen-free, diamond-like films, of relevance to nuclear reactor components, with a high-power and high-repetition-rate laser facility.

A small group was formed in Accelerator Physics Branch to assess the potential of the IMPELA technology as a basis for a far-infrared free electron laser (FEL), and to survey potential applications, particularly in CANDU reactor research and development. The study concluded that with relatively modest modifications to the IMPELA prototype accelerator, it would be possible to build an internationally competitive far-inbred FEL user facility. An IMPELA-based FEL facility could meet the needs of basic and applied research over a wide area within AECL and create new scientific opportunities for university-based researchers in Canada.

A study was done to identify consequences of mechanical failure of the dump switch in the network of resistors and diodes that connects the magnet power supplies to the superconducting cyclotron magnet coils. A code, DISCHRGE, was modified to model discharging of the magnet when any one of the three legs of the dump switch does not open when required. This low-probability situation could result in loss of precompression on the coils and possible movement that would require realignment of the magnet windings.

During the last seven years, a simple but unique system was developed for measuring high-temperature (up to 1500°C) dielectric properties, based on the resonant cavity perturbation technique. The system is automated for measurements above 400°C, which covers most ceramics work. Both in-house system development work and collaborative projects with outside groups have continued.

3. RESEARCH REPORTS

3.1 Condensed Matter Science

Materials Science

Real-Time Oxidation

J.H. Root *(AECL)*, H. Abuluwefa and R. Guthrie *(McGill University)*

Oxide scales form on the surface of steel during hot fabrication. Neutron diffraction has provided a unique opportunity to study the kinetics of iron oxidation at realistic, high temperatures, of the order 1200°C. Previously, we have reported an initial experiment to track the growth of three main oxide phases (wüstite, Fe_xO; magnetite, Fe_3O_4; and hematite, Fe_2O_3) on the surface of a ferritic steel cylinder [1]. The initial experiment was performed in a contained environment with a partial pressure of oxygen equivalent to that of air. In the early stages of oxidation, there was a predominance of wüstite and hematite, the oxygen-poor and oxygen-rich phases, respectively. However, after 30 minutes, the intermediate phase, magnetite grew at the expense of the other two phases. After about 90 minutes, there was a clear predominance of magnetite, and a very low volume fraction of wüstite. The low volume fraction of wüstite was a surprise. Previous studies of scale formation, by post-oxidation examination of specimens at room temperature, revealed a wüstite volume fraction of 95% [2].

Neutron diffraction measurements of oxide growth were repeated this year, at a reaction temperature of 1127°C, under varying oxygen partial pressures. As the concentration of oxygen was reduced, the volume fractions of the three oxide phases were redistributed. In figure 1, we show the relative predominance of the wüstite phase at a low oxygen concentration (3%), after two hours of oxidation. The higher concentration of wüstite is indicated by the increased intensity of the $Fe_xO(220)$ diffraction peak compared with the peak obtained at an oxygen concentration of 12%. Interestingly, the total of the intensities from the three oxide phases appears to be insensitive to the concentration of oxygen in the reaction chamber.

REFERENCES

[1] Physics Division Progress Report, PR-PHY-8:2.3.1.48 AECL–11234, 1995.

[2] M.H. Davis, M.T. Simand and C.E. Birchenall, Journal of Metals, Transaction AIME 5 (1951) 827.

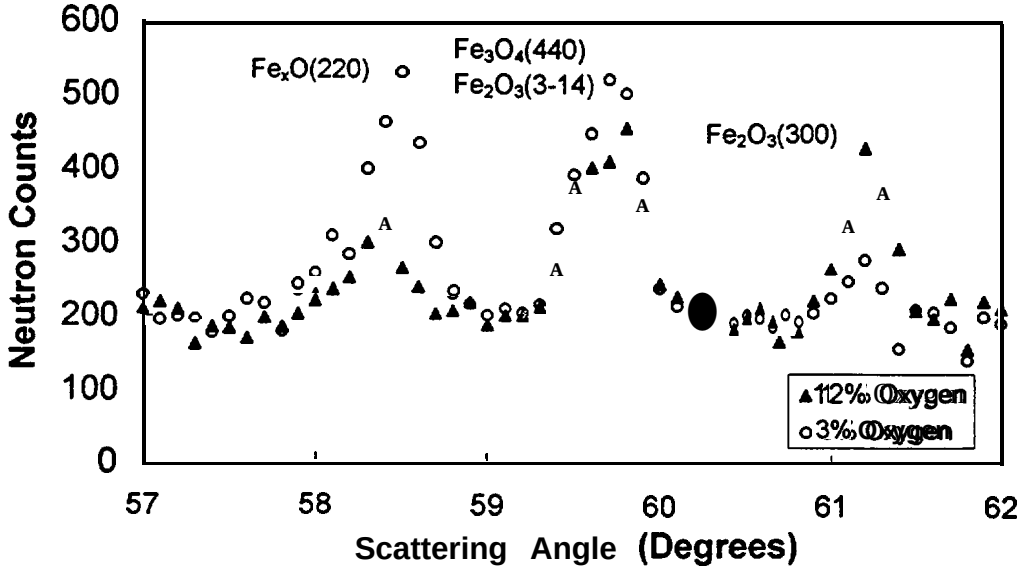

Fig. 1 Neutron diffraction patterns of oxide phases after 2 hours of oxidation of iron at 1127°C.

Neutron Measurements of Plasticity in Pressure Hull Steel (HY-80) and Frigate Steel (350-WT) Samples

T.M. Holden, A.P. Clarke and J.H. Fox *(AECL)*

Non-destructive methods of measuring plastic deformation or fatigue damage in marine components that have been subjected to stresses beyond the yield point or to cyclic loading are of importance to estimates of remaining life in naval vessels. Plastic deformation generates dislocations within the crystallites that make up the polycrystalline component. These permit a non-uniform strain distribution to exist within grains, enhance the differences between the strains in grains oriented with a particular crystalline direction along the deformation axis and can break up the grain into smaller sub-grains. All these processes contribute to the linewidth of the diffraction peak that can therefore be used as a tool to diagnose plastic deformation.

The linewidth of the (110) diffraction peak was measured on a number of standard " 'dog-bone" samples of HY-80 subjected to known plastic deformation. A one-to-one correlation of intrinsic linewidth Δ_D with true strain, &, was observed that may be described by

$$\Delta_D = 0.025 \text{ in } \varepsilon + 0.284 . \qquad (1)$$

The plastic deformation also changes the grain orientation and rotates the $\langle 110 \rangle$ axes of bcc materials along the tensile axis. The intensity of diffraction from a fixed volume of steel depends on the plastic deformation as follows,

$$I = I_0 + b\varepsilon \qquad (2)$$

and this may also be used to measure plastic deformation. Experiments were also carried out on samples of HY-80 that had been subjected to fatigue loading below and above the yield point (560 MPa). No change in diffraction linewidth was observed for those samples fatigued up to 550 MPa, except for cases where the samples were imperfectly made and had broken. However large increases in linewidth were noted for samples fatigued above the yield point at 652 MPa. When the dimensions of these latter fatigue samples were examined it was noticed that they had deformed plastically and the true strain, &, was deduced from the shape changes. The measured linewidths were in good agreement with the relation expressed in equation 1. This shows that the linewidths were a result of the plastic deformation, not fatigue.

A series of measurements *were also* made on eleven standard "hour-glass" samples of 350 WT steels for the Canadian Frigate Program; these steels had been subjected to a number of fatigue cycles at known stresses. Experiments were carried out on samples that had broken in the course of establishing the S-N curve (the stress, S, versus number of cycles, N, at failure), which had the form

$$\log_{10} N = +118.3 - 42.2 \times \log_{10} S . \qquad (3)$$

The linewidth of the broken samples depends on the true strain (as established by the change of diameter of the hour-glass samples) according to the relationship

$$A = (0.071 \pm 0.001) \ln \varepsilon + 0.322 \pm 0.002, \qquad (4)$$

which is very similar to the result for the HY-80 steels. Three of the unbroken samples showed no dimensional change and no linewidth increases to within the experimental uncertainty, but four samples showed a dimensional change of about 6% and linewidth increases of 0.15°. The latter fall on the curve established for the broken samples. Thus in the case of 350 WT steels as well as HY-80 steels our findings are that the linewidth is related to plastic deformation and not to fatigue damage in the regime of stress and number of cycles investigated, which is essentially low-cycle fatigue.

Residual Stresses in an Aluminium Ring and Plug Sample

J. Pang *(University of Toronto)*, A.P. Clarke and T.M. Holden *(AECL)*

In the past decade many neutron laboratories have begun programs of residual stress measurement with a view to industrial applications. Industrial customers in general require a uniformity of approach in making measurements as well as an indication of the accuracy of the results. An example of this required uniformity is the setting up a residual stress standards group under the auspices of VAMAS (Versailles Agreement on Measurements and Standards). The use of steel and aluminum standard samples has been investigated at Chalk River. The form of sample chosen was a ring-and-plug. A plug with the diameter of 25.094 mm and a ring with the internal diameter of 25.00 mm and external diameter of 75.0 mm were machined from high strength Al 7050 alloy. The difference in diameters is termed the interference, δ. The ring was first cooled to 77 K and then warmed to 300 K. The plug was then cooled to 77 K and inserted in the ring. This procedure ensured that both parts had the same thermal history. The interference was calculated to give a tensor stress field in the plug given in cylindrical coordinates, rr, θθ, by

$$\sigma_{rr} = \sigma_{\theta\theta} = -p \qquad (1)$$

and in the ring

$$\sigma_{rr} = \frac{a^2 p}{b^2 - a^2}\left(1 - \frac{b^2}{r^2}\right) \qquad (2)$$

$$\sigma_{\theta\theta} = \frac{a^2 p}{b^2 - a^2}\left(1 + \frac{b^2}{r^2}\right). \qquad (3)$$

Here a and b are the inner and outer radii of the ring and, p is the pressure at the interface of the ring and the plug given by

$$p = \frac{(b^2 - a^2)}{6ab^2}\delta E \qquad (4)$$

for a material of Young's modulus, E. No where does the stress exceed the yield point (400 MPa) of Al 7050; thus the stress field is completely elastic.

Measurements were made of the axial, hoop and radial strain components in the ring and the plug by neutron diffraction with the L3 spectrometer. The (331) planes of a Ge crystal were used to provide a monochromatic beam of neutrons. The lattice spacing for the (113) planes of Al were investigated with neutrons of wavelength 1.7409 Å as determined by calibration with a standard Si sample from the National Institute of Standards and Technology, Washington. For the radial and hoop measurements, the gauge volume was defined by slits 1.5 mm wide before and after the sample and 20 mm high. For the axial component, measurements were made at the mid-thickness of the assembly with a slit height of 10 mm in the ring and 5 mm in the plug.

Because the sample will be tested in many laboratories throughout the world and the results intercompared, the detailed results obtained in the experiment cannot be presented in this progress report.

However, the agreement between the measurements and the theory is very close. There are, however, slight differences that can be attributed (a) to the finite spatial resolution of the gauge volume, and (b) to the finite length of the ring and plug assembly.

A preliminary investigation of a steel ring-and-plug assembly was carried out. This sample is far less suitable than aluminium because of the relatively high neutron beam depletion by iron compared with aluminium for a similar path length in the sample.

Residual Stresses in Diffusion-Bonded SiC-Mo Joints

R.B. Rogge *(AECL)*, A.E. Martinelli and R.A.L. Drew *(McGill University)*

The use of ceramics such as SiC for high-temperature applications and in chemically hostile environments has increased dramatically. Among the properties that make SiC suitable for these applications are high strength at high temperatures, good wear resistance, and excellent chemical stability. However, ceramics are also brittle and are thus often married with metals in the form of composites, ceramic coatings, and joined structures. The integrity of such metal-ceramic bonds is therefore crucial for the overall performance of the engineering component and residual stresses generated in the bonding process will clearly impinge on the integrity of the bond.

Various joining technologies are available, but solid-state diffusion bonding is known to provide joints resistant to high temperatures and chemical attack. Diffusion bonding is realized at high temperatures and metals have coefficients of thermal expansion (CTE) 2 to 7 times greater than ceramics. Thus the metal contracts more than the adjoining ceramic of the diffusion couple resulting in potentially detrimental stresses near the interface. The high penetration of neutrons allow for the investigation of stresses in both materials in the interfacial region of an intact diffusion couple. We report on neutron diffraction stress measurements for a series of hot-pressed diffusion-bonded SiC-Mo joints.

The series of samples were designed to evaluate the distribution in thermomechanical stresses as a function of joining temperature and cooling rate. Strains were scanned along paths perpendicular to and parallel to the interface in both materials. Measurements were made with a spatial resolution of 0.25 mm. For each position both the in-plane and normal components of strain were measured and the stresses were calculated assuming a biaxial stress state.

Similar stress distributions were observed across the various samples. Specifically the in-plane component was tensile in the Mo and compressive in the SiC. This is a direct consequence of the CTE mismatch between the materials: the metal contracts more, so it applies a compressive force on the ceramic which in turn attempts to hold up the metal, resulting in a tensile stress in the metal. The normal component is near-zero throughout the range. The stresses observed in a sample that was hot-pressed at 1200°C and furnace-cooled are shown in figure 1.

A sample hot-pressed at 1400°C was observed to exhibit stresses of larger magnitude than the 1200°C sample. This is believed to be a consequence of the larger temperature change on cooling the couple. Another sample hot-pressed at 1400°C, but slowly cooled, was observed to exhibit lower magnitude stresses, particularly in the metal. It is believed that the slower cooling rate allowed the materials to better accommodate residual stresses through structural rearrangement.

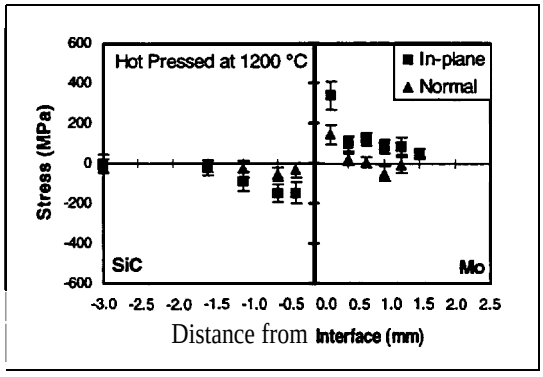

Fig. 1 Stress distribution observed in sample hot-pressed at 1200°C and furnace-cooled.

Volubility of Hydrogen in Zr-2.5Nb Pressure Tube Materials

J.H. Root and R.W.L. Fong *(AECL)*

During the operating lifetime of CANDU nuclear reactors, the hydrogen content in the Zr-2.5Nb pressure tubes increases. When the concentration of hydrogen exceeds the solid solubility, at a given temperature, zirconium hydride precipitates may form in the metal matrix. These hydrides embrittle the material, and may lead to delayed hydride cracking or formation of hydride blisters. Knowledge of the volubility of hydrogen in zirconium alloys is necessary to make realistic decisions on the fitness-for-service of a pressure tube that contains a given level of hydrogen. This year, the precipitation and dissolution of zirconium hydrides in Zr-2.5Nb pressure tube material were tracked successfully by neutron diffraction both as a function of temperature for specimens with fixed hydrogen content and as a function of time during hydrogen ingress at the operating temperature of CANDU nuclear reactors. The direct nature of the neutron measurements is expected to resolve a number of uncertainties about the interpretation of data from other experimental techniques and to shed new light on aspects of hydrogen volubility in zirconium alloys.

The solvus line, obtained by heating two hydride-bearing specimens, agrees with equations that fit earlier results, [1,2] except in the early stages of dissolution, when large hydride precipitates are present in the matrix (figure 1). On cooling, the solvus line is shifted by about 20°C towards higher temperature, compared with that of Slattery [2] for Zr-2.5Nb (figure 2). Hydrides may appear in two possible phases in pressure tube materials: an fcc δ-phase and a face-centred tetragonal γ-phase. The γ-phase is thought to be metastable at room temperature created by rapid cooling, or low hydrogen concentrations. However, in the specimens with fixed hydrogen concentration, a substantial fraction of the hydrides persisted in the γ-phase, through a number of thermal cycles in which the specimen was soaked at temperatures over 400°C for several hours, then cooled slowly to room temperature. In a specimen subjected to continuous hydrogen ingress at 250°C for 7 days and subsequent cooling to room temperature, all of the hydrides were found to be in the δ-phase. Work on the hydride: zirconium system is continuing.

REFERENCES

[1] J.J. Kearns, J. Nucl. Mater. **22** (1967) 292.

[2] G.F. Slattery, J. Inst. Metals **95** (1967) 43.

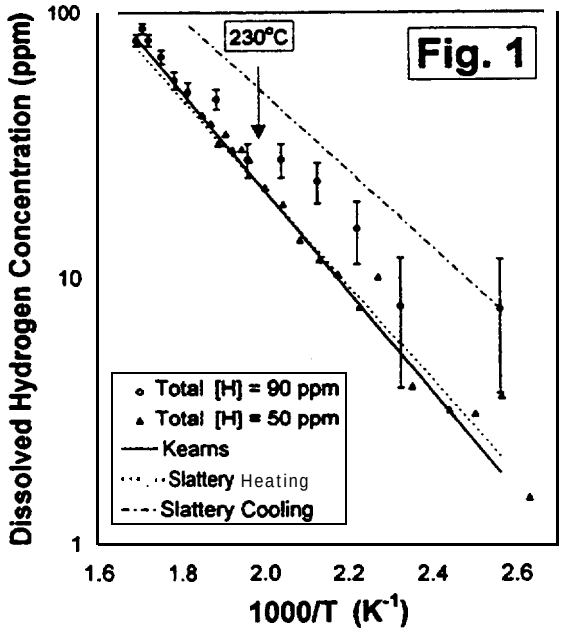

Fig. 1 Solvus line, measured by various techniques during heating (dissolution).

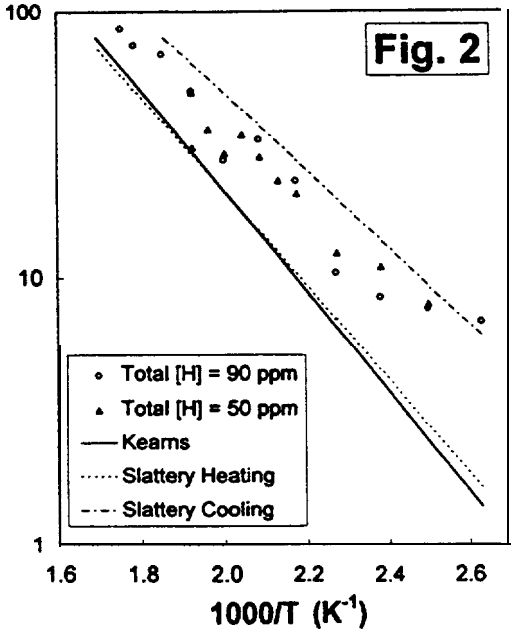

Fig. 2 Solvus line, measured during cooling (precipitation).

Volubility of Hydrogen in Single-Phase Zirconium Alloys

J.H. Root and D. Khatamian *(AECL)*

CANDU pressure tubes are currently made from a two-phase zirconium alloy, Zr-2.5Nb. The alloy contains a majority of the hcp a-phase and a minority of bcc β-phase, which is metastable at room temperature and contains about 20 wt % Nb. The volubility of hydrogen in these two metal hosts is very different. Hydride precipitation and dissolution in real pressure tube materials may therefore be influenced by the microstructure and composition of the distinct metal hosts, in addition to a large number of other factors, such as thermo-mechanical history, presence of trace elements, and stress state. Matrix alloy effects on hydrogen volubility are best investigated with single-phase metals.

For this project, specimens of pure a-phase zirconium and a pure β-phase alloy, Zr-20%Nb, were pre-loaded with deuterium to levels of 220 μg/g and 1100 μg/g, respectively. Critical temperatures for the completion of dissolution (TSSD) were evaluated by differential scanning calorimetry (DSC). There are two popular ways to obtain TSSD from a DSC. One is to select the temperature at which the heat flow curve vs. temperature passes through a maximum or a minimum. The other is to select the temperature where the heat flow curve passes through an inflection point. Neutron diffraction provides an unambiguous indication of TSSD, based on the temperature dependence of hydride diffraction peak intensities. Comparing neutron diffraction and DSC values of TSSD (Table 1), it appears that the temperature of the peak maximum in DSC is the most reliable. A surprising discovery, made during the course of the neutron diffraction measurements, was the long time required for the hydride precipitates to reach equilibrium after cooling to room temperature from the solution heat treatment temperature of 400°C. The conversion of initial δ-phase hydrides to y-phase hydrides requires many hours, as shown in figure 1.

Table 1 TSSD Values (°C)

Technique	a-Matrix	B-Matrix
Neutron	361 ± 3	134 ± 2
DSC Peak Max.	357 ± 1	134 ± 1
DSC Max. Slope	376 ± 1	146 ± 1

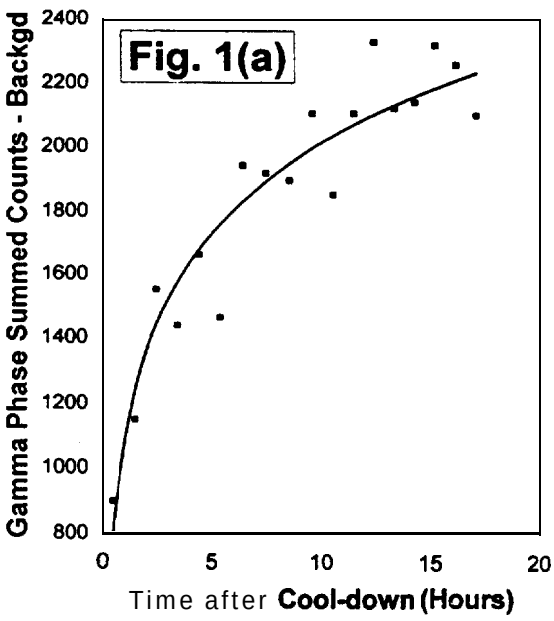

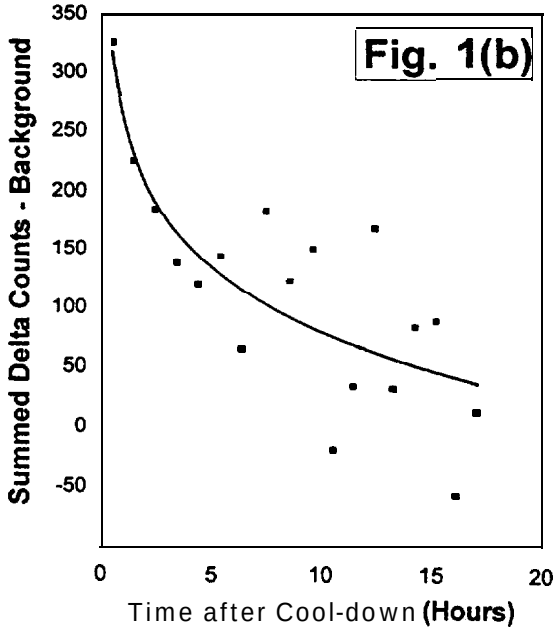

Fig. 1 Transformation of δ-phase hydrides into γ-phase hydrides, tracked by variations of (111) diffraction peak intensities with time at fixed temperature, 57°C.

Changes in a Ti Thin Film Probed by In-situ Neutron Reflectometry

J. Noel, D.W. Shoesmith and Z. Tun *(AECL)*

We have carried out neutron reflectometry measurements on a thin Ti film in contact with a liquid electrolyte, subjected to an in-situ electrochemical reaction. The ~150 Å thick film was grown by sputtering onto a Si substrate doped as a p-type semiconductor to provide good electrical conductivity. The electrolyte was a 0.27 M NaCl solution. The other electrode of the cell was a thin Pt foil positioned parallel to the Ti electrode. Figure 1 shows a schematic view of the cell and the neutron scattering geometry. Neutrons are incident on the Ti film from the Si side as they cannot propagate far in the aqueous electrolyte and the specular reflectivity was measured with θ/2θ scans. The experiment measured changes in the Ti film, and its air-grown oxide layer, as a dc potential was applied across the cell (Pt positive and Ti negative).

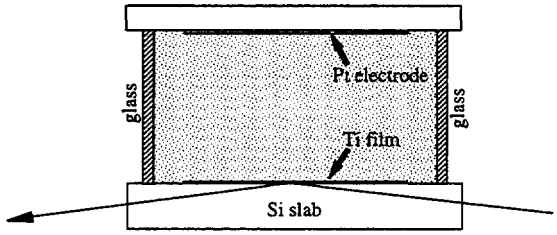

Fig. 1 Schematic view of the electrochemical cell and the scattering geometry.

Measurements were made with the following conditions:

Condition 1 The Ti film was submerged in ultra-pure water and air-dried. The cell was assembled but not filled with electrolyte.

Condition 2 The cell was filled with the NaCl solution, but no external circuit was connected.

Condition 3 The external circuit was completed and either constant voltage or constant current was applied. Several scans were taken over a 5-day period. The maximum current applied, during the last set of scans, was 500 μA.

Figure 2 shows the results (circles) measured under Condition 2. They are given as counts versus momentum transfer, Q_z, normal to the sample surface. The observed peaks are broad because of a non-periodic layer structure, and the background is high because of incoherent scattering from water.

We have proposed a model layer profile to reproduce the experimental points in figure 2. The minimum parameter model consists of the Si substrate, Ti layer, a natural oxide layer, and water. Assuming the oxide to be TiO_2 and the water to be pure H_2O, scattering densities of the layers were assigned to nominal bulk values. A least-squares refinement of layer thicknesses, t, gave t(Ti) = 140 Å and t(TiO_2) = 21 Å. The curve in figure 2 is the reflectivity calculated with the model.

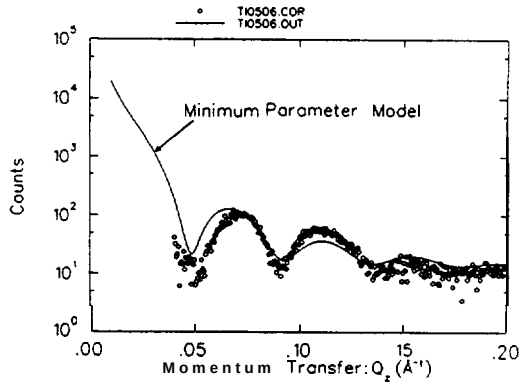

Fig. 2 Neutron reflectometry profile measured before an external potential was applied.

Figure 3 shows the reflectivity of the same sample after ~5 days of in-situ electrochemical reaction (Condition 3). Compared with figure 2 the sample reflectivity has changed, most notably in the growth of the peak at 0.11 Å^{-1}. Scans performed between figures 2 and 3 show that the change started, soon after the cell current was increased to 500 μA. Since the specular reflectivity decreases very rapidly as a function of Q, a second-order peak nearly as strong as the first-order peak is anomalous. We are so far unable to explain the observed change. We plan to investigate this surprising result further.

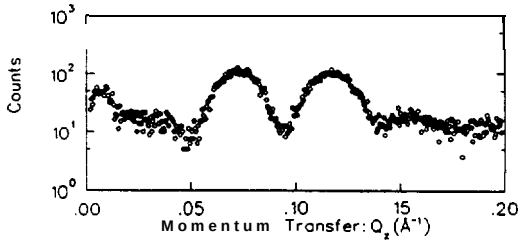

Fig.3 Neutron reflectometry profile after 500 μA current was applied to the cell, with the Ti electrode connected to negative terminal.

Long-Range Order and Vacancies in Fe_3Al and $Fe_3Al(Cr)$ Alloys

S.M. Kim *(AECL)* and D.G. Morris *(University of Neuchâtel)*

The Fe_3Al and $Fe_3Al(Cr)$ alloys are currently receiving considerable attention from the materials science community for possible use as new high-temperature structural materials because of their high strength and corrosion resistance at elevated temperatures. A recent ILL (Grenoble), GKSS (Geesthacht) and Münster (Institut Metallforschung) collaboration measured *in situ* neutron diffraction profiles in several Fe_3Al alloys and reported that both the $D0_3$ and B2 long-range order parameters (S) remain almost unchanged up to well above the critical temperatures [1]. They suggested that the phase boundaries shown in the current Fe-Al phase diagram are not the phase boundaries at all, but have bearing only on the size of antiphase domains. We find, however, that they used an incorrect expression for S, which does not go to zero for a completely disordered alloy. In addition, because single crystals were used, they could not determine the temperature dependence of S accurately below the critical temperatures.

We have carried out *in situ* neutron powder diffraction measurements on $Fe_{.62}Al_{.28}$, $Fe_{.675}Al_{.325}$ and $Fe_{.62}Al_{.28}Cr_{.05}$ alloys from room temperature to 1100°C using the C2 DUALSPEC powder diffractometer. The observed neutron powder diffraction profiles were analyzed using the Rietveld analysis program GSAS.

We found that S defined by Krivoglaz and Smirnov [2] and also used by the ILL-GKSS-Münster collaboration, is not applicable for the $D0_3$ or B2 phase of Fe_3Al. Their formula is applicable only for the nearly stoichiometric compositions in ordered alloys having two different sublattices. We define a new long-range order parameter as $S = (p-c)/(1-c)$ where p is the fraction of the chosen atom types (Fe or Al) occupying a given sublattice (A, B, A + B or C) and c is the fraction of the chosen atoms in the two sublattices concerned, i.e. A and B for the $D0_3$ order, and (A + B) and C for the B2 order.

For $Fe_{.62}Al_{.28}$ and $Fe_{.675}Al_{.325}$, the $D0_3$ (Al on the A sublattice) and B2 (Fe on the C sublattice) long-range order parameters decreased rapidly below the critical temperatures, indicating a second-order phase transition, in sharp contrast to the claims of the ILL-GKSS-Münster collaboration. In $Fe_{.675}Al_{.325}$, S ($D0_3$) had a low value of 0.581(7) at room temperature caused by the freezing-in of the atom mobility below about 375°C, as also was observed in the present measurements. For $Fe_{28}Al$, S($D0_3$) at room temperature was slightly incomplete 0.979(7) caused also by the freezing-in of the atom mobility. S (B2) for $Fe_{.62}Al_{.28}$ and $Fe_{.675}Al_{.325}$ were 0.994(5) and 1.004(5), respectively, at room temperature. The small departure from a perfect B2 order (S = 1.000) is most likely caused by a slight deviation (> 0.1%) in the alloy composition from the nominal value. No indication of vacancy formation was observed to an accuracy of ±0.1 %. In $Fe_{.62}Al_{.28}Cr_{.05}$ alloy, appreciable $D0_3$ and B2 disorder was observed as the temperature was lowered, indicating decreasing ordering energies. The increased ductility (by a factor of 2) observed in this alloy at room temperature may be due to this lowering of the ordering energies with addition of 5 at % Cr.

REFERENCES

[1] K. Hilfrich, W. Petry, O. Scharpf and E. Nembach, Acts Metall. Mater. 42 (1994) 731, and references therein.

[2] M.A. Krivoglaz and A. Smirnov, The Theory of Order-Disorder in Alloys (MacDonald, London, 1964) 2.

Defect Structure in NiAl Alloys Observed by Neutron Diffraction

S.M. Kim *(AECL)*, Y. Takeda and M. Kogachi *(University of Osaka Prefecture)*

In situ neutron powder diffraction measurements on several B2 NiAl alloys (45.3, 47.6, 50.0, 51.0 and 52.3 at % Al) from room temperature to 1400°C, reported previously (PR-PHY-8:2.3.1.54; AECL-11234), have now been analyzed with the Rietveld analysis program, GSAS. The small composition change caused by Al evaporation during the measurements has been taken into account in the analysis.

The observed Ni and Al antistructure atom concentrations (closed circles) and the Ni or Al vacancy concentrations (open circles) determined at 900°C are shown in figure 1(a). The Ni antistructure atom concentration and Ni vacancy concentration at room temperature obtained from the Bradley-Taylor (BT) structure model [1] are also shown with open and closed triangles, respectively. It is seen that in $Ni_{54.9}Al_{45.1}$ alloy, the Ni antistructure atom concentration is appreciably higher than the BT model, and that appreciable Al antistructure atoms are also present. The defect concentrations observed at room temperature are very similar to those at 900°C, except that the antistructure atom concentrations are slightly higher than at 900°C.

The defect concentrations observed at 1300°C are shown in figure 1(b). In Ni-rich NiAl, the antistructure atom concentrations are appreciably smaller than at 900°C. For Al-rich compositions, Ni vacancy concentrations are also appreciably smaller than those at 900°C. The most interesting result, however, is that appreciable Al vacancies form in $Ni_{52.7}Al_{47.3}$, $Ni_{50.3}Al_{49.7}$ and $Ni_{49.3}Al_{50.7}$ at this temperature, which was entirely unexpected. It is also interesting to note that appreciable Al antistructure atoms are also created in $Ni_{50.3}Al_{49.7}$, $Ni_{49.3}Al_{50.7}$ and $Ni_{48}Al_{52}$ alloys in sharp contrast to previous expectations.

REFERENCES

[1] A.J. Bradley and A. Taylor, Proc. R. Soc. Lond. **159** (1937) 56.

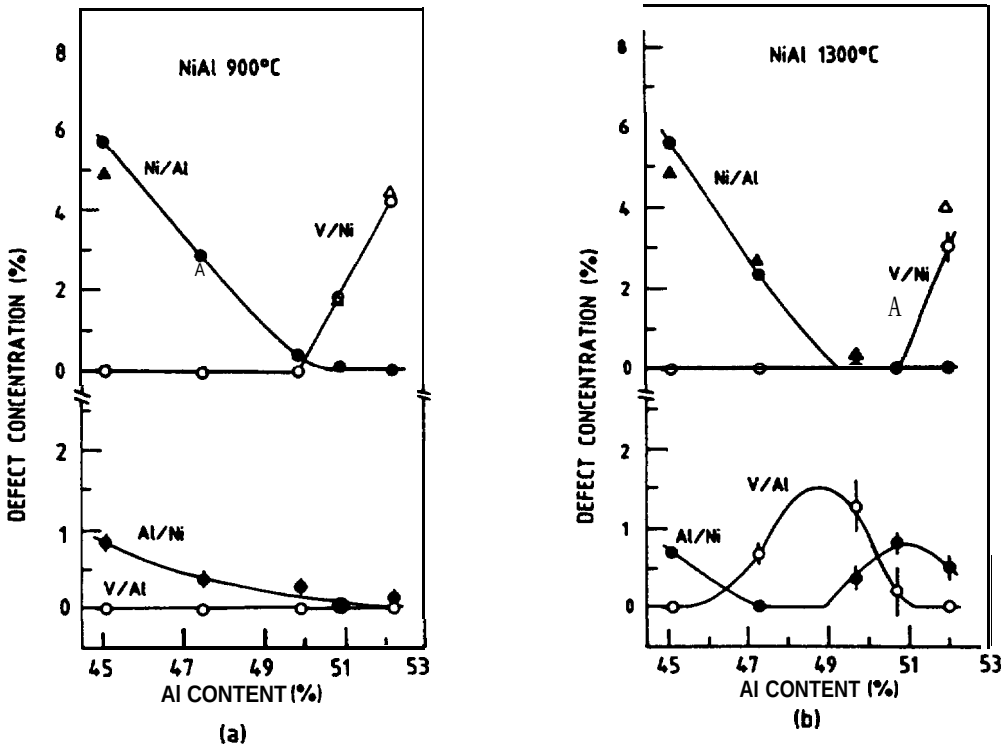

Fig.1 The defect concentrations in NiAl alloys observed at 900°C (a) and 1300°C (b). Ni/Al (V/Al) denotes the fraction of Ni atoms (vacancies) on the Al sublattice.

Physics

Magnetism and Superconductivity in UPt_3

B. Lussier and L. Taillefer *(McGill University)*,
T.E. Mason *(University of Toronto)* and W.J.L. Buyers *(AECL)*

To explain the two superconducting phases of the heavy fermion compound UPt_3, many theories require a symmetry breaking field (SBF) to lift the degeneracy in the two-dimensional order parameter. A likely candidate for such a SBF is the small antiferromagnetic moment ($0.02\,\mu_B$) lying in the basal plane of this hexagonal crystal. In the presence of a magnetic field, some theories require the moment to rotate in the basal plane, whereas others postulate the formation of a single thermodynamically stable magnetic domain. Our experiment consisted in a study of these magnetic domains down to 1.8 K under a magnetic field using the DUALSPEC triple axis spectrometer with a graphite monochromator, analyser and filter at a neutron energy of 3.52 THz. The sample, used in previous neutron experiments was a high-quality single crystal of UPt_3 that exhibits two sharp successive superconducting transitions, a moment of $0.03\,\mu_B$/U atom and a Néel temperature of approximately 6 K. It was aligned with its hexagonal plane in the scattering plane of the spectrometer and mounted in a horizontal field cryostat that enabled a field of up to 3.2 T to be applied at any angle in the basal plane.

Our results, shown in figure 1, indicate that a magnetic field of up to 3.2 Tesla has no effect on the magnetic order in UPt_3, whether it be in rotating the moments or in selecting a particular q-vector (or domain). Because the upper critical field of UPt_3 is less than 3.2 T, the absence of rotation makes it difficult to reconcile the fact that experimentally a kink in $H_{C2}(T)$ is always observed for a field in any direction in the basal plane, with the prediction of current theories that it should only occur when $\mathbf{H} \perp \mathbf{M}_S$. A calculation with three fixed domains would prove very helpful. Our results also invalidate the respective assumptions (moment rotation and domain selection) underlying two recent explanations for the slight 60° variation of H_{C2} in the basal plane.

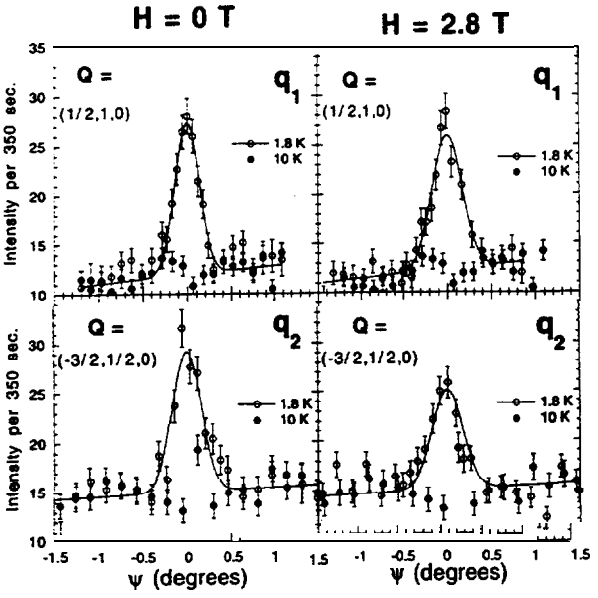

Fig. 1 Magnetic Bragg intensity versus crystal angle ψ with and without an applied field in the [-1, 2, 0] direction.

Low-Energy Magnetic Fluctuations in UNi_4B

S.A.M. Mentink and T.E. Mason *(University of Toronto)*,
J.A. Mydosh *(Leiden University)* and W.J.L. Buyers *(AECL)*

The hexagonal uranium compound, UNi_4B, forms a partially ordered antiferromagnetic structure [1] below T_N = 20 K. We have studied the magnetic fluctuations of this material below T_N, which are anticipated to behave anomalously, since part of the uranium moments stay disordered at low temperature. Earlier high-resolution inelastic spectra taken at the Risø spectrometer TAS-7, making use of the multicrystal vertically focussing RITA analyzer have, for the first time, shown the existence of a dispersive spin-wave excitation around 0.58 THz, at the magnetic wave vector $Q = (\frac{1}{3}\ 0\ 2)$. Near dispersionless magnetic scattering was observed throughout the zone, typical of the overdamped response often present in uranium intermetallic compounds. Alternatively, it could also be contributed to the magnetic fluctuations of the non-ordering moments.

The attempt to reproduce the 0.58 THz excitation and to measure its dispersion relation with the DUALSPEC C5 triple axis spectrometer on the same UNi_4B crystal has failed, both when using a fiat and a focussing monochromator. This is due to the very weak magnetic scattering of UNi_4B and the tight resolution (0.5 THz) necessary in this experiment. It suggests that only cold-source experiments may reveal the complete magnetic excitation spectrum of UNi_4B. Scans taken with coarser resolution (1.3 THz) could not resolve the spin-wave excitation, but did confirm the existence of weak but real, strongly broadened magnetic fluctuations at various wave vectors. Figure 1 displays the very weak scattering at the magnetic wave vector and an energy scan with coarse resolution over the broad scattering. All data were taken at 4.2 K.

REFERENCES

[1] S.A.M. Mentink, A. Drost, G.J. Nienwenhuys, E. Frikkee, A.A. Menovsky and J.A.. Mydosh, Phys. Rev. Lett. 73 (1994) 1031.

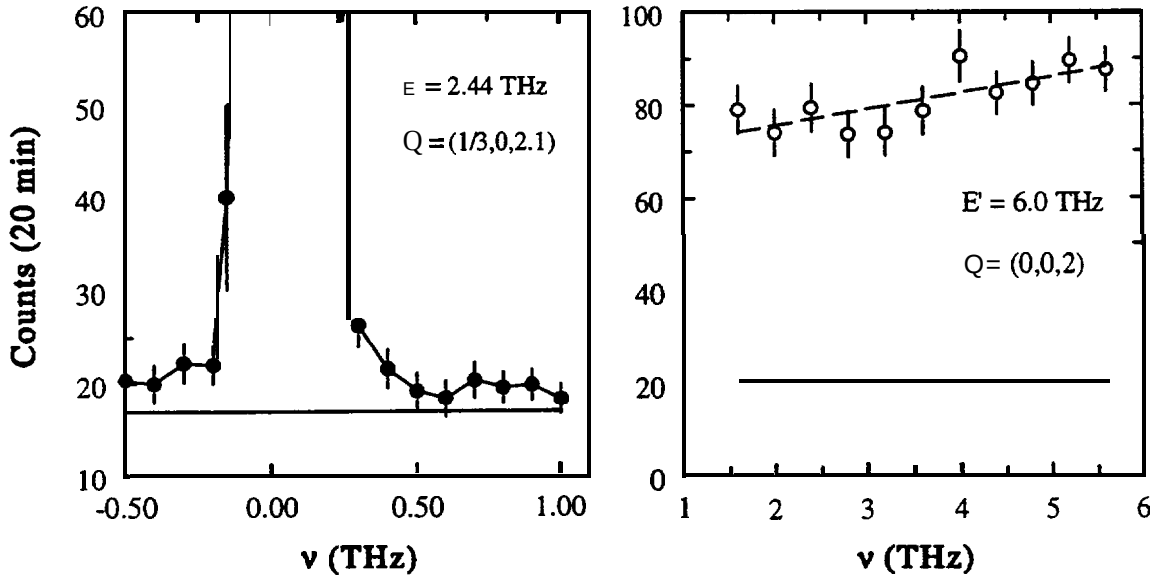

Fig. 1 Constant-Q scans at various wave vectors in the (h O 1) zone of UNi_4B with tight (left) and coarse (right) resolution taken at 4.2 K. Thick solid lines represent the analyzer-turned background.

Elastic and Inelastic Neutron Scattering Studies of $KNiCl_3$

O.A. Petrenko, M.F. Collins and B.F. Collier *(McMaster University)*, and Z. Tun *(AECL)*

Experiments on the C5 and N5 triple-axis spectrometers, and the DUALSPEC powder diffractometer, C2, have allowed us to investigate the structural and magnetic phase transitions of $KNiCl_3$.

The room-temperature crystal structure of $KNiCl_3$ is a modified form of stacked triangular structure found in a series of hexagonal ABX_3 compounds, where A is an alkali metal, B a divalent 3d metal and X a halogen. Antiferromagnetic exchange interactions along the hexagonal *c* axis are two to three orders of magnitude stronger than those in the basal plane. There is magnetic frustration in the basal plane arising from the triangular arrangement of spins. This is the reason for current interest in this class of materials since it results in different "physics" from that found in unfrustrated systems, notably novel critical exponents and phase diagrams.

We have investigated three large crystals of $KNiCl_3$. At room temperature (RT), 298 K, all three crystals gave identical scattering patterns consistent with the space group $P6_3cm$. This structure is derived from the simple stacked triangular lattice (space group $P6_3/mmc$) by shifting two thirds of the $NiCl_3$ chains along the *c* axis. Machida *et al.* [1] have reported that $KNiCl_3$ undergoes structural distortions just below room temperature. We observe dramatic differences between our crystals after cooling through these transitions.

In crystal #1 scans in the (*hhl*) plane of the reciprocal lattice revealed new Bragg peaks at position (*h*/3, *h*/3, *l*) when the sample was cooled through ~270 K. The intensity of these peaks was small, increasing gradually as the temperature decreases, though even at the lowest temperature (4 K) it did not exceed 0.5% of the main Bragg peaks. No new peaks were found for scans in the (*h0l*) plane and none of the main Bragg peaks changes in intensity when passing through 270 K. We conclude that first, the distorted low temperature (LT) unit cell is rotated through 30° about the *c* axis from the RT cell and enlarged to $\sqrt{3}a$, $\sqrt{3}a$, and *c*, and second, the distortion is small so that the LT structure does not differ very much from the RT structure. Measurements on a powder sample have confirmed these conclusions. We call the LT structure of this particular sample "phase A".

In crystal #2, instead of RT peaks at position (*h0l*) with *l* even, new peaks appeared at $(h+q, 0, l)$ with $q = 0$ for $h = 3n$ (n is an integer), $q = -1/4$ for $h = 3n + 1$ and $q = 1/4$ for $h = 3n + 2$. We call this LT structure, which is clearly different from that of crystal #1, phase B.

Close inspection of LT scattering patterns from crystal #1 and #2 shows neither of them is homogeneous; that is a small amount of phase B is present in crystal #l, and vice versa for crystal #2. This can be seen in figure 1, where each panel shows small peaks from the minority LT phase. Our rough estimate of phase ratio A:B gives 97:3 for crystal #1 and 10:90 for crystal #2. For each crystal, this ratio is repeatable and does not depend upon the cooling rate. To investigate the spatial distribution of phases A and B in crystal #2, we restricted the horizontal size of the incident neutron beam to 2 mm and scanned the sample across the beam while the intensities of selected peaks from the both phases were measured. We observed phase A is mostly located at the tips of the roughly cylindrical crystal (mounted on its side), whereas phase B occurs mostly in the middle.

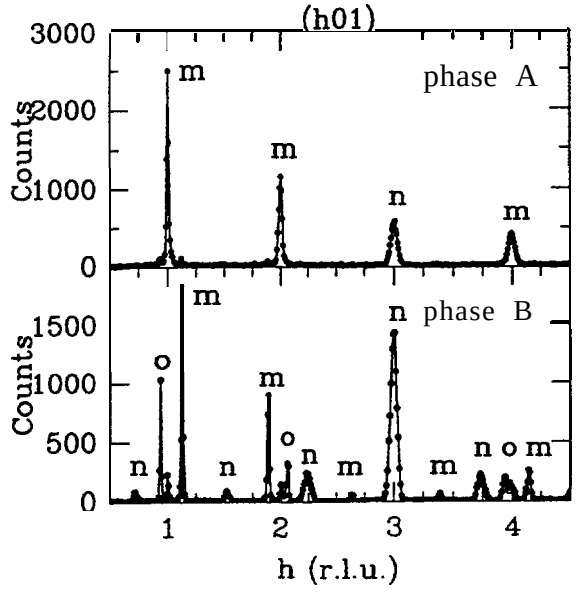

Fig. 1 Bragg-peak intensity of $KNiCl_3$ at T = 4.2 K for phase *A* (top) and *B* (bottom) along the (h0l) direction of the reciprocal lattice. Nuclear peaks are designated by n, in-plane magnetic peaks m and out-of-plane magnetic peaks o.

Like many other ABX_3 materials, $KNiCl_3$ is hygroscopic, and one plausible reason for the sample-dependent LT structures is the amount of non-crystallized water trapped in the lattice. To investigate this possibility, crystal #3 was prepared and its neutron diffraction pattern measured immediately after preparation and again after annealing for 12 days at 250°C. No significant change was found and in both cases the diffraction pattern is consistent with phase B indicating that water is not the source of the sample dependence.

As a consequence of the existence of two different LT structures, two different magnetic structures developed at very low temperatures (<12K). However, in both cases, the (hkl) magnetic Bragg reflections with even l are systematically absent indicating that spin ordering within each chain is strictly antiferromagnetic because of the dominating intrachain exchange interaction.

In crystal #1 with majority phase A, the magnetic ordering takes place at TN = 12.5 K. The magnetic Bragg peaks appear at $(h0l)$ where l is an odd integer (see figure 1a). The pattern is consistent with a 120° spin structure confined in the basal plane. However, the (001) Bragg reflection is clearly present, indicating that the actual canting angle is significantly different from 120°. This is an expected result as structural distortions lead to lower symmetry among the interchain exchange interactions.

In crystal #2 with majority phase B, the magnetic ordering sets in at TN= 8.6 K. Unlike crystal #1, not all the magnetic Bragg peaks lie in the $(h0l)$ scattering plane. The peaks located in the plane can be indexed as $((3/8)(2h+1), 0, 2l+1)$, but there are also peaks slightly above and below the scattering plane. These out-of-plane peaks are sufficiently close to the scattering plane that they can be seen if the vertical divergence spectrometer is large (see figure 1b). This diffraction pattern, including peaks above and below the scattering plane, is identical to that observed in another distorted ABX_3 material, $RbMnBr_3$.

We have also measured the spin wave dispersion relations in phase A along the hexagonal axis and the results are shown in figure 2.

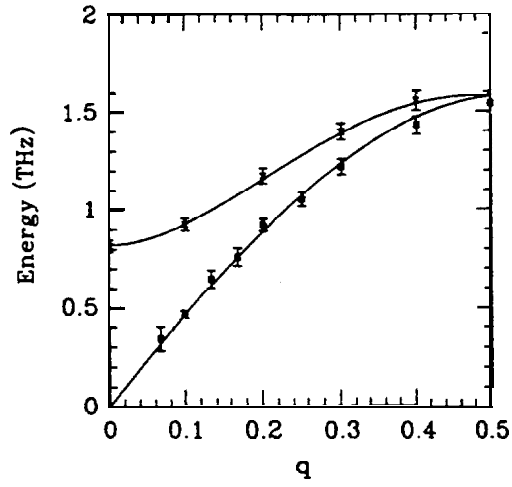

Fig. 2 Spin-wave dispersion relation in $KNiCl_3$ at 4.5 K along the hexagonal axis. The solid points give the observed spin-wave energies at $Q = (1, 0, 0-q)$ and the crosses give the spin-wave energies at $Q = (1, 1, 1+q)$. The lines are given by equations (1) and (2) with $J = 0.365$ THz. $D = 0.115$ THz.

The lines in the figure, which agree well with experiment, are fit to a model with only two parameters;

$$\hbar w_1(q) = 4J \sin\frac{q}{2}\sqrt{4\cos^2\frac{q}{2} + \frac{D}{J}} \qquad (1)$$

$$\hbar w_2(q) = 4J \cos\frac{q}{2}\sqrt{4\sin^2\frac{q}{2} + \frac{D}{J}} \qquad (2)$$

where J and D are intrachain exchange and easy-plane anisotropy parameters.

REFERENCES

[1] K. Machida, T. Mitsui, T. Kato and K. Iio, Solid State Comm. 91 (1994) 17.

Magnetic Phases in UNiGe

H. Nakotte, A. Purwanto and R.A. Robinson *(Los Alamos National Laboratory)*
and Z. Tun *(AECL)*

In studies of the magnetic anisotropy of uranium compounds, most materials manifest the following features that relate the moment configuration to the geometrical surrounding of U ions:

1. The nearest-neighbour exchange between U ions is ferromagnetic.
2. The *5f* moments tend to be perpendicular to the shortest inter-uranium vector. For U compounds with an orthorhombic TiNiSi structure, this vector lies along the crystallographic *a*-axis, with a slight zig-zag because of some small displacement of U ions parallel to the *c*-axis. Therefore, one would anticipate that the moments will be located in the *b-c* plane.

UNiGe is one of the U compounds with the TiNiSi structure. It orders antiferromagnetically into a commensurate magnetic structure below 42 K, with $\mathbf{q} = (0,1/2,1/2)$ [1]. A collinear arrangement of magnetic moments that lie in the *b-c* plane was found, but there was some evidence that the x component along *a was* nonzero. Between 42 and 51 K, an incommensurate phase appears [2] with propagation vector $\mathbf{q} = (0, \delta, \delta)$. A third magnetic phase with $\mathbf{q} = (0,1/3,1/3)$ occurs upon application of a magnetic field higher than 2 T above 20 K.

We have performed polarized and unpolarized neutron-diffraction experiments on a single crystal of UNiGe in horizontal magnetic fields up to 3 T in order to answer the following questions:

1. Is the x component of the U moment in UNiGe nonzero in the commensurate phase?
2. What is the magnetic structure in the incommensurate phase between 42 and 51 K?
3. What is the nature of the transitions between the commensurate phase, incommensurate phase and the 1/3-phase?

Polarized neutron experiments were performed on the C5 spectrometer of the DUALSPEC facility. The sample *b-c* plane was arranged to be in the scattering plane and the neutron polarization could be rotated to any direction in this plane by turning the sample inside the cryostat. A difference in the minimum response for spinflip and non-spinflip scattering is then clear evidence for an x component. The result plotted in figure 1 clearly shows a difference in the minimum response for the two scattering channels. Our analysis gives a non-collinear arrangement of the moments with canting angle out of the *b-c* plane by $17 \pm 4°$, indicating that UNiGe is an exception among U compounds.

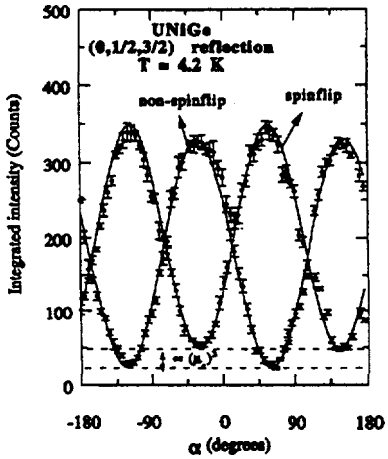

Fig. 1 Non-spinflip and spinflip scattering of the (0, 1/2, 3/2) Bragg peak as the polarization vector is rotated within the *b-c* plane.

The second and third part of the experiment were performed on the N5 spectrometer in the temperature range between 40 and 55 K and for magnetic fields up to 3 T. For the incommensurate phase, we find an ordering wave vector $\mathbf{q} = (0, \delta, \delta)$, where δ is slightly temperature dependent and increases from 0.35 at 50 K to 0.37 at 44 K. At 42 K, the structure locks in to the commensurate one with $\delta = 1/2$. At low magnetic fields, only little change in δ was found, but around 2 T the incommensurate structure locks into the l/3-phase with $\delta = 1/3$. There is evidence for a nonzero x component also in the incommensurate phase.

REFERENCES

[1] A. Purwanto, V. Sechovský, L. Havela, R.A. Robinson, H. Nakotte, A. Larson, K. Prokeš, E. Brück, F.R. de Boer; Phys. Rev. B (in press).

[2] V. Sechovský, L. Havela, P. Svoboda, A. Purwanto, A.C. Larson, R.A. Robinson, K. Prokeš, H. Nakotte, F.R. de Boer, H. Maletta; J. Appl. Phys. 76 (1994) 6217.

Neutron Depolarization Study of **Meso-Scale** Ordering in Frustrated **Magnetic Systems**

D.H. Ryan *(McGill University)*, J.M. Cadogan *(University of New South Wales)*,
Z. Tun *(AECL)* and S.J. Kennedy *(Australian Nuclear Science and Technology Organization)*

Partially frustrated magnetic systems exhibit two magnetic transitions, the first at T_c to a ferromagnetic state, followed at a lower temperature T_{xy}, by a second transition in which transverse spin components freeze at random perpendicular to the ferromagnetic ordering direction. We have carried out an extensive study of both bulk and microscopic behaviour in these systems [1] and now turn to neutron scattering techniques to probe the ordering on intermediate length scales.

We used neutron depolarization to investigate the following issues:

(i) Isa ferromagnetic state established at T_c?
(ii) Is the ferromagnetic order affected by the ordering of the transverse spin components at T_{xy}?
(iii) How does the ferromagnetic state evolve as we increase the level of frustration?

Two systems were studied: a-Fe_xZr_{100-x} with $90 < x < 93$, and a-$Fe_{90-x}Ru_xZr_{10}$ with $0 < x < 4$. In both cases the frustration increases with x. Although the former system is cleaner and has been more extensively studied, it is not possible to reach the spin-glass by increasing x, as samples beyond $x = 93$ are not stable. The Ru-doped series appears to be a spin-glass for $x \geq 3$ and provides an alternative system in which to watch a ferromagnet evolve into a spin-glass.

A piece of ribbon 20 μm thick was mounted over a 1 mm × 5 nun window in a cadmium mask. Measurements were performed on the C5 DUALSPEC triple axis spectrometer, using the (111) reflection from two Heusler crystals as polarizer and analyzer. A base polarization of close to 96% was obtained at a wavelength of 2.37 Å. Both H8 and D3 cryostats were used to record data during free cool and controlled heating runs in a "straight through" or $q = O$ geometry.

Visual inspection of the data on both series clearly shows that the ferromagnetic state formed at T_c leads to a significant depolarization of the beam, as expected, and persists to the lowest temperatures studied (~2 K) confirming that the ordering at T_{xy} does not destroy the ferromagnetic order. It is also clear that the increasing frustration leads to a reduction of the depolarization signal as the ferromagnetic order weakens. Although it is not visible on the scale used in figure 1 the $Fe_{93}Zr_7$ sample does in fact depolarize the beam slightly below T_c, while neither the $x = 3$ nor the $x = 4$ Ru-doped samples yield any depolarization, confirming that we need the Ru in order to fully frustrate this system.

The observed depolarization signal in a-Fe-Zr can be fitted assuming a constant domain size and a conventional temperature-dependent magnetization, confirming the formation of a ferromagnetic state below T_c. However deviation from such a fit is observed at low temperatures as the polarization rises slightly. Both the extent of the recovery and the temperature at which it starts increase with increasing frustration. The effect is most marked in the Ru-doped samples. One possible explanation for the recovery is a destruction of ferromagnetic domains associated with the onset of transverse spin freezing; however the recovery starts significantly above T_{xy}. A second possibility is the development of some spin-dependent scattering associated with fluctuations in the transverse spin components. Distinguishing between these possibilities will be the subject of further experiments.

REFERENCES

[1] H. Ren and D.H. Ryan, Phys. Rev. B **51** (1995) 15885.

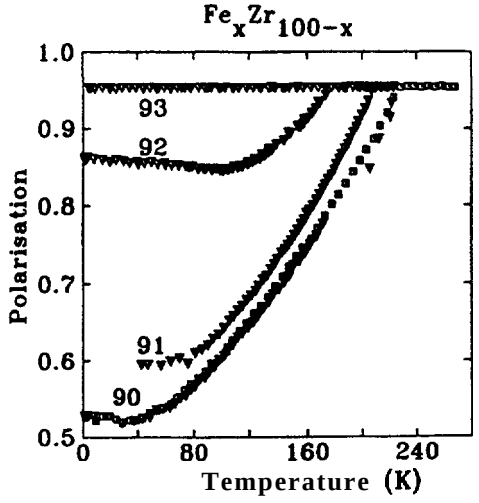

Fig. 1 Transmitted beam depolarization as a function of sample temperature.

Observation of Spin Kinetics at 1.3 Kin a Random Anisotropy System

D.R. Taylor *(Queen's University)* and W.J.L. Buyers *(AECL)*

This experiment studied the development of magnetic ordering in $Dy(As_{0.35}V_{0.65})O_4$, a system that provides a random anisotropy environment with no dilution, mixing, or structural disordering of the magnetic ions. The case of a three-dimensional lattice with two spin components is of special interest to investigate the existence of a transition to long-range order.

The experiment was run at N5 using the H5 cryostat and the Edwards 275/Roots blower pump to reach temperatures as low as 1.1K. A flexible rubber hose link allowed cryostat rotations of ±45° at the lowest temperatures. The monochromator was Si(111) giving neutrons a wavelength 2.37 Å. Graphite filters before and after the sample reduced half-wavelength contamination. Quasi-elastic (no analyzer) scans in radial and transverse directions were carried out at the (100) point where scattering due to antiferromagnetic ordering was expected.

In general the scattering at (100) showed both a broad and a sharp component as seen in figure 1. The broad peak was visible up to 8K. Its width decreased as the temperature was lowered, but by only a factor of two down to 1.3 K. Its intensity changed very little down to 2K, but then increased smoothly by a factor of ~5 as the temperature was reduced to 1.3 K. Its lineshape was well fitted by a Lorentzian-squared function.

The narrow peak was temperature-independent and resolution-limited above 2K, where it is attributed to residual feedthrough from (200). Below about 1.6 K its intensity increases dramatically, as shown in figure 2, suggesting an antiferromagnetic transition. Examination of this peak below 1.7 K with tighter resolution, however, showed that the width was never resolution-limited in this range.

Throughout the experiment the magnetic scattering was observed to require a significant time to reach equilibrium. The equilibration times ranged from about 1 hour at 2.5 K to 10 hours at 1.3K.

We conclude that the random anisotropy suppresses antiferro-magnetic ordering from about 3.0 K (where it occurs in the pure compounds) to about 1.6 K. However this is not a true long-range ordered state with diverging susceptibility, in agreement with most theoretical predictions. This state coexists with, and competes against, configurations of short-range order that resemble correlated spin-glass states. Random anisotropy also causes slow equilibration and associated hysteresis effects.

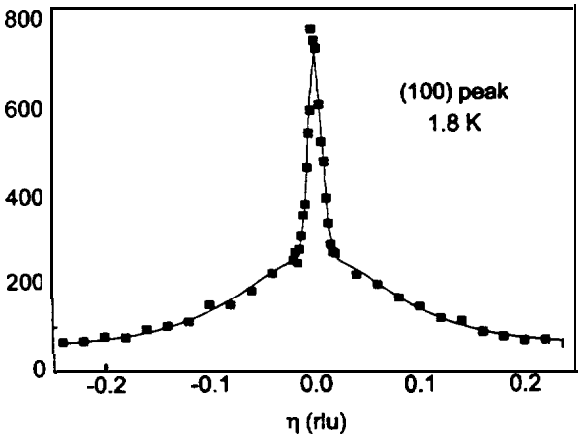

Fig.1 Broad and sharp elastic scattering in scans along line [170].

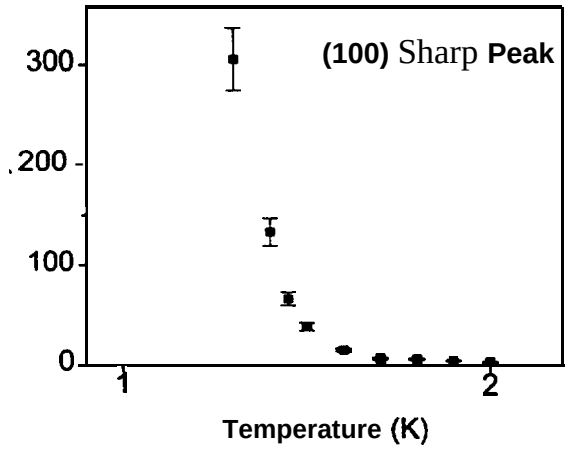

Fig. 2 Approach to antiferromagnetism, as seen in the intensity of the sharp peak at (1, 0, 0).

Chemical and Magnetic Structure of NiCo/Cu Multilayers

M. Mao, B.D. Gaulin and S.Nguyen *(McMaster University)*, Z. Tun *(AECL)*,
X. Bian, Z. Altounian and J.O. Strom-Olsen *(McGill University)*

Synthetic multilayers of alternating NiCo alloy and Cu layers exhibit the phenomenon of giant magnetoresistance (GMR), but with an unusual property: the GMR effect at a Cu layer thickness of ~20 Å persists over a relatively wide range of Cu thickness. We have carried out a detailed structural study of two samples with layer sequence:

$$Si/Ni_{80}Co_{20}50Å/[Ni_{80}Co_{20}15Å/Cu20Å]_n$$

where n = 12 and 60. The samples were prepared by *dc* magnetron sputtering at McGill University. X-ray and polarized neutron reflectivity measurements performed, respectively, at McMaster University and Chalk River Laboratories provided data to determine chemical and magnetic layer profiles. Figure 1 shows the x-ray data (filled symbols), along with the model profile for the n = 12 sample (inset).

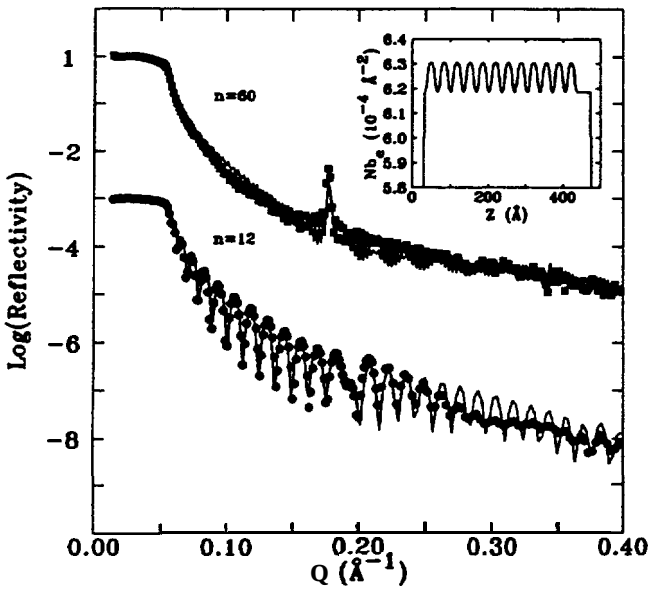

Fig. 1 X-ray reflectivity of NiCo/Cu multilayers.

The model for the n = 60 sample is essentially the same. The parameters of the models, refined by least-squares method, are the thickness of NiCo and Cu layers, their density (i.e. electron density), and the width of the inter-layer diffusion region represented as an error function. All parameters converge to values close to nominal values, and the agreement between the calculated reflectivity (curves) and the experimental data is generally good. However, for the n = 12 sample, intensity oscillations cease beyond Q ~ 0.27 Å^{-1} while the model predicts oscillations extending to larger wave vectors. We conjecture that the disagreement is due to some kind of sample roughness that has not been taken into account in the model. The argument is based on the fact that any kind of roughness will affect high-Q regions more than low-Q regions (analogous to Debye-Waller factors predominantly affecting high-angle Bragg reflections). Apart from this deficiency the models obtained with x-ray reflectometry are good and their parameters can be held fixed in determining the magnetic structure from neutron reflectometry.

Polarized neutron reflectivity measurements were carried out on the DUALSPEC polarized beam spectrometer on both samples with almost zero applied field (15 Oe) and with a field strong enough to saturate the GMR effect (230 Oe). The data were corrected for diffuse background, finite sample size and <100% polarization of the neutron beam. Figures 2 and 3 show the corrected data, along with the calculated reflectivity curves. The last panels of the figures show the nuclear scattering length and magnetic scattering length profiles for the 12-repeat sample. The labels x, y, z in the figures refer to a Cartesian system defined as follows: z is the film growth direction, y is the in-plane direction parallel to the vertical applied field, and x = y × z.

The calculated reflectivity agrees well with experiment at low Q but is significantly different for Q > 0.1 Å^{-1}. However, we can draw several important conclusions. In the 15 Oe field (figure 2) there is no evidence of ferromagnetic alignment between layers since the R^{++} and R^{--} reflectivities at the nuclear peak position (Q ~ 0.17 Å^{-1}) are the same. The interlayer magnetic order is entirely antiferromagnetic as evident by the strong peaks at Q ~ 0.09 Å^{-1}. For the 12-repeat sample the peaks in the R^{++} and R^{--} channels and the R^{+-} and R^{-+} channels are roughly equal suggesting that the moment distribution is isotropic within the xy-plane. This, however, is not the case for the 60-repeat sample. The antiferromagnetic signal is mostly in the R^{+-} and R^{-+} channels suggesting moments are mostly along ±x. In other words the spin-flop in this sample is complete even in a field of only 15 Oe! Since the anisotropy energy and the magnetic moment per unit volume are

supposed to be independent of the number of repeats, this difference between the two samples is puzzling and warrants further investigation.

In the 230 Oe field (figure 3) there is no neutron intensity in the R^{+-} and R^{-+} channels. Magnetic scattering contributes only to the nuclear peak, making $R^{++} \neq R^{--}$. The interlayer magnetic order is therefore entirely ferromagnetic with the moments in the y direction. This result agrees with the known GMR behavior.

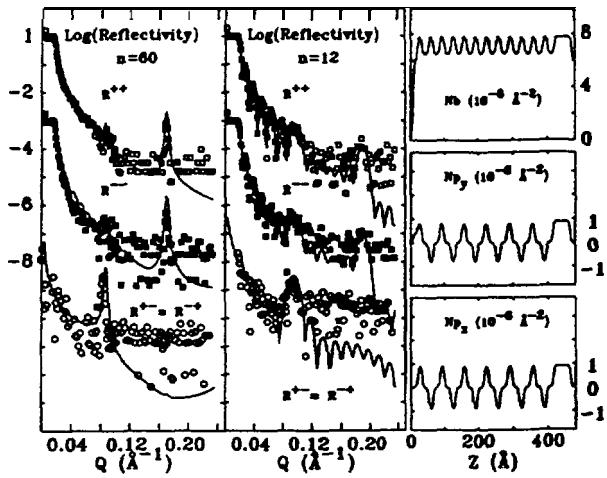

Fig. 2 Neutron reflectivity of NiCo/Cu multilayers in a 15 Oe field applied parallel to the layers.

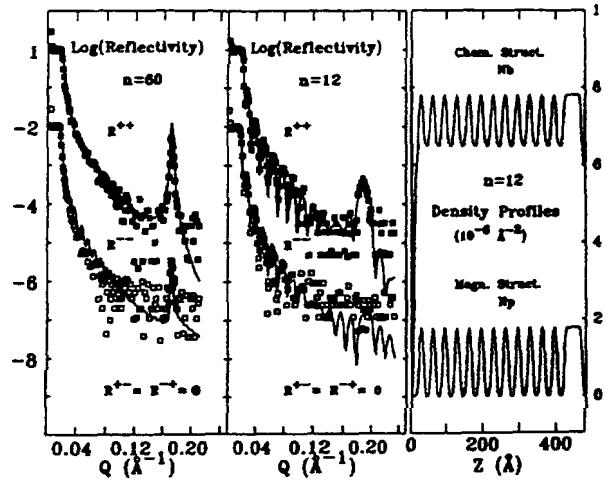

Fig. 3 Neutron reflectivity of NiCo/Cu multilayers in a 230 Oe field applied parallel to the layers.

Neutron Diffraction Studies on $ZnCl_2$

E. Kartini *(McMaster University/Hahn Meitner Institute)*, M.F. Collins *(McMaster University)*, E.C. Svensson *(AECL)* and F. Mezei *(Hahn Meitner Institute)*

A neutron diffraction experiment has been performed on the DUALSPEC high-resolution powder diffractometer to study the temperature dependence of glassy, liquid and crystalline $ZnCl_2$. Molten $ZnCl_2$ at 500°C was poured into a thin-walled cylindrical niobium can with inner diameter 0.40 cm, and then quenched in liquid nitrogen to obtain a glass sample. This sample was then mounted in a furnace for the diffraction measurements that were carried out using 1.5 Å neutrons from a Si(531) monochromator at $2\theta_m = 110°$. The melting point of $ZnCl_2$ is 598 K and the glass transition temperature T_g is 375 K [1].

Measurements of 2 hour duration were taken at temperatures between 300 K and 680 K, over the angular range $3° \leq 2\Theta \leq 83°$. On heating the specimen from 300 K, there was no dramatic change in the diffraction pattern until 410 K when crystallization commenced. At 410 K, and at 420 K, the time dependence of the crystallization was followed by making half-hour counts for a period of 20 hours. The peaks were still growing in intensity at the end of this period. The intensity of the powder peaks was then followed as the temperature was increased from 420 K to 600 K. Diffraction patterns from molten $ZnCl_2$ were also measured for several temperatures from the melting point to 680 K. Molten $ZnCl_2$ could not be supercooled below 570 K during the neutron experiment, as crystallization occurred.

1. Temperature dependence of the structure factor S(Q)

Figure 1 shows the neutron diffraction patterns of $ZnCl_2$ for 300 K and 610 K, when the sample is a glass and a liquid, respectively. The spectra show the features typical of amorphous materials and are generally similar for the glass and liquid. Several broad peaks show small but systematic changes with temperature. The scattering pattern exhibits two broad peaks, centred at about 2.1 $Å^{-1}$ and 3.8 $Å^{-1}$, with an additional small peak centred at about 1.0 $Å^{-1}$. The main diffraction peak corresponds to the Zn-Cl nearest neighbour distance. The Zn-Cl distance is almost unchanged between the liquid (2.35 Å [2]; 2.29 Å [3]) and the glass (2.35 Å [3]). The coefficient of volume expansion is 2.30×10^{-4} in the liquid but only 0.87×10^{-4} in the glass [1,4]. The first peak of the neutron diffraction pattern corresponds to the Zn-Zn and Cl-Cl distances that, in the glass, are about the same (3.76 Å). In the liquid state these distances are different, Zn-Zn being 3.66 Å and Cl-Cl being 3.85 Å.

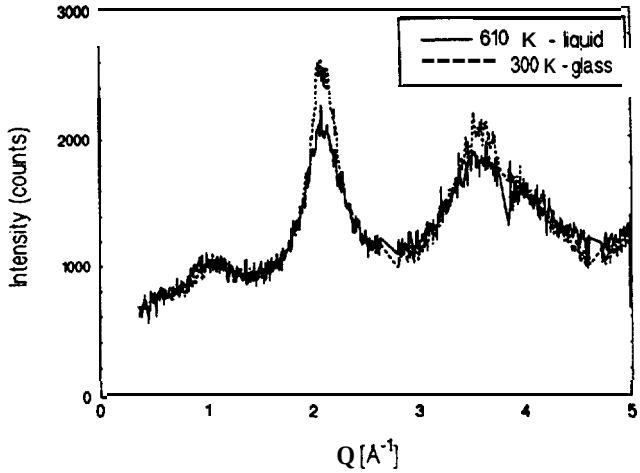

Fig.1 The neutron diffraction patterns of $ZnCl_2$ in its glass and liquid phases. Note that there are "gaps" in the spectra at Q values of 2.7, 3.8 and 4.6 $Å^{-1}$ due to the presence of strong powder lines from the niobium sample holder.

2. Crystallization of $ZnCl_2$

The glass-forming tendencies of $ZnCl_2$ are well known, but its structure has been very little studied because of its extreme water sensitivity. The structure of $ZnCl_2$, along with BeF_2, has been considered a weakened structural analogue of the oxide glasses SiO_2 and GeO_2. The Zn-Cl bond is, however, much more ionic in character than the Si-O bond, as demonstrated by the fact that molten $ZnCl_2$ is more like a typical ionic liquid, though there is a tendency towards covalency with four-fold coordination for Zn and two-fold coordination for Cl, forming something analogous to SiO_2. Early studies identified α, β, and γ polymorphs of crystalline $ZnCl_2$, but later work suggests that these are all found only in $ZnCl_2$ contaminated with water. Desa *et al.* [5] give the stable form of dry $ZnCl_2$ at room temperature as orthorombic δ-$ZnCl_2$.

In our neutron diffraction studies of the crystallization process in $ZnCl_2$, we observe three distinct patterns in the temperature variation of the powder peaks. Figure 2 shows the intensity of the three different types (A, B and C), of powder lines as a function of temperature for Q values of 3.589, 2.138 and 3.024 $Å^{-1}$, respectively [referred to T = 584, 584 and 440 K, respectively]. The intensities given are after subtraction of the temperature-dependent backgrounds.

It is apparent that the powder lines of type A and B have a similar temperature dependence, one where the intensities grow continuously with increasing temperature until they reach a maximum at 580 ± 5 K, and then decrease and finally disappear at the melting point (595 ± 5 K). The important difference is that the lines of type A appear when crystallization starts at 410 K, but the lines of type B only appear at 480 K. From comparison with known crystallographic results, we find that, at temperatures above 530 K, types A and B are both from the same crystal structure, namely δ-$ZnCl_2$ [5]. This has been checked by using the TREOR fit program, which show that the crystal structure at 588 K is δ-$ZnCl_2$. At 530 K the pattern is also pure δ-phase, but not at 490 K. Our observations show that at this temperature the crystal structure is a mixture of δ-$ZnCl_2$ and of some other phase.

The third type of powder peak, type C, behaves differently from type A and B as is illustrated in figure 2 for 3.024 $Å^{-1}$. The peaks start to grow in intensity at low temperatures, reach a maximum at 430 ± 5 K, and then decrease slowly and disappear, not at the melting point but at 530 ± 5 K. In the temperature range where the type C peaks are observed, there is still a large liquid-like background (as in figure 1) which makes the determination of the crystallographic structure more difficult. In the temperature region below 460 K, there is a phase that includes lines of both type A and C. Close examination shows that, after allowing for thermal expansion, there are small differences in the Q values of the type A lines between the values observed above 530 K for δ-$ZnCl_2$ and those for the (unknown) phase observed below 460 K.

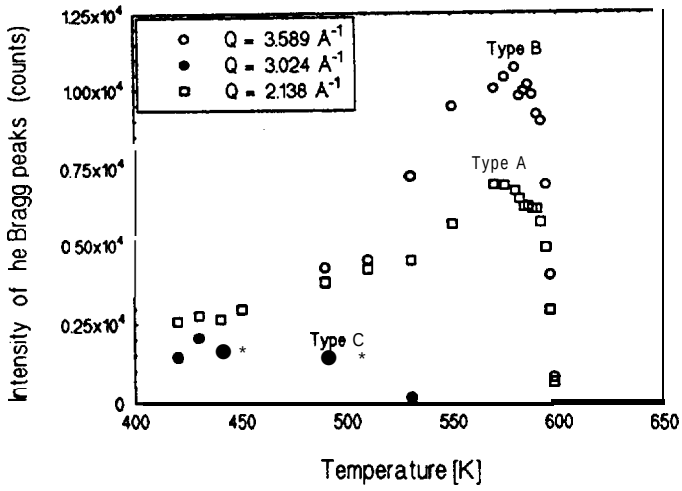

Fig.2 The temperature dependence of the intensities of the powder lines of crystalline $ZnCl_2$.

The results show that there is a transformation from the (unknown) low-temperature phase to δ-$ZnCl_2$, occurring over the range 460 K to 530 K. Above this temperature the crystal structure is purely δ-$ZnCl_2$ and the maximum intensity is found at 580 K. The melting point is determined as 595 ± 5 K, which is in agreement with other measurements [4,5]. When $ZnCl_2$ was cooled from above the melting temperature, powder lines corresponding to pure δ-phase began appearing below 570 K, and we observed only pure δ-phase all the way down to 300 K.

REFERENCES

[1] J. Wong and F.W. Lytle, J. Non. Crys. Solids. 37 (1980) 273.

[2] M. Imaoka, Y. Konagaya and H. Hasegawa, Yogyo Kyokai Shi. 79 (1971) 97.

[3] J. Dianoux, J. Phys. C. 18 (1985) 1115.

[4] S. Biggin and J.E. Enderby, J. Phys. C. 14 (1981) 3129.

[5] J.A.E. Desa, A.C. Wright, J. Wong, and R.N. Sinclair, J. Non. Crys. Solids. 51 (1982) 57.

Inelastic Neutron Scattering from $ZnCl_2$ Glass and Liquid

E. Kartini *(McMaster University/Hahn Meitner Institute)*, M.F. Collins *(McMaster University)*, E.C. Svensson *(AECL)* and F. Mezei *(Hahn Meitner Institute)*

We have used the DUALSPEC (C5) triple axis spectrometer to study the neutron scattering by $ZnCl_2$. The primary objective was to study the dynamic properties of the glasseous state. The sample for the inelastic measurements was a large, rectangular slab of 0.5 cm thickness contained in a niobium holder with thin (0.35 mm) incident and exit windows. It was masked to an area 6 cm wide by 4 cm high on the incident-beam side, and the measurements were carried out with the sample in symmetric transmission using a Si(113) monochromator and a Ge(113) analyzer. The scattered neutron frequency was fixed at 3.52 THz. Sapphire and pyrolytic graphite filters were placed in the incident and scattered beams, respectively, to suppress higher-order neutrons. The resolution at the elastic position (frequency transfer $\nu = 0$) was 0.105 THz (FWHM). Measurements were carried out at temperatures between 300 and 680 K, with the sample in either a normal liquid, supercooled liquid, crystalline or glassy state. The melting point is 598 K and the glass transition temperature T_g is 375 K.

At the cooling rates achievable in the furnace used for the measurements, $ZnCl_2$ crystallized well before the glass transition was reached. However, if the sample and its holder were quenched from high temperature into liquid nitrogen, the glass state was formed. On heating, this sample did not crystallize until about 410 K. Because of this we were unable to obtain data in the supercooled liquid state for temperatures between 410 K and 550 K.

Glass transformations show a range of behaviour. At one extreme are the "strong" glasses like SiO_2, where the viscosity exhibits an exponential divergence, and where there is no marked specific heat anomaly at the glass transition. At the other extreme are the "fragile" glasses such as the ionic glass calcium potassium nitrate (CKN) that we recently studied [1] and the polymer glasses [2,3]. Here the viscosity diverges more strongly at the glass transition, and there is a jump in the specific heat on passing from the glass to the supercooled liquid. This jump is attributed to a softening of certain vibrational modes, often referred to as boson peaks, which have been observed by neutron and Raman scattering [4].

$ZnCl_2$ is intermediate in character between the strong and fragile glasses. The structure in the liquid and glass phases contains chains similar to those found in silica glass, so the bonding is more covalent than ionic. The data shown in figure 1 have been corrected for background and empty sample-holder scattering, while simple thermal population effects have been removed by multiplying by a Bose factor. Our results show the presence of a well-defined boson peak in the glass state. In the liquid state we see that there are excitations below 0.6 THz, but no well-defined peaks, whereas in the crystalline state there are no excitations. Our work on CKN [1] shows a peak that is more damped, such as that seen in the liquid phase of $ZnCl_2$. Similar boson peaks have been observed in polymer glasses [2,3]. The temperature dependence of our boson peak is that expected for harmonic phonons. This was found in the polymer glasses studied by Kanaya *et al.* [3], but not in the polymer glass studied by Frick *et al.* [2].

REFERENCES

[1] E.C. Svensson, E. Kartini, M.F. Collins and F. Mezei, see the following report.

[2] B. Frick and D. Richter, Phys. Rev. B **47** (1993) 14795.

[3] T. Kanaya, T. Kawaguchi and K. Kaji, J. Non-Crys. Solids **172-174** (1994) 327.

[4] A.P. Sokolov, A. Kisliuk, D. Quitmann, A. Kudlik, E. Rössler, J. Non-Crys. Solids **172-174** (1994) 138.

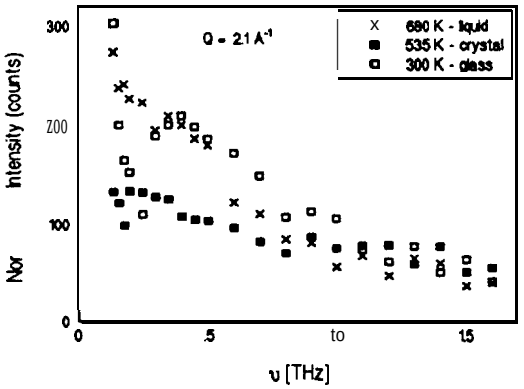

Fig. 1 The inelastic scattering by $ZnCl_2$ in various phases, showing the Boson peak centred at 0.4 THz in the glass phase.

Inelastic Neutron Scattering by $Ca_{0.4}K_{0.6}(NO_3)_{1.4}$

E.C. Svensson *(AECL)*, E. Kartini *(McMaster University/Hahn Meitner Institute)*, M.F. Collins *(McMaster University)* and F. Mezei *(Hahn Meitner Institute)*

We have previously reported [1] preliminary results from a study of the inelastic neutron scattering by $Ca_{0.4}K_{0.6}(NO_3)_{1.4}$ (CKN) carried out using the C5 DUALSPEC triple-axis spectrometer. CKN is an ionic glass with a glass-transition temperature, T_g, of 335 K [2]. The primary aims of our inelastic measurements, carried out on glasseous and liquid CKN, were to obtain signatures of the liquid-to-glass transition and results to test critically the predictions of mode-coupling theories [3]. Detailed analysis of the results of this study has now been completed and we report here a selection of the most interesting observations and conclusions.

The temperature dependence of the position (wave vector transfer, Q_o, in the range 1.76 to 1.87 $Å^{-1}$) of the main peak of $S(Q, co= 0, T)$ in the liquid phase gives a value of $(2.3 \pm 0.2) \times 10^{-4}$ for the linear coefficient of thermal expansion. This is approximately double the value, 1.28×10^{-4}, obtained [4] from density measurements, indicating that the thermal expansion of liquid CKN is accompanied by substantial structural rearrangements. The Debye-Waller factor, as determined from the intensity of the main peak of $S(Q, \omega = 0, T)$ (see Fig. 2.3.1.2 in [1]), shows an anomaly (change in slope) at the glass-transition temperature, $T_g = 335$ K, but the anomaly at the critical temperature, T_c, predicted by mode-coupling theory [3] is not seen. In contrast, the change in the effective root-mean-square displacement, $\langle r^2 \rangle_T - \langle r^2 \rangle_{300}$, deduced from the Q dependence of the temperature variation of the quasielastic scattering over a wide range of Q values (2 - 4 $Å^{-1}$, i.e. at values substantially higher than Q_o) shows a change in slope at a temperature of 368 ± 5 K, as shown in figure 1. The results in figure 1 give the first direct signature of a critical temperature, T_c, above the glass-transition temperature, T_g, as predicted by mode-coupling theory [3], and the value $T_c = 368 \pm 5$ K, inferred from these results is the first model-independent value of T_c. Previous neutron spin-echo [5] and time-of-flight [6] measurements gave similar values for T_c, 370 ± 5 K and 368 ± 5 K, respectively, but in these cases T_c could only be identified tentatively by fitting the data with two scaling functions assuming a *priori the* existence of T_c. Note that the results in figure 1 give no indication of an anomaly at T_g and that, contrary to the predictions of mode-coupling theory, they do not show a variation of the form $(T_c - T)^{1/2}$ between T_g and T_c.

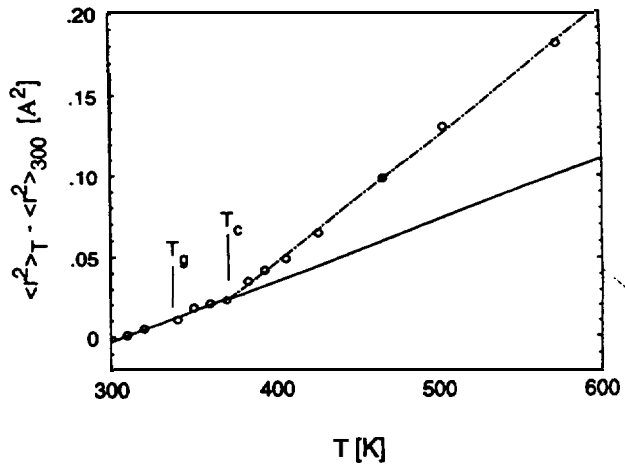

Fig. 1 The change in the effective root-mean-square displacement, $\langle r^2 \rangle_T - \langle r^2 \rangle_{300}$, as a function of temperature.

If one removes the scattering arising from thermal population effects by dividing-by the Bose factor, one obtains the quantity $S_n(Q, \omega, T)$, which is temperature-independent for harmonic phonon scattering. Such temperature-independent behaviour is what we observe for CKN for all frequencies $\nu = \omega/2\pi$ 20.6 THz and for all frequencies at temperatures below T_g. However, for $T \geq T_g$ and $\nu \leq 0.5$ THz we observe "excess intensity", which is proportional to $(T - T_g)$, and which we attribute to the fast-relaxation or β process of mode-coupling theory [3]. The frequency dependence of this excess intensity is shown in figure 2. Similar excess intensity in the frequency range below 0.5 THz was observed in previous time-of-flight measurements [6] for $Q = Q_o$, but the present study is the first to give detailed information on the Q and ν dependence of the β process. If we extract from our results a quantity that reflects the amplitude of the β process, we find that it exhibits a minimum in the region of the peak of the structure factor (at $Q = Q_o$), as predicted by mode-coupling theory [3,7]. Similar behaviour to that shown in figure 2 has been observed [8,9] in

polymer glasses, where the excess intensity is referred to as a *boson peak*.

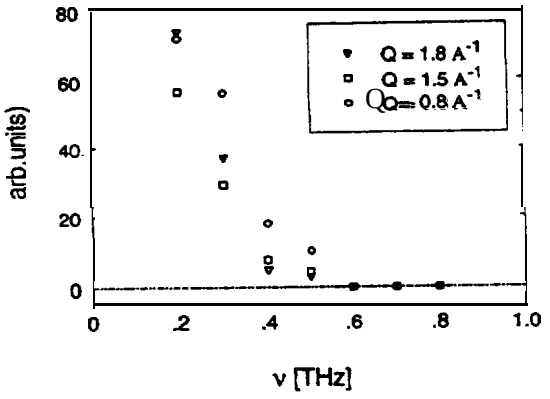

Fig. 2 The frequency dependence of the excess intensity at T = 350 K for Q values of 0.8, 1.5 and 1.8 $Å^{-1}$. The data are normalized to S(Q, ω = 0) at T = 300 K.

In conclusion, our broad study of the inelastic scattering by CKN has revealed a complex variety of features and given clear signatures of both the glass-transition temperature, T_g, and the critical temperature, T_c. Some aspects of the behaviour we observe support the predictions of mode-coupling theory, whereas others show serious shortcomings of this theory. Clearly, more work, both experimental and theoretical, needs to be done before we can claim a fundamental understanding of glass-forming systems, and of what happens at T_g and T_c in particular.

REFERENCES

[1] Physics Division Progress Report, PR-PHY-8:2.3.1.18, AECL–11234, 1995.

[2] E. Kartini, M.F. Collins, B. Collier, F. Mezei and E.C. Svensson, Can. J. Phys. **73** (1995) 748.

[3] See, e.g., W. Götze in *Liquids, Freezing and the Glass Transition*, D. Levesque, J.P. Hansen and J. Zinn-Justin, eds. (Elsevier, Amsterdam, 1991).

[4] A. Dietzel and H.P. Poegel, in *Proc. Intern. Glass Congr. 3rd, Venice,* (1963) 319.

[5] F. Mezei, W. Knaak and B. Farago, Phys. Rev. Lett. **58** (1987) 571; Phys. Scripts **19** (1987) 571.

[6] W. Knaak, F. Mezei and B. Farago, Europhys. Lett. **7** (1988) 529.

[7] F. Mezei, in Ref. 3.

[8] B. Frick, D. Richter and B. Farago, J. Non. Crys. Solids **131-133** (1991) 169; B. Frick and D. Richter, Phys. Rev. B **47** (1992) 14795; B. Frick, D. Richter, R. Zorn and L.J. Fetters, J. Non. Crys. Solids **172-173** (1994) 272.

[9] T. Kanaya, T. Kawaguchi and K. Kaji, J. Chem. Phys. **98** (1993) 8262; T. Kawaguchi, T. Kanaya and K. Kaji, Physics B **213&214** (1995) 510.

Temperature Dependence of the Roton in Liquid ^{4}He

W. Montfrooij *(ISIS Facility, Rutherford Appleton Laboratory)* and E.C. Svensson *(AECL)*

The temperature dependence of the roton excitation in liquid ^{4}He has been of long-standing interest and has generated a great deal of controversy. (For reviews, and extensive references to experimental and theoretical studies, see [1-3].) The study of Woods and Svensson [4] at saturated vapour pressure (SVP), which approached the superfluid transition temperature T_λ (2.173 K at SVP) to within 0.023 K from below, was the first to show a qualitative difference in the dynamic structure factor, $S(q, \nu)$, on passing through T_λ. In particular, it showed that sharp excitations in the maxon-roton region of the dispersion relation were unique to the superfluid phase. In a more recent study [5] at a constant density of 0.1715 g.cm^{-3} (pressure P ≈ 20 bar), T_λ (1.9202 K at this density) was approached to within 0.0026 K. This study gave evidence for soft-mode behaviour of the roton at P ≈ 20 bar. As T_λ was approached from below, there was an increasingly rapid decrease (increase) in the roton propagation frequency (intrinsic width), with a collapse to non-propagating behaviour (i.e. central modes only) above T_λ. In new measurements at SVP, we have now probed to within 0.0007 K of T_λ, i.e. almost four times closer to T_λ than achieved previously [5] in any neutron scattering study and more than thirty times closer than achieved previously [4] at SVP.

The new measurements were carried out using the N5 triple-axis spectrometer with a Si(111) monochromator and a pyrolytic graphite (002) analyzer. Sapphire and beryllium filters, both at 77 K, were placed in the incident and scattered beams, respectively, and the scattered-neutron frequency was held fixed at 1.19 THz. The frequency resolution at the roton frequency (ν = 0.18 THz) at the lowest temperature (1.05 K) of our study was 0.06 THz (FWHM). Measurements of the dynamic structure factor, $S(q, \nu)$, were carried out for wave-vector transfers q of 0.8 Å^{-1} and 1.918 Å^{-1} (the roton) for T_λ - T values of 1.12, 0.27, 0.17, 0.071, 0.021, 0.011, 0.0051, 0.0011, 0.0007 and -0.029 K. For the measurements below T_λ, the temperature stability was typically ± 0.0001 K. The scattering by the empty sample container was also determined.

As in our other recent studies on liquid ^{4}He [5,6], we have focussed, in the analysis of the results, on the symmetric relaxation function

$$S_{sym}(q,\nu) = \frac{1-\exp(-\beta h\nu)}{\beta h\nu} S(q,\nu), \qquad (1)$$

since this quantity best reveals the intrinsic behaviour of the system, and especially clearly shows the dramatic changes that occur very close to T_λ. The exact Mori-Zwanzig projection formalism [7] states that $S_{sym}(q,\nu)$ *can* always be described by a sum of Lorentzians. In the present case, only the two Lorentzians describing the extended sound modes (at frequencies $\pm\nu_s$) are required to give an excellent description of $S_{sym}(q, \nu)$, and the only "free" parameter in the analysis is the damping rate of the momentum fluctuations, $z_u(q, T)$. Values of $z_u(q, T)/2$ for rotons (at SVP) from our new measurements and from our analysis of the results of Woods and Svensson [4] in terms of $S_{sym}(q,\nu)$ *are* given in figure 1. Note that there is excellent agreement in the region of overlap. Also shown in figure 1 are values of $f_{un}(q, T)$, the coupling parameter between number density (n) and momentum density (u). This is the only other parameter in our analysis, and its values are determined by the f-sum rule for $S(q, \nu)$. If $f_{un}(q, T) > z_u(q, T)/2$, the eigenvalues and amplitudes of the two Lorentzians are complex and are each others complex conjugate, and the extended sound modes are propagating. On the other hand, if $f_{un}(q, T) < z_u(q, T)/2$, then the eigenvalues and amplitudes are real and different, and the modes are overdamped (non-propagating). Note that this latter situation is not reached in figure 1, so the roton at SVP does not go completely soft though there is a marked softening as one approaches T_λ from below, as shown by figure 2. In contrast, our results for the roton at a pressure of 20 bars [5] give $f_{un}(q, T) < z_u(q, T)/2$ for $T > T_\lambda$ so in this case the roton does go completely soft, apparently right at T_λ. Results for $S_{sym}(q,\nu)$ at 20 bars are shown in figure 3. The different behaviour on passing through T_λ exhibited by figures 2 and 3 can be attributed to the different q values and the different densities.

Note that the crucial parameter $z_u(q, T)$, the damping rate of the momentum correlations, changes very rapidly (figure 1) just below T_λ. The very rapid

increase of $z_u(q, T)$ as one approaches T_λ from below is the most salient feature of the results for both SVP (figure 1) and 20 bars [5]. Such behaviour is of course what one might expect on going from a superfluid phase, characterized by long-range momentum correlations, to a normal-fluid phase. The results, especially those from the much closer approach to T_λ in the present study, also indicate that $z_u(q, T)$ and $f_{un}(q, T)$ are continuous through T_λ. It thus appears as if there is a continuous transition from the superfluid phase to the normal-fluid phase, driven by a dramatic change in the damping rate of the momentum correlations. Our results give no indication of the sudden appearance of a well-defined mode (a renormalized single-particle mode) as one goes below T_λ, as had been inferred [1,2] from earlier measurements and as is expected from theoretical considerations [3,8]. Pushing the measurements ever closer to T_λ continues to give us an increasingly clearer picture of the changes that occur as one passes from the superfluid to the normal-fluid phase, changes that are of crucial importance for a fundamental understanding of liquid ^{4}He, the protype example of a quantum fluid of interacting bosons.

REFERENCES

[1] E.C. Svensson in *Elementary Excitations in Quantum Fluids*, K. Ohbayashi and M. Watabe, eds. (Springer-Verlag, Heidelberg, 1989) p. 59.

[2] E.C. Svensson in *Excitations in Two-Dimensional and Three-Dimensional Quantum Fluids*, A.F.G. Wyatt and H.J. Lauter, eds. (Plenum Press, New York, 1991) p. 59.

[3] A. Griffin, *Excitations in a Bose-Condensed Liquid* (Cambridge University Press, Cambridge, 1993).

[4] A.D.B. Woods and E.C. Svensson, Phys. Rev. Lett. **41** (1978) 974.

[5] W. Montfrooij and E.C. Svensson, Physics B **194-196** (1994) 521.

[6] W. Montfrooij, E.C. Svensson and I.M. de Schepper, J. Low Temp. Phys. **89** (1992) 437.

[7] H. Mori, Prog. Theor. Phys. **33** (1965) 423.

[8] H.R. Glyde and A. Griffin, Phys. Rev. Lett. **65** (1990) 1454.

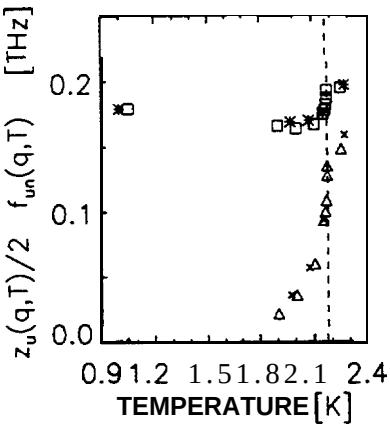

Fig. 1 $z_u(q, T)/2$ (lower) and $f_{un}(q, T)$ (upper) for the roton in liquid ^{4}He at SVP from the present study (Δ and ❑ l) at $q = 1.918$ Å^{-1} and from our analysis of the results of Woods and Svensson [4] (x and *) at $q = 1.926$ Å^{-1}. T_λ is shown by the vertical dashed line.

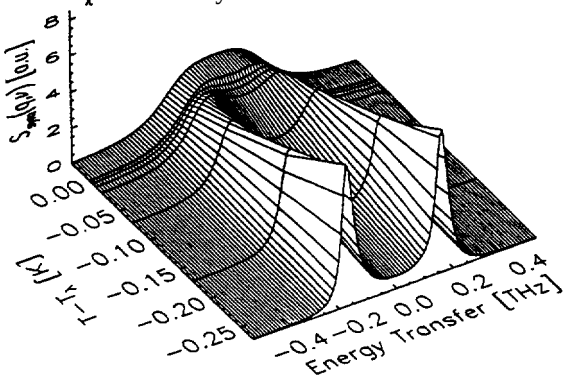

Fig. 2 $S_{sym}(q, \nu)$ for rotons ($q = 1.918$ Å^{-1}) in liquid ^{4}He at SVP and temperatures near T_λ from the present study. Above T_λ, the modes are strongly damped and overlapping.

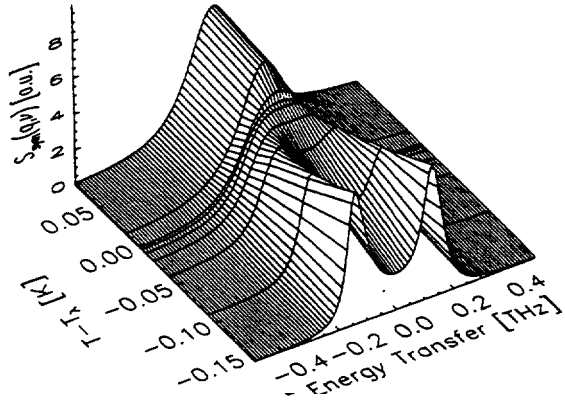

Fig. 3 $S_{sym}(q, \nu)$ for rotons ($q = 2.0$ Å^{-1}) in liquid ^{4}He at P ≈ 20 bars and temperatures near T_λ from our earlier measurements [5]. Above T_λ, the modes are overdamped (non-propagating).

Multiexcitation Scattering by Superfluid ^{4}He

R.M. Crevecoeur, H.E. Smorenburg and I.M. de Schepper *(Delft University of Technology)*,
W. Montfrooij *(ISIS Facility, Rutherford Appleton Laboratory)* and E.C. Svensson *(AECL)*

As has been repeatedly emphasized [1-4], one of the most urgent needs for the advancement of our understanding of liquid ^{4}He is to better determine and understand the multiexcitation component, $S_M(q, \nu)$, of the dynamic structure factor $S(q, \nu)$ in the superfluid phase. This component, which occurs mainly at frequencies ν higher than those of the strong single-excitation peak in $S(q, \nu)$, is known (see, e.g., figure 4 in [2]) to consist of a mixture of sharp and broad features and to vary rapidly with momentum transfer, q. Although the theoretical understanding of the detailed shape of $S_M(q, \nu)$ is inadequate (see [3] for an extensive discussion), the sharp features undoubtedly correspond primarily to two-roton, roton-plus-maxon and two-maxon processes. The work of Glyde and Griffin [5] leads one to also expect the possibility of a broad zero-sound contribution in the multiexcitation frequency region, for certain q values.

To address the need for more extensive high-quality data for $S_M(q, \nu)$, we have carried out a new study at the ISIS spallation-neutron facility of the Rutherford Appleton Laboratory, U.K. The IRIS spectrometer, an inverted-geometry time-of-flight instrument, was used with pyrolytic graphite (002) analysers in backscattering geometry. This gave very high-energy resolution, FWHM = 15μeV = 0.004 THz at the elastic position, $\nu = 0$. Measurements were carried out at 1.4 K on superfluid ^{4}He at saturated vapour pressure (SVP) and under applied pressures of 10 and 20 bars. The scattering by the empty sample container was also determined. Three-dimensional plots of the data show that $S_M(q, \nu)$ exhibits a rich topography with multiple ridges in (q, ν) space, and rapid variations with q. Preliminary results for constant-q values of 1.12 and 1.92 Å^{-1}, obtained by interpolation from the constant-angle data given by the IRIS spectrometer, are shown in figures 1 and 2. These q values correspond to the well-known "maxon" (1.12 Å^{-1}) and "roton" (1.92 Å^{-1}) single-excitation modes of superfluid ^{4}He which give rise to the very strong peaks at low frequency in figures 1 and 2. Detailed analysis of the results is continuing.

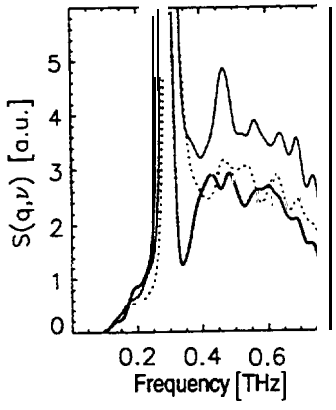

Fig. 1 $S(q, \nu)$ for superfluid ^{4}He at 1.4 K for $q = 1.12$ Å^{-1} and three pressures: SVP (heavy solid curve), 10 bars (light solid curve) and 20 bars (dashed curve).

REFERENCES

[1] E.C. Svensson in *Elementary Excitations in Quantum Fluids*, K. Ohbayashi and M. Watabe, eds. (Springer-Verlag, Heidelberg, 1989) p. 59.

[2] E.C. Svensson in *Excitations in Two-Dimensional* and *Three-Dimensional Quantum Fluids*, A.F.G. Wyatt and H.J. Lauter, eds. (Plenum Press, New York, 1991) p. 59.

[3] A. Griffin, *Excitations in a Bose-Condensed Liquid* (Cambridge University Press, Cambridge, 1993), especially chapter 10.

[4] K.J. Juge and A. Griffin, J. Low Temp. Phys. **97** (1994) 105.

[5] H.R. Glyde and A. Griffin, Phys. Rev. Lett. **65** (1990) 1454.

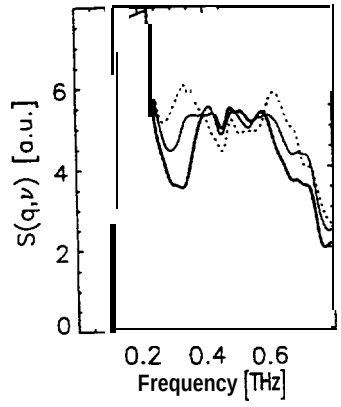

Fig. 2 As for figure 1, but for $q = 1.92$ Å^{-1}.

Structural Science

Structure of Ice Grown in an Electric Field

E.C. Svensson *(AECL)*, J. Bouillot and Y. Teisseyre *(Université de Savoie)*,
M. Farzaneh and P. Dubouchet *(Université du Québec à Chicoutimi)* and R.L. Donaberger *(McMaster University)*

Studies of ice accretion on high-voltage conductors have shown that the quantity and the physical appearance of the accreted ice are strongly dependent on the electric field strength at the surface of the conductor and the polarity of the applied voltage [1,2]. This work prompted us to carry out neutron powder diffraction measurements [3] on D_2O ice samples grown in high electric fields to investigate possible effects of such growth on the structural parameters of ice. The results [3,4] from this initial study showed that ice grown in a high electric field retains a memory of its growth conditions, as revealed by changes in the structural parameters, an effect that had not been observed previously. One very puzzling feature of the observations was that the sign, but not the magnitude, of the change in the lattice constants (and, hence, in the unit cell volume) induced by growth in an electric field depended on the polarity of the applied voltage.

In a continuation of this program, we have carried out neutron diffraction measurements at a lower temperature on new samples of D_2O ice grown in high electric fields and cooled rapidly to liquid nitrogen temperature (77 K) immediately after growth. As previously, the special ice samples were made in the "High Voltage Laboratory" of the Université du Québec à Chicoutimi by allowing small droplets of high-purity D_2O vapour to freeze onto a rotating conductor held at -12 ± 0.5°C. Samples were made for electric fields of& 15 and $\pm$ 20 kV cm-*. A reference sample was also made at zero applied voltage. Immediately after they were made, the samples were broken from the conductor, placed in canisters and quickly cooled to 77 K by immersion in liquid nitrogen. While continuously being kept at this temperature, they were transported to Chalk River Laboratories, ground into fine powders, and placed in thin-walled cylindrical vanadium cans of inner diameter 0.50 cm. Measurements on the five samples and on an empty cell were carried out at 70 K using the DUALSPEC powder diffractometer with 1.5 Å neutrons from a Si(531) monochromator at $2\theta_m = 110°$. The measurements covered the range of scattering angles $5 \leq \phi \leq 120°$ in 0.05° steps. The samples were rotated continuously during the measurements and the total counting time for each sample was ~18 hours.

Rietveld refinement of the results has now been completed and in all cases an excellent description of the observed diffraction profiles is obtained. An example is shown in figure 1. All samples have the $P6_3/mmc$ space group of ordinary ice Ih. The changes in the unit cell parameters obtained from our new measurements at 70 K and from the earlier measurements [3,4] at 225 K (on samples that had been stored at temperatures in the range -10 to -30°C from the time of production to the time they were ground into fine powders at liquid nitrogen temperature and placed in the cryostat for the diffraction measurements) are shown in figure 2.

In contrast to our expectation that quenching to 77 K immediately after growth would prevent possible relaxation of the structural changes induced by the electric field and, hence, might be expected to lead to larger observed effects, we see that the lattice parameter changes observed in the new study are almost an order of magnitude smaller than those observed in the earlier study. This, we believe, is a result of the different temperatures at which the measurements were carried out (rather than the different thermal histories of the samples which, we now suspect, are of relatively minor importance) and can be understood on the basis of the unusual thermal expansion of ice Ih as revealed by a recent study [5]. This study has shown that the lattice constants, a and c, both decrease with increasing temperature until about 70 K and then increase at higher temperatures. Where the coefficient of linear expansion is zero, i.e. at about 70 K, precisely where we carried out the present measurements, one would expect effects of an enharmonic type, such as those induced by an external electric field, to be minimized.

The results in figure 2 show very clearly the dependence of the sign of the change in a and c on the polarity of the applied voltage and also indicate saturation at large fields. The changes induced by the electric fields are, we believe, related to the delocalization of deuterons on the oxygen-oxygen bonds caused by defects. Two types of defects are considered in a paper [6] that discusses tetrahedral

jumps of deuterons in ice Ih, based on NMR measurements. The first type are the Bjerrum defects, which correspond to bonds in which either zero or two deuterons are located, instead of the normal one. The second type are ionic defects that arise from

$$2H_2O \leftrightarrow H_3O^+ + OH \quad (1)$$

and that are normally much less numerous than the Bjerrum defects. Because of the growth in a high electric field, these ionic defects, whose numbers increase with increasing electric field, may however be preponderant in our samples. This can readily account for a change in lattice parameters induced by growth in an applied field. Since the mobility of H_3O^+ ions is more than one hundred times larger than that of OH^- ions, and since the interaction between the two types of defects plays an important role, it is also perhaps not surprising that the polarity of the applied voltage has an important influence on the change in lattice parameters. The precise mechanism, or why the magnitude of the change should be independent of the polarity as shown in figure 2, is however not understood at present. We plan to carry out additional measurements to determine more completely the dependence of the lattice parameter changes on the magnitude of the applied electric field at several temperatures. Hopefully these will allow us to develop a more thorough understanding of the effect on the structural parameters of ice of growth in electric fields, based on the behaviour of the different types of known defects.

REFERENCES

[1] M. Farzaneh and J.L. Laforte, Int. J. Offshore and Polar Eng. 1 (1994) 40.

[2] Y. Teisseyre and M. Farzaneh, Cold Regions Science and Techn. 18 (1990) 1.

[3] Physics Division Progress Report, PR-PHY-7:2.3.1.8, AECL-11016, 1994.

[4] Physics Division Progress Report, PR-PHY-8:2.3.1.23, AECL-1 1234, 1995.

[5] K. Rôttger, A. Endriss, J. Ihringer, S. Doyle and W.F. Kuhs, Acts Cryst. 50 (1994) 644.

[6] F. Fujara, S. Wefing and W.F. Kuhs, J. Chem Phys. 88 (1988) 6801.

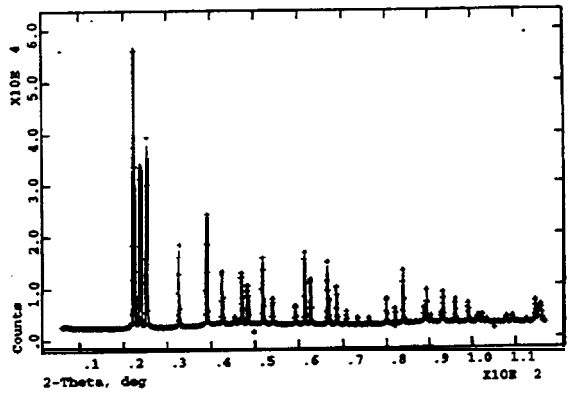

Fig. 1 Comparison of the measured spectrum (crosses) and the calculated spectrum given by the Rietveld analysis program for a fine powder of D_2O ice grown under an electric field of -15 kV cm^{-1}. The measurements were performed at 70 K.

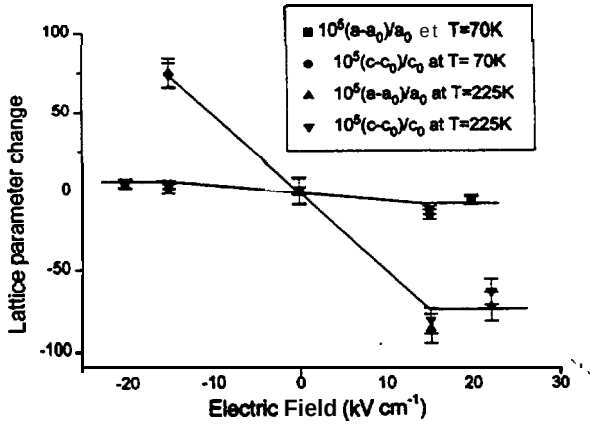

Fig. 2 Changes in the lattice constants a and c of ice Ih (relative to the values a_o and c_o for zero applied voltage) caused by growth in an electric field, obtained by Rietveld analysis of the present measurements at 70 K and earlier measurements [3,4] at 225 K. Solid lines are simply a guide to the eye.

Domain Walls in Deuterated KDP

D.R. Taylor *(Queen's University)* and I.P. Swainson *(AECL)*

The experiment was designed to detect neutron diffraction from unit cells in the domain walls of a twinned orthorhombic crystal and thus to determine the width of the domain walls. In a simple tetragonal-orthorhombic transition such as those that occur in the KDP family of compounds and many of the cuprate superconductors, a Bragg peak such as (h00) splits into two when (h00) and (0h0) become inequivalent. The orthorhombic phase is normally multidomain with regularly spaced {110} domain walls. Unit cells within a domain wall will have cell parameters intermediate between those in adjoining domains, and will therefore contribute scattering intensity in a broad peak between the two main peaks. From its lineshape and intensity an average domain wall width can be calculated.

The experiment used a single crystal of KDP deuterated to about 80%, mounted with tetragonal axis vertical in cryostat H8 on the DUALSPEC high-resolution powder diffractometer C2. The monochromator was Si (531), producing a wavelength of 1.5 Å. The sample was rotated about the vertical axis while data were collected by the 800 wire detector. This arrangement avoids the line broadening and structure expected in a single-crystal diffraction experiment because of crystal mosaic and structure effects while giving better statistics than a powder experiment.

It was found that rotating the cryostat by only 10° about the scattering angle of a desired Bragg peak gave optimum statistics and a clean baseline by suppressing other peaks. The results were encouraging a broad peak was found that was centred between the two split peaks in the orthorhombic phase (see figure 1). The main peaks gave excellent fits to Gaussian lineshapes, indicating that it should be possible to separate accurately the intensities of the domain wall peak and the bulk domain peaks. The data shown in figure 1 were collected in two days of counting. To obtain a convincing set of results, comparison data with similar statistics will be needed at other temperatures.

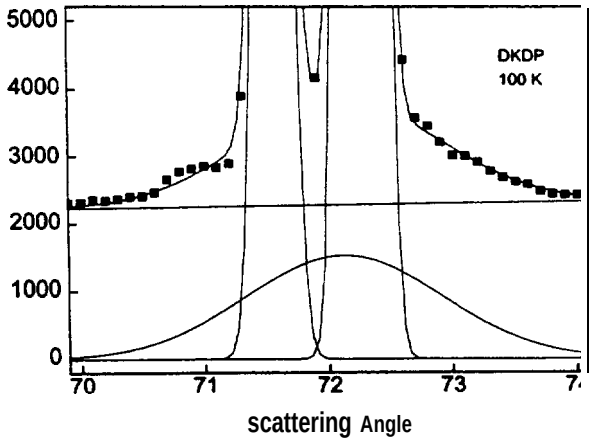

Fig. 1 The split (350) peak of DKDP at 100 K. Data are shown as closed squares with the best fit shown as a line. The fitted background-subtracted main Gaussian peaks and broad domain wall peaks are shown.

Anomalous Inelastic Scattering from Calcite ($CaCO_3$)

I.P. Swainson and B.M. Powell *(AECL)*, M.T. Dove *(Cambridge University)*,
M.J. Harris *(ISIS Facility, Rutherford Appleton Laboratory)* and M.E. Hagen *(Keele University)*

In a series of experiments made on the N5 triple-axis spectrometer at the NRU reactor, Chalk River, and on the PRISMA time-of-flight inelastic spectrometer, at the ISIS facility, Rutherford-Appleton Laboratory, UK, an unusual feature was noticed in the inelastic scattering from calcite. It occurs at particular *F* zone boundary points of the Brillouin zone. These zone boundary points also exhibit strong diffuse scattering in single-crystal x-ray diffraction studies. The feature takes the form of a "column" of scattering when viewed on conventional dispersion plots of frequency against wavevector. The column extends from the frequency of the transverse acoustic mode (TA) down to $h\nu = O$, and the intensity of the scattering is approximately independent of the energy transfer.

An order-disorder transition $R\bar{3}c \Rightarrow R\bar{3}m$ *exists* in calcite at *ca.* 1260 K, and is associated with an instability at the Z-zone boundary point (not symmetrically related to *F*). A plot of the room temperature ordered structure is shown in figure 1.

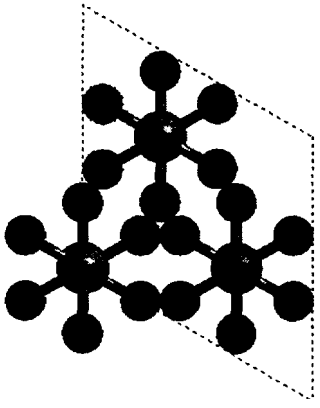

Fig. 1 Structure of ordered $R\bar{3}c$ calcite, viewing the (0001) plane of the CO_3 groups.

The disordering mechanism was determined from a previous experiment performed on the C2 DUALSPEC powder diffractometer, and appears to be one of continuous growth of vibrational amplitude in the crystal [1]. In particular, the L_{33} in-plane libration of the CO_3 grows until it reaches an angular amplitude of 30°, and the crystal then enters the $R\bar{3}m$ disordered phase. As calcite is heated towards this transition, the F-point TA mode softens continuously, becomes more strongly damped and the scattered intensity increases in the column. This is depicted in figures 2 and 3.

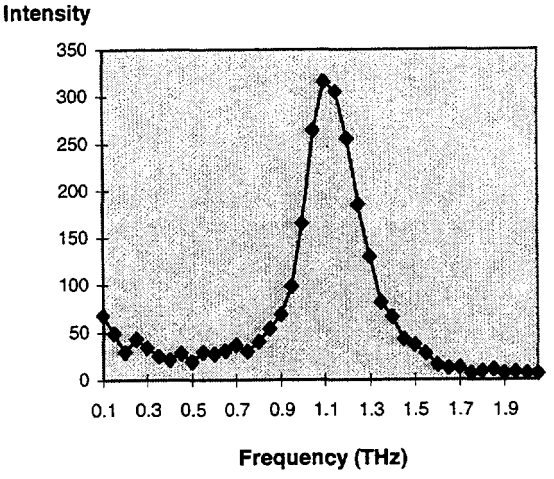

Fig. 2 Constant-Q scan through the (2.5, 0, 2) F-point at 300 K. Note that there is a column of scattering between the TA peak and the elastic point, revealed as a higher "background" below the frequency of the TA node.

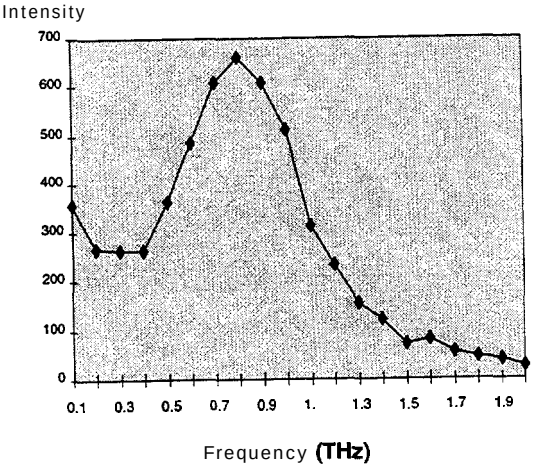

Fig. 3 Constant-Q scan through the (2.5, 0, 2) F-point at 500 K. Note the softening of the TA frequency with temperature.

Recently, we have been able to suggest an origin for the column. A symmetry-analysis of the F-point TA

mode reveals that it is of symmetry F_2^- [2]. This is also the symmetry of the soft mode phase transition to the lowest high-pressure form of calcite, $CaCO_3$ (II) [3], stable above 15 kbar. This monoclinic cell (space group $P2_1/c$) is characterized by in-plane rotations of the CO_3 groups, and out-of-plane displacements of the Ca ions. The structure is depicted in figure 4.

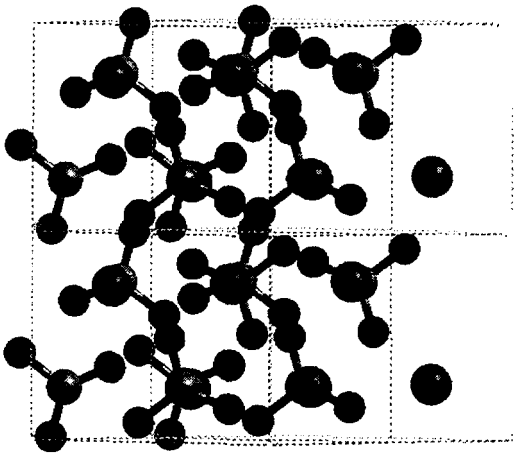

Fig. 4 Structure of $P2_1/c$ $CaCO_3$ (II), viewing the same geometric plane of CO_3 groups.

It appears that the column is, therefore, the result of a competing ordering scheme present in calcite. It is an important part of the nature of calcite, since it is not a critical effect seen only close to T_c, but distinct F-point scattering is seen even at 5 K. The fact that a column is not observed in the "isostructural" system $NaNO_3$, which undergoes a very similar Z-point transition, shows that the presence of the column is a delicate feature due to mode coupling: there is no stable high-pressure F-point phase in $NaNO_3$. There are very few other known examples of this effect: they include β-Ti [4] and β-Zr [5], and KCP ($K_2Pt(CN)_4Br_{0.3}\,3.2D_2O$) [6]. In all cases it appears that an incipient ordering appears in systems in which another transition actually occurs.

REFERENCES

[1] M.T. Dove, I.P. Swainson, B.M. Powell and D.C. Tennant, Phys. Chem. Mineral, (In Press).

[2] L. Merrill and W.A. Bassett, Acts Cryst. B **31** (1975) 343.

[3] M. Ferrario, R.M. Lynden-Bell and I.R. McDonald, J. Phys.: Condens. Matter **6** (1994) 1345.

[4] C. Stassis, J. Zaretsky and N. Wakabayashi, Phys. Rev. Lett. **41** (1978) 1726.

[5] W. Petry, T. Flottman, A. Heiming, J. Trampenau, M. Alba and G. Vogl, Phys. Rev. Lett. **61** (1988) 722.

[6] K. Carneiro, G. Shirane, S.A. Werner and S. Kaiser, Phys. Rev. **13** (1976) 4258.

Phase Transition in Ammonium Perrhenate (ND_4ReO_4)

I.P. Swainson *(AECL)* and R.J.C. Brown *(Queen's University)*

ND_4ReO_4 crystallises in the scheelite structure (space group $I4_1/a$). It does not undergo a phase transition between liquid He and *ca.* 400 K, but shows a remarkable thermal expansion. The unit cell expands along the c-axis, but contracts along the a-axis, so that the cell volume is approximately constant. We have re-analyzed previously published powder diffraction data from the E3 triple-axis spectrometer, NRU, run in two-axis mode [1]. In this re-analysis we used a new rigid body constraint to describe the tetrahedral geometry of the ND_4 molecule, which was not available previously. The analysis of the higher temperature data using a single orientation resulted in a very elongated thermal ellipsoid. This is hard to reconcile with measurements of the nuclear spin-relaxation time and Raman spectra, which do not suggest such a "soft" direction. However, recent molecular dynamics simulations [2] showed no evidence for a split site. The evidence was, therefore, contradictory. We found that a split orientation for the ND_4 ion gave an excellent description of the diffraction spectra and much more reasonable temperature factors. The fitted parameters also correspond well with the pseudo-spin theory developed by Taylor [3,4]. The observed occupation factors for the two orientations agree well with the predictions of the theory, and the difference between the axial and equatorial NO distances decreases on heating, also as predicted in the theory. This establishes ND_4ReO_4 as an example of a co-operative disordering process, which is well represented by an Ising model with a longitudinal field.

REFERENCES

[1] B.M. Powell, R. J.C. Brown, A.M.C. Harnden and J.K. Reid, Acts Cryst. **B49** (1993) 463.

[2] R.J.C. Brown and R.M. Lynden-Bell, J. Phys.: Condens. Matt. **6** (1994) 9903.

[3] D.R. Taylor, J. Chem. Phys. **87** (1987) 773.

[4] D.R. Taylor, Phys. Rev. B **40** (1989) 49.

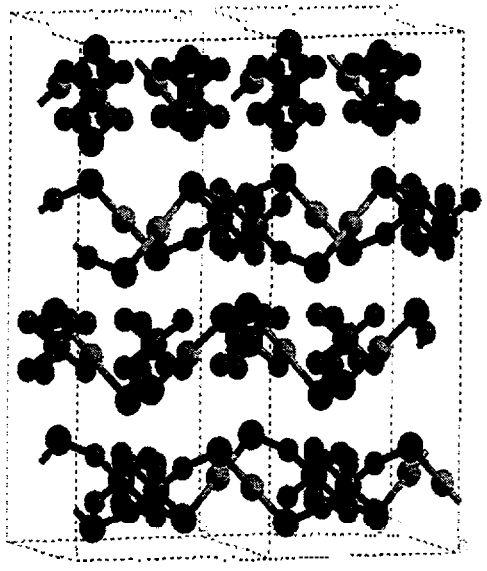

Fig. 1 Two unit cells of ND_4ReO_4 refined at room temperature. The ND_4 ion is shown as an octahedron as it sits in two partially occupied orientations.

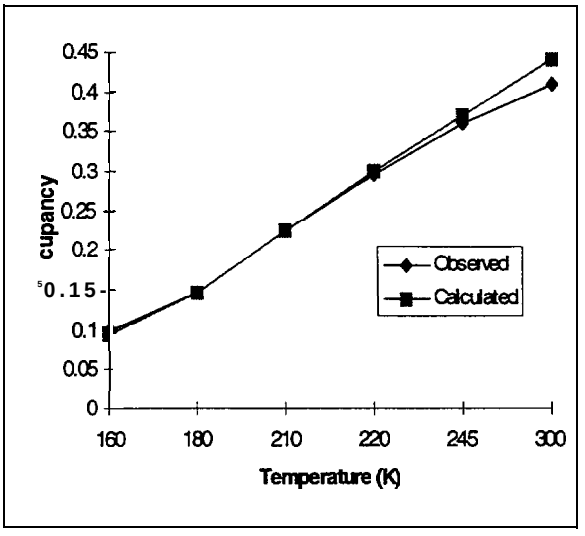

Fig. 2 Comparison of the refined and calculated (using the pseudo-spin model) partial occupancy of the equatorial site of ND_4ReO_4 as a function of temperature.

Nuclear and Magnetic Structure of RFe_7 Compounds and Their Nitrides

O. Mao and Z. Altounian *(McGill University)* and I.P. Swainson *(AECL)*

We have measured the crystal structures of several RFe_7 compounds (R = Tb, Y, Nd) and their corresponding nitrides with the DUALSPEC powder diffractometer. These are the first neutron diffraction measurements performed on the RFe_7 compounds. The measurements have shown interesting results on the crystalline and magnetic structures of the compounds, which are particularly useful for understanding the magnetic properties of the compounds and developing new magnetic materials. They were believed to be $TbCu_7$-type disordered structures. The measurements have concluded that RFe_7 is a disordered structure based on the $CaCu_5$ structure with random replacement by the R elements on the Ca site, and the replacement of some of the individual Cu atoms with Fe dumb bell pairs, where each Fe-atom is positioned $\pm z$ above and below the Cu-site.

The magnetic components of each of the Bragg peaks of $TbFe_7$ and its nitrides has been deduced by measuring the diffraction patterns below and above their Curie temperatures. Using this method, the direction of spontaneous magnetization in these compounds was determined to be along the (100) axis, which can be explained by the in-plane anistropy. Magnetic hysteresis measurements made at McGill University showed that the nitride of $TbFe_7$ has a coercivity of 3 kOe, which is unusual for a material with easy-plane magneto-crystalline anisotropy. The results of our neutron experiments have suggested that the disordering in the RFe_7 compounds may induce this intrinsic coercivity.

Preliminary measurements have been made, and further measurements are planned, of $NdFe_{7\pm x}$ compounds with a range of Fe-compositions, from $NdFe_{6.6}$ to $NdFe_8$. These are being made to investigate the volubility of Fe in the $NdFe_7$ phase, which could affect the magnetic properties. Modelling of the structures of these RFe_7 compounds will give detailed information on the atomic positions as a function of Fe-composition. Of particular interest is the variation in the Fe-dumbbell structure.

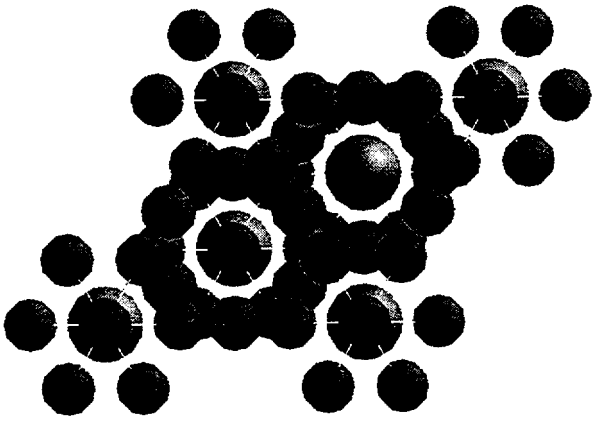

Fig. 1 View of the $NdFe_7$ structure looking down the c-axis. The large atom is Nd.

Site Substitution of $Nd_2Fe_{16.5}X_{0.5}$ Hard Magnets: (X = Al, Si, Ti, V, Cr, Mn, Co, Nb, Mo, W)

E. Girt and Z. Altounian *(McGill University)* and I.P. Swainson *(AECL)*

The preferential substitutions of X elements (X = Al, Si, Ti, V, Cr, Mn, Co, Nb, Mo, W) in the $Nd_2Fe_{16.5}X_{0.5}$ samples were investigated using neutron diffraction measurements. The measurements were performed on the C2 DUALSPEC powder diffractometer, closed-cycle cryostats were used for measurements of the fully magnetically ordered structures, and a cartridge heater system, for temperatures above the magnetic ordering temperature. Neutron diffraction measurements are essential as they utilize the much greater diffraction contrast between the transition metal elements allowing a more accurate determination of the site-substitution. This would be very difficult from powder x-ray measurements. The bulk samples measured also reduce the texturing problems encountered using x-ray diffraction.

The $Nd_2Fe_{16.5}X_{0.5}$ samples investigated were all single phase samples. Nd_2Fe_{17} crystallises in the trigonal space group R3 in the Th_2Zn_{17} structure. In this structure Nd occupies only a single crystallographic site, *(6c)* whereas Fe occupies four different crystallographic sites, designated *6c, 9d, 18f, 18h. The* substitutional X-elements in the $Nd_2Fe_{16.5}X_{0.5}$ samples replace only the Fe atoms in this structure. The results of our measurements show that X elements do **not** randomly substitute across all the Fe sites. For the cases of Ti, V, Nb, Mo and W, the *main* substitution occurs in the *6c* site. For Si the chief substitution is in the *18f* and *18h* sites. For Al, Cr, Mn and Co a more complicated substitution occurs in more than two sites. These results can be explained using the following arguments:

1) The four Fe sites do not have same volume. The size of the polyhedra surrounding these sites are in the sequence, *6c>18h>18f>9d*, causing the bigger elements to preferentially occupy the larger Fe site.

2) The four Fe sites have a different number of nearest neighbours, so that the mixing energy between the X element and the elements in the different neighbouring sites are different.

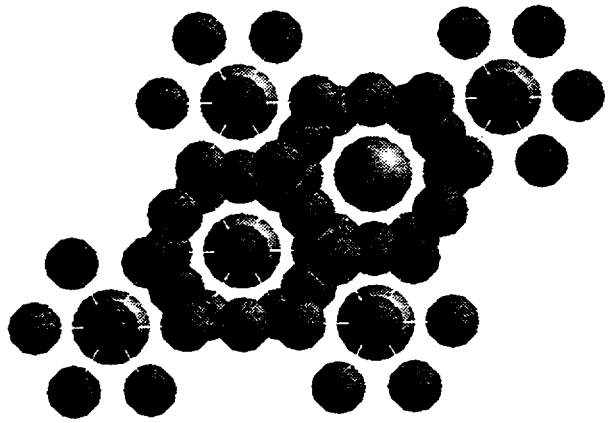

Fig. 1 View atom the c-axis of Nd_2Fe_{17}. The large atoms are Nd, which is surrounded by various Fe-sites at which preferred substitution may occur.

Magnetic Structures of $CuFeX_2$: (X = S, Se, Te)

G. Lamarche, A-M. Lamarche and J. Wooley *(Université d'Ottawa)*,
M. Quintero *(Universidad de Los Andes)*, I.P. Swainson and T.M. Holden *(AECL)*

The semimagnetic semiconductors of the I-III-VI_2 class with the chalcopyrite ($CuFeS_2$) structure have been widely studied. $CuFeS_2$ is a magnetic semiconductor with a very high Neel temperature. It was decided to extend the data to the selenides and tellurides. Such substitution has a strong effect on the magnetic, electrical and crystal properties: $CuFeSe_2$, for instance, has metallic character, it does not possess the chalcopyrite structure and the magnetic properties are much weaker than $CuFeS_2$.

$CuFeS_2$: occurs as the natural mineral chalcopyrite. This is a well-studied structure, but shows magnetic anomalies at low temperature, that could not be explained from the previous structural work. The structure has long been known to crystallize in the space group $I\bar{4}2d$ in terms of both its nuclear and magnetic structure, with the Fe-spins in an antiferromagnetic arrangement up the *c*-axis. The ordering temperature for the magnetic ordering of the Fe spins is very high: $T_N = 823$ K. Using the C2 DUALSPEC powder diffractometer the ordered Fe-moment was refined to $3.42 \pm 0.07\ \mu_B$.

It was suspected from magnetic susceptibility measurements that an additional magnetic ordering transition occurred near 50 K. Measurements of the *a* and *c* lattice parameters show distinct changes close to 50 K, indicating the possible presence of a transition. Below 50 K, the pure nuclear lines show a marked drop in intensity, but the mixed nuclear and magnetic lines show a corresponding increase in intensity. The data can be interpreted only by the presence of a transition in which the Cu-spins order antiferromagnetically. The refined value of the Cu-moments is approx. $0.05\ \mu_B$.

Measurements of lattice parameters of $CuFeSe_2$ as a function of temperature showed a break in slope at around 80 K. This is in agreement with magnetic susceptibility measurements that show a magnetic phase transition in this region. Rietveld analysis of the nuclear structure above 80 K showed a good fit to a tetragonal unit cell with space group $P\bar{4}2c$. For temperatures below 80 K the positions of the magnetic lines indicated a doubling of the *a* unit cell parameter. The magnetic moments on the Fe atoms appear to have components along all three axes and a magnitude of approximately $1.75\ \mu_B$. The Fe atoms on the two sublattice sites have slightly different moments resulting in weak ferrimagnetism, as suggested by magnetic susceptibility measurements.

The nature of the detailed nuclear and magnetic structures of $CuFeTe_2$ are still being actively investigated. The crystal structure is quite different from that of $CuFeS_2$. Both $CuTe_2$ and $FeTe_2$ crystallise in the Cu_2Sb structure, which has the space group $P4/nmm$. A peak is observed in measurements of the magnetic susceptibility near 64.5 K; however, there is no direct evidence from the diffraction patterns of changes in long-ranged magnetic order at this temperature.

Nuclear and Magnetic Structure of $UCu_{1.5}Sn_2$ and UCuSn

A. Purwanto, H. Nakotte and R.A. Robinson *(Los Alamos)* and I.P. Swainson *(AECL)*

Previously it was thought that UCuSn crystallized in the hexagonal $CaIn_2$ form [1,2]. Using data collected on the C2 DUALSPEC powder diffractometer, and the HIPD powder diffractometer at Los Alamos, it has been shown, on the basis of a large number of nuclear reflections which were not indexable in this phase, that UCuSn does not form in the $CaIn_2$ structure. Instead, it forms an orthorhombic $P2_1\,cn$ structure, and must be considered an ordered ternary compound. This structure is shown in figures 1 and 2.

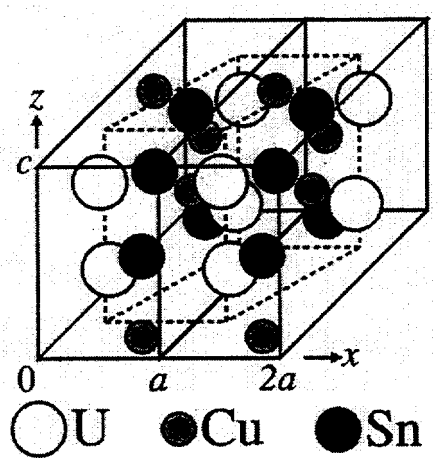

Fig. 1 The structure of UCuSn, represented in a doubled cell showing the relationship to the "parent" $CaIn_2$ hexagonal cell. For the sake of clarity the z-position were shifted by 0.25.

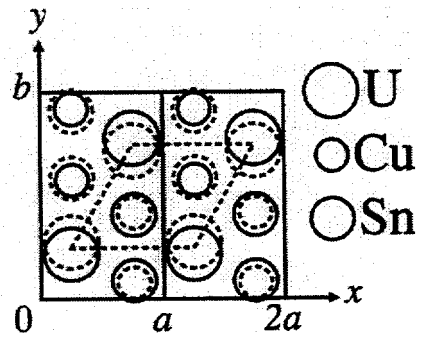

Fig. 2 Projection onto the *a-b* plane is shown, where the dashed lines represent the lower *z* position. The hexagonal cell is represented by dashes.

Structure refinements were also made as a function of temperature below the T_N of 62 K. Bulk measurements of magnetisation, resistivity and specific heat show anomalies around 25 K. However, measurements of the diffraction patterns through this temperature show no evidence for a second phase transition. One possible explanation is that UCuSn is similar to UPdSn, in which one component of the moment keeps fluctuating below T_N, while the others become permanent. However, for the case of UCuSn the fluctuations must slow down until 25 K where they stabilize to a zero value.

The Cu-deficient compound $UCu_{1.5}Sn_2$ has previously been studied with x-rays [3]. It crystallizes in the tetragonal $CaBe_2Ge_2$ structure type with space group $P4/nmm$. It has an unusually high TN for a U-intermetallic. This x-ray study found all the Cu on 2c sites, and the Sn atoms split over the other 2c sites with two different z-parameters.

The results of the experiments on the C2 DUALSPEC powder diffractometer showed no evidence for split Sri-sites, but did agree with the Cu-deficiency on the 2c sites. Three extra peaks were seen at low temperatures, below T_N, indexed as (010), (012) and (111). No extra intensity is seen at the (001), (002) or (110) low-angle peaks, and so it is assumed that these new peaks arise from pure magnetic scattering. The magnetic unit cell is the same size as the nuclear cell. As no (001) magnetic component is seen, it is assumed that the spins lie along the c-axis, in a simple linear antiferromagnetic order. U-based intermetallic antiferromagnets typically show strong magnetic anisotropies, with moments aligned perpendicular to the closest U-U distance. In this case, the closest U-U distance lies in the a-b plane with U-U= 4.39A. This exceeds the "Hill limit", beyond which localised U-moments are expected.

REFERENCES

[1] F.R. de Boer, et al., Physics B **176** (1992) 275.

[2] V.H. Tran and R. Troc, Int. J. Mod. Phys. B **7** (1993) 850.

[3] R. Pottgen, J.H. Albering, D. Kaczorowski and W. Jeitschko, J. Alloys Compounds **196** (1993) 111.

Biological ***Science***

The $L_{\beta'} \rightarrow L_{c'}$ Phase Transition in Phosphatidylcholine Lipid Bilayers: A Disorder-Order Transition in Two Dimensions

J. Katsaras *(AECL)* and V.A. Raghunathan *(Raman Research Institute, Bangalore)*

Lipid molecules exhibit a number of lamellar phases, when hydrated, which are characterized by the absence of interlayer correlations in the molecular arrangement. In the high-temperature, L_{α}, phase the hydrocarbon chains of the molecules are in a melted state and hence the ordering of the molecules within each layer is "liquid-like". On the other hand, in the lower temperature, $L_{\beta'}$ and $L_{c'}$ phases, the chains are fully stretched and are ordered within the plane of the bilayer. Most of the lipids studied consist of two hydrocarbon chains attached to a hydrophilic headgroup and it is possible for these chains to be ordered on a two-dimensional lattice, whereas the headgroups are not. X-ray diffraction studies indicate that the structure of the $L_{\beta'}$ phase is consistent with such a picture (figure 1(a)). Thus all the reflections caused by the in-plane ordering can be attributed to the hydrocarbon chains whereas the electron-rich headgroups give rise to a diffuse background [1].

From x-ray diffraction studies on oriented bilayers, we have recently shown that below the $L_{\beta'} \rightarrow L_{c'}$ phase transition in DPPC, the molecules are ordered in the plane of the bilayer [2]. Interestingly, this ordering process takes place without destroying the chain lattice, and the simultaneous existence of the two lattices requires the molecular lattice to be a superlattice of the chain lattice (figure 1(b)). This transition can thus be looked upon as a disorder-order transition on a two-dimensional lattice and is likely to be driven by the interactions between the headgroups. Hence lipids with the same headgroup can be expected to have similar structure in the $L_{c'}$ phase.

In order to confirm this, we have fitted the model given in figure 1(b) to the powder data reported by Stümpel et al. [3] on lipids having the phosphatidylcholine (PC) headgroup, but different in the length of their hydrocarbon chains and their position in the glycerol backbone. The data summarized in table 1, shows that the calculated and observed spacings of the different reflections are in good agreement, confirming the model shown in figure 1(b) for the structure of the $L_{c'}$ phase.

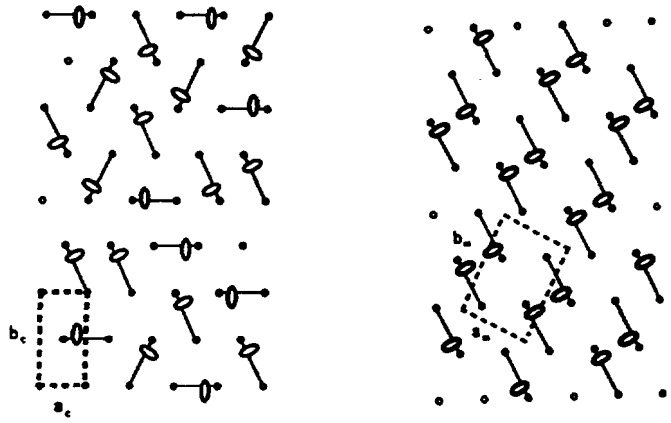

Fig. 1 (a) Schematic representation of the in-plane molecular ordering in the $L_{\beta'}$ phase of hydrated lipids. The small circles represent the hydrocarbon chains, whereas the larger oval symbols represent the headgroups. Note that even though the chains are ordered on a lattice, the molecules themselves are not. a_c and b_c represent the lattice parameters of the hydrocarbon chain lattice. *(b)* The in-plane structure of the $L_{c'}$ phase of DPPC deduced from x-ray studies on oriented bilayers. The molecules are now ordered on a superlattice of the chain lattice. The figure shows one of a possible six molecular arrangements within the superlattice, a_m and b_m represent the lattice parameters of the molecular lattice.

We should mention here that an attempt was made by Stümpel et al. [3] to index all the observed non-lamellar reflections on a two-dimensional lattice in the plane of the bilayer. However, they did not get satisfactory agreement between the calculated and measured spacings as the hydrocarbon chain reflections were not corrected for tilt and as the reflection caused by the secondary maximum of the chain form factor was treated on an equal footing with the others. Consequently, they were not able to establish the in-plane structure of the bilayers.

REFERENCES

[1] W.-J. Sun, R.M. Suter, M.A. Knewtson, C.R.. Worthington, S. Tristram-Nagle, R. Zhang and J.F. Nagle, Phys. Rev. E. **49** (1994) 4665.

[2] V.A. Raghunathan and J. Katsaras, Phys. Rev. Lett. **74** (1995) 4456.

[3] J. Stümpel, H. Eibl and A. Nicksch, Biochim. Biophys. Acts **727** (1983) 246.

Table 1 The spacings observed in the powder diffraction data presented by Stümpel et al. [3] and those calculated from the model shown in figure 1(b). The letters M, P and S in the names of the lipids stand for acyl chains containing 14, 16 and 18 carbon atoms, respectively. The numbers 1, 2 and 3 denote the position of the chains in the glycerol backbone.

Lipid	1S-2S-PC		1M-2S-PC		1P-2M-PC		1M-3M-PC		1S-3M-PC		IS-3P-PC	
Chain Lattice												
a (Å)	8.70		8.70		8.70		8.40		8.56		8.40	
b (Å)	5.32		5.13		5.13		5.14		5.07		5.24	
θ (°)	35		33		33		25		34		37	
Chain Reflections	Obs. (Å)	cal.	Obs.	Cal.	Obs.	Cal.	Obs.	Cal.	Obs.	Cal.	Obs.	Cal.
02	4.41	4.35	4.34	4.35	4.40	4.35	4.25	4.20	4.33	4.28	4.26	4.20
11, 1$\bar{1}$	3.88	3.88	3.86	3.86	3.84	3.84	4.07	4.07	3.76	3.76	3.76	3.76
Molecular Lattice												
a (Å)	10.20		10.10		10.10		9.85		9.95		9.90	
b(Å)	9.09		8.84		8.84		8.79		8.73		8.91	
Superlattice Reflections	Obs. (Å)	cal.	Obs.	Cal.	Obs.	Cal.	Obs.	Cal.	Obs.	Cal.	Obs.	Cal.
01	10.10	10.20	9.98	10.10	9.96	10.10	9.73	9.85	9.82	9.95	9.82	9.90
11, 1$\bar{1}$	6.80	6.78	6.75	6.65	6.74	6.65	6.69	6.56	6.69	6.56	6.64	6.62

Evidence for a Two-Dimensional Molecular Lattice in Subgel Phase DPPC Bilayers

J. Katsaras *(AECL)*, V.A. Raghunathan *(Raman Research Institute, Bangalore)*,
E.J. Dufourcq and J. Dufourcq *(CNRS, Pessac)*

In 1980, Chen et al. [1] observed a new phase transition at about 18°C, in a dipalmitoyl phosphatidylcholine (DPPC) multilamellar suspension using differential scanning calorimetry. Until then, DPPC suspensions were known to have only two thermotropic phase transitions. However, this newly discovered phase, commonly referred to as the subgel phase, was observed only after the sample was stored at ≈ 0°C for several days. Since then, there have been many diffraction experiments carried out to characterize the structure of this phase.

The structural changes accompanying the subtransition, from the gel phase, have been well documented [2,3]. There is a decrease in the lamellar periodicity and the appearance of a number of Bragg reflections in addition to the commonly observed lamellar and wide-angle reflections (1/4.2 and 1/4.1 $Å^{-1}$ of the $L_{\beta'}$ phase). These "additional" reflections have been cited as evidence that the low-temperature phase of DPPC has a much more ordered hydrocarbon chain structure than the $L_{\beta'}$ phase [2]. Also, ^{31}P nuclear magnetic resonance studies (NMR) have shown that in the subgel phase there is an incomplete motional averaging of the ^{31}P shift tensor not unlike dry DPPC samples [4].

Using oriented films and multilamellar liposomes of DPPC, we find that the structure of the subgel phase is characterized by a two-dimensional molecular lattice containing two lipid molecules. From the hydrocarbon chains we were able to precisely define the oblique hydrocarbon chain lattice, from which we derived the two-dimensional molecular lattice. From the proposed two-dimensional molecular lattice, six different molecular arrangements are possible (figure 1).

REFERENCES

[1] S.C. Chen, J.M. Sturtevant and B.J. Gaffney, Proc. Natl. Acad. Sci. U.S.A. 77 (1980) 5060.

[2] M.J. Ruocco and G.G. Shipley, Biochim. Biophys. Acts 684 (1982) 59.

[3] S. Tristram-Nagle, R.M. Suter, W.-J. Sun and J.F. Nagle, Biochim. Biophys. Acts 1191 (1994) 14.

[4] H.H. Füldner, Biochemistry 20 (1981) 5707.

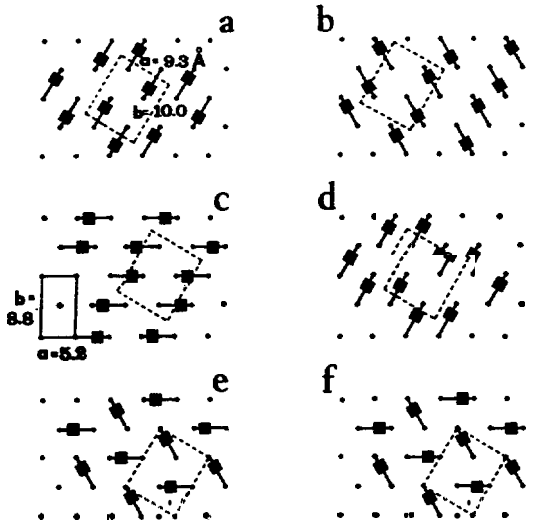

Fig. 1 The possible in-plane molecular arrangements in the subgel phase of hydrated DPPC. The chains are denoted by (●)'s and the headgroups by (■)'s. By connecting two nearest neighbour hydrocarbon chains with one headgroup, we obtain one DPPC molecule. The molecular superlattice is shown by dashed lines and the hydrocarbon chain sublattice by solid lines. Molecular arrangements (a)-(c) belong to the plane group ***p2***, while the rest belong to ***p1***. Unit cell parameters are given in Å.

Hydration/Entropic Repulsion Forces in the Various Phases of DPPC Multibilayers

J. Katsaras *(AECL)*, S. Presser *(University of California, San Diego)*
and K.R. Jeffrey *(University of Guelph)*

Lipid multilayer membrane systems, which consist of lipid bilayers separated by water, are of fundamental importance as good model systems for biological membranes. Of importance to biology, are the intermembrane interactions. The basic forces between bilayers are van der Waals attractive forces and repulsive forces, arising from either direct hydration or from entropic fluctuations [1,2], all are thought to play an important role in protein assembly, cell-cell interactions and cell fusion.

Both experimental [1,3] and theoretical studies [4] demonstrate that, at small bilayer-bilayer separations (≤ 20 Å), the presence of a strong repulsive interaction between the bilayers is the result of lipid molecules perturbing the water structure near the lipid-water interface [5]. More recently, it has been proposed that the existence of the hydration force is a result of partial charge transfer between the polar headgroups and the water molecules, resulting in a sort of "chemical hydration" of the bilayer surface [6].

In the last few years, a completely different explanation has been proposed. It argues that the repulsive forces between dynamic interfaces, such as lipid bilayers, are due primarily to entropic fluctuations that arise from undulations, protrusions and headgroup overlap [2,8]. Experimentally, it has been demonstrated that entropic steric repulsions dominate intermembrane interactions in a sodium dodecyl sulfate (SDS) fluid membrane system at a large intermembrane distance of $38 \text{ Å} \leq d \leq 16.3 \text{ Å}$ [9]. Monte Carlo simulations, [4] have predicted the presence of both entropic and direct hydration interaction regimes, depending on the whether the system was above or below its transition temperature [4]. Since the two "pictures" for the nature of the intermembrane interactions are so disparate, this area of research has become rather controversial [2,10].

X-ray diffraction [1,3,7,9] is one of the commonest techniques employed in the construction of the pressure-distance curves [1-3,7] used for the determination of the various repulsive forces between bilayers. Plotting the log of pressure *vs.* surface separation should yield a force of the following form:

(a) Exponential dependence in the case of the hydration force.

(b) Power law dependence in the case of undulatory steric repulsion of the type predicted by Helfrich [11] and demonstrated at large intermembrane spacings in the SDS fluid membrane system [9].

(c) Discontinuity in the pressure-distance curve at distances between 3-5 Å because of headgroup collisions [3,8] and molecular protrusions.

However, commonly cited problems in the construction of the pressure-distance curves are that the x-ray diffraction data used was of low resolution and that steric forces can probably be more accurately described by using a probe more sensitive to changes in the polar region (e.g. neutron diffraction or nuclear magnetic resonance) [12].

We have attempted to resolve this problem for the subgel and gel phases of dipalmitoyl phosphatidylcholine (DPPC) multibilayers using high-resolution one-dimensional scattering profiles obtained from a combination of neutron and x-ray diffraction experiments. A comparison of scattering density profiles obtained from x-ray and neutron diffraction experiments for DPPC at $\approx 100\%$ RH is shown in figure 1. The two distributions emphasize different features of the bilayer. The phase portion of the structure factors was obtained by describing lipid bilayers as a series of multiatomic quasimolecular fragments, each represented by a Gaussian distribution in composition space [13]. The scattering density profiles obtained at various relative humidities, were used to plot pressure-distance curves.

In figure 2 we present a pressure-distance curve of gel phase bilayers. The points fall, to a first approximation, on a straight line lending support to the hydration pressure theory. In addition, we have also examined previously published data of subgel phase DPPC bilayers [3] in which a sharp upward break in the pressure-distance curve occurs, indicative of steric repulsion. We explain, using two-dimensional x-ray diffraction patterns, that this break in the pressure-distance curve is a result of a phase transition in the bilayers from $2D \rightarrow 3D$.

In conclusion, the repulsive hydration pressure will dominate in ordered phases with the steric repulsive force increasing as the bilayers tend towards disorder.

REFERENCES

[1] R.P. Rand and V.A. Parsegian, Biochim. Biophys. Acts **988** (1989) 351.

[2] J.N. Israelachvili and H. Wennerström, J. Phys. Chem. **96** (1992) 520.

[3] T.J. McIntosh and S.A. Simon, Biochemistry **32** (1993) 8374.

[4] R. Lipowsky and S. Grotehans, Europhys. Lett. **23** (1993) 599.

[5] S. Marcelja and N. Radic, Chem. Phys. Lett **42** (1976) 129.

[6] G. Cevc, J. Chem. Soc. Faraday Trans. **87** (1991) 2733.

[7] S.H. White and G.I. King, Proc. Natl. Acad. Sci. USA **82** (1985) 6532.

[8] M.K. Granfeldt and S.J. Miklavic, J. Phys. Chem. **95** (1991) 6351.

[9] C.R. Safinya, D. Roux, G.S. Smith, S.K. Sinha, P. Dimon, N.A. Clark and A.M. Bellocq, Phys. Rev. Lett. **57** (1986) 2718.

[10] S. Leiken, V.A. Parsegian and D.C. Rau, Annu. Rev. Phys. Chem. **1993** (1993) 369.

[11] W. Helfrich, Z. Naturforsch **33a** (1978) 305.

[12] R.P. Rand and V.A. Parsegian, in *The Structure of Biological Membranes,* edited by P. Yeagle, (CRC Press, 1992).

[13] M.C. Weiner and S.H. White, Biophys. J. **59** (1991) 174.

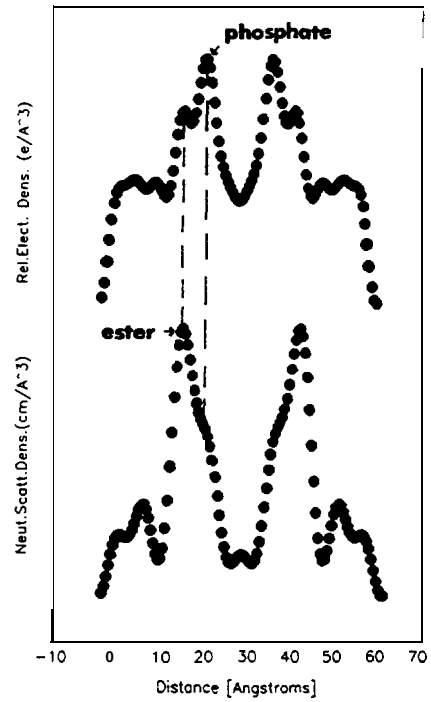

Fig. 1 A comparison of one-dimensional scattering density profiles of DPPC multibilayers obtained from x-ray (top) and neutron (bottom) diffraction experiments.

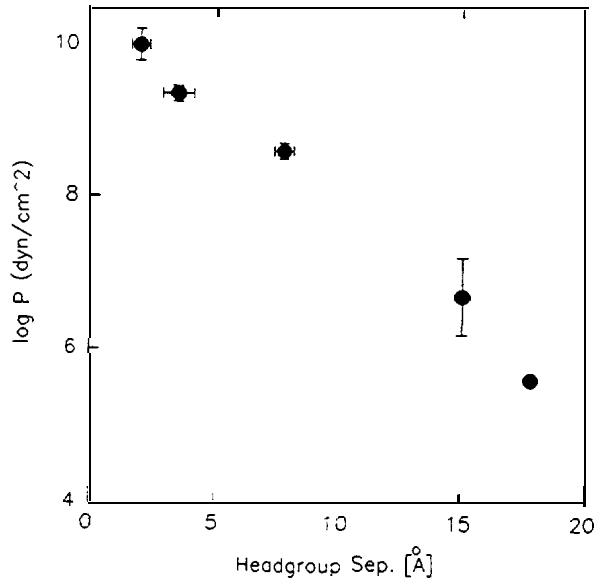

Fig. 2 Logarithm of applied pressure *(vs.)* headgroup separation in oriented DPPC multibilayers at 25°C.

Neutron Reflectivity from Lipid Multibilayers

J. Katsaras and Z. Tun *(AECL)*

Lipid multilayer membrane systems, which consist of lipid bilayers separated by water, are of fundamental importance as good models for biological membranes. Moreover, lipids are also lyotropic liquid crystals, which exhibit a variety of interesting structures (e.g. lamellar, hexagonal, "ripple", cubic, etc.) and serve as prototype models for certain one-dimensional and two-dimensional phase transitions [1]. However, despite a great number of studies over the past three decades, the precise structure of some of these phases was not known until recently [2] and for some, such as the ripple $P_{\beta'}$ phase, the details are still not well understood [3]. Recently Lubensky and Mackintosh [4] described the various symmetric and asymmetric $P_{\beta'}$ phases using a continuum Landau theory.

Using the C5 DUALSPEC spectrometer, we performed a pilot reflectivity experiment on oriented dipalmitoyl phosphatidylcholine (DPPC) multibilayers under hydration. The specular reflectivity obtained is presented in figure 1. The most important advantage of using the C5 spectrometer, rather than the Bio-Science diffractometer (normally used for the study of biologically relevant materials), is the availability of a tuneable wavelength, which enables us to collect data for momentum transfer, $Q \leq 0.05$ Å^{-1}, as demonstrated in figure 1. The low Q region is crucial to the determination of the $P_{\beta'}$ phase structure and until now, the data arising from this region in reciprocal space has been contradictory.

Using high-resolution specular reflectivity data we will be in a position to determine the structure of the $P_{\beta'}$ phase and compare it to the models proposed by Lubensky and Mackintosh [4].

REFERENCES

[1] G.S. Smith, E.B. Sirota, C.R. Safinya and N.A. Clark, Phys. Rev. Lett. **60** (1988) 813.

[2] V.A. Raghunathan and J. Katsaras, Phys. Rev. Lett. **74** (1995) 4456.

[3] J. Katsaras and V.A. Raghunathan, Phys. Rev. Lett. **74** (1995) 2022.

[4] T.C. Lubensky and F.C. MacKintosh, Phys. Rev. Lett. **71** (1993) 1565.

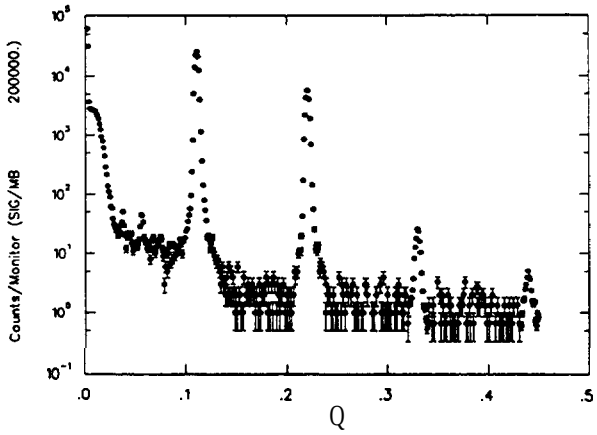

Fig.1 Specular reflectivity pattern of oriented DPPC multibilayers in the $L_{\beta'}$ phase. Critical $|Q|$ is ~ 0.1 Å^{-1}.

Theory

The Optical Conductivity in $Ba_{0.6}K_{0.4}BiO_3$

F. Marsiglio *(AECL)* and J.P. Carbotte *(McMaster University)*

The high-T_c superconductor, $Ba_{0.6}K_{0.4}BiO_3$ ($T_c \approx 28$ K) is believed to have an order parameter with s-wave symmetry. Experimental support comes mainly from single-electron tunnelling measurements and far-infrared experiments. Tunnelling measurements further suggest that the electron-phonon mechanism is responsible for the superconductivity in this compound. We have undertaken a study of the optical conductivity in a conventional electron-phonon driven s-wave superconductor to elucidate precisely what the optical conductivity measurements indicate about both the symmetry of the order parameter and the mechanism responsible for superconductivity.

An important signature of the symmetry of the order parameter is the presence or absence of a gap in the single-particle density of states. Both tunnelling and, to some extent, reflectivity measurements indicate a gap, and therefore an s-wave order parameter. This conclusion has been reinforced by analyzing the imaginary part of the conductivity. In figure 1 we show the imaginary part of the conductivity (multiplied by the frequency), $\nu\sigma_2(\nu)$ vs. frequency, measured in $Ba_{0.6}K_{0.4}BiO_3$ at two different temperatures. Theoretical curves are shown for comparison. At 9 K, the dip above 10 meV in the data is unequivocal evidence for the existence of a gap, of roughly this size ($2\Delta \approx 10.4$ meV).

The issue of whether or not the electron-phonon interaction is responsible for the superconductivity is a more subtle issue. One means of probing this, which is valid in the normal state, is to fit the high-temperature data for both the real and imaginary parts of the optical conductivity to a Drude form, and thereby extract the coupling strength (through fits from Eliashberg theory) [1]. Another is to examine the structure present in the real part of the conductivity, which increases as the coupling strength increases. In either case the derived coupling is very small — far too small to account for superconductivity in this compound. This discrepancy remains an outstanding puzzle at this time.

In related work, we have investigated the relationship between the electron scattering rate, as extracted from the optical or microwave conductivity, and the quasiparticle inverse lifetime in an s-wave superconductor. Aside from trivial geometric factors, we find that the two are in qualitative agreement for electron-phonon plus impurity scattering, over a wide range of parameters. In particular, the electron lifetime increases significantly in the superconducting state, because of phase space (Anderson's "theorem") arguments. Accurate quantitative agreement is lacking, however, so that too rigid an interpretation following a two-fluid prescription is not possible.

REFERENCES

[1] F. Marsiglio and J.P. Carbotte, Phys. Rev. B **52** (1995) 16192.

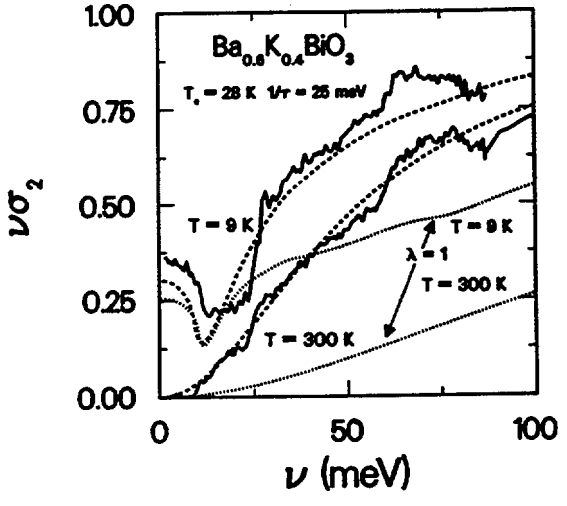

Fig. 1 The measured imaginary part of the conductivity, $\nu\sigma_2(\nu)$ vs. frequency at T = 9 K and T = 300 K (solid curves), along with theoretical fits with $\lambda = 0.2$ (dashed curves). Also shown are fits with $\lambda = 1$ (dotted curves), which are incompatible with the data.

Statistical Transmutation of the Heisenberg Spin Chain

M. Couture *(AECL)*

In the study of many body systems, it is often useful to think of them in terms of spins, fermions or bosons, whatever the nature of the original system. This is particularly true in one-dimensional physics where the possibility of transmuting the statistics of a particular model has often been used as a means of solving it. The $S = 1/2$ Heisenberg spin chain is probably the best example. On the lattice, this model can be shown to be equivalent to a spinless fermion model by using a Jordan-Wigner transform. Then by mapping the resulting model in the continuum one may, through bosonization, show the equivalence with a free massless bosonic field theory. This allows one to calculate correlation functions in the long wavelength limit. Recent developments in mathematics open up the possibility of re-examining the transmutation of statistics in one-dimensional from a more fundamental point of view. We have examined the transmutation on a lattice of the $S = 1/2$ Heisenberg spin chain. It is well known that this model has a rich underlying algebraic structure that is rooted in topology and in the symmetries of non-commutative spaces. One might expect that essentially all properties of the model can be traced back to properties of these structures. In this project we have studied the transmutation of the model by examining the transmutation of its algebraic roots (which are examples of Hopf algebras) using a recently developed transmutation theory [1] of Hopf algebras. The objective was to gain a more basic understanding of the process with the hope that it might lead to generalizations of the Jordan-Wigner transform and to extensions to two- and three-dimensional. This work has lead to the identification of the symmetry that lies at the origin of the Jordan-Wigner transform. Having understood the foundation of this transform, we have generalized it to higher spins ($S > 1/2$) and to more general statistics (braided). This led us to define new equivalences for the Heisenberg model ($S \geq 1/2$). There are several directions one might go from here. In this work we have examined the simplest type of transforms that Majid's theory permits (which turned out to be a generalization of the Jordan-Wigner transform). It would be interesting to consider the other possibilities which will be most probably unrelated to the Jordan-Wigner transforms but which, will nevertheless lead to a transmutation of the model. One might also attempt to adapt Majid's transmutation theory in the continuum limit. Having understood the symmetry behind the Jordan-Wigner transform, we hope to extend this idea to formulate two- and three-dimensional generalization of this transform.

REFERENCES

[1] S. Majid, Math. Proc. Comb. Phil. Soc. **113** (1993) 45.

Exact Correlation Functions for the S = 1/2 Heisenberg Spin Chain

M. Couture *(AECL)* and H. Bougourzi *(State University of New York, Stony Brook)*

The understanding of the physics of the S = 1/2 Heisenberg spin chain has constituted a major challenge for theoretical physicists over the last sixty years. Initially, it was considered as a possible first step in understanding the three-dimensional case. H. Bethe [1] showed that the one-dimensional isotropic case was exactly solvable (Bethe ansatz). This result has had an enormous impact in our understanding of the physics of the problem. Over the next sixty years, this led to the uncovering of a rich underlying mathematical structure whose intense study has led, to the discovery of new symmetries that are continuous deformations of the classical ones.

The interest in Heisenberg spin chains increased considerably when it became clear, that the model was most probably realized in certain quasi one-dimensional materials. In their seminal work, Faddeev and Takhtajan [2] developed a theory explaining the spectrum of the model in terms of elementary excitations, now referred to as spinons. This spinon-based theory predicts a continuum of magnetic excitations.

A further motivating factor in understanding this model is the fact that it belongs to the "Luttinger liquid" universality class of which, certain properties are believed to carry over into two-dimensions. This was suggested by Anderson [3] in 1987 in the context of high T_c superconductivity, and has, since then, motivated a lot of work on the one-dimensional models which belong to this class.

Recently, neutron scattering experiments on $KCuF_3$ [4] have tested the predictions of the spinon-based theory mentioned above. Correlation function are of course a key ingredient in comparing theory and experiment. In the above-mentioned experiments, the correlation functions provided by Müller [5] and those obtained within a field theoretical framework (valid only in the low-energy and long-wavelength limit) were used. Although the overall agreement is good, the interpretation of these results in terms of the spinon picture needs clarification. Müller's formula was obtained through some ansatz and its physical meaning is still obscure. A major advance in our understanding of the Heisenberg model was made when a hidden symmetry of the model was discovered [6]. This new symmetry is of the type mentioned above and is referred to as quantum affine sl (2). The existence of such a symmetry implies that the physics of the problem (description of ground state, excited states, dispersion relations, spinon creation operators, correlation functions) can be completely described within the framework of the representation theory of the quantum affine sl (2). This is the spinon space as opposed to spin space. The important point is that this theory allows one to calculate correlation functions exactly. Moreover, since we are working in spinon space, one can calculate the contributions of the various processes (2, 4, 6 ... spinons) separately. The difficulty is that the expressions are given in the form of complicated integrals and therefore impossible to use in the present form. The object of this work is to obtain exact and usable expressions for the contribution of the two-spinon process to the correlation functions and, compare the results with those used in the analysis of the neutron experiments [4]. The first task was to understand the theory and given its mathematical sophistication, this was not a trivial task. Significant progress has been made. We have succeeded in simplifying the expression for the two-spinon contribution provided by the theory. We are now comparing it with Müller's [5] expression. The next step will be to tackle the four-spinon case.

REFERENCES

[1] H. Bethe, Z. Phys. **71** (1931) 205.

[2] L.D. Faddeev and L.A. Takhtajan, J. Sov. Math. **24** (1984) 241.

[3] P.W. Anderson, Phys. Rev. Lett. **64** (1990) 1839, and **65** (1990) 2306.

[4] D.A. Tennant, R.A. Cowley, S.E. Nagler and A.M Tsvelik, Phys. Rev. B. **52** (1995) 13368.

[5] G. Müller, H. Thomas, H. Beck and J.C. Bonner, Phys. Rev. B. **24** (1981) 1429.

[6] B. Davies, O. Foda, M. Jimbo, T. Miwa and A. Nakayashiki, Commun. Math. Phys. **151** (1993) 89.

Reflecting Properties of Neutron Monochromator Crystals

V.F. Sears *(AECL)*

As discussed in the preceding report, we have obtained the general solution of the Darwin equations for a mosaic crystal slab for both the Laue case (transmission geometry) and the Bragg case (reflection geometry). This now allows us, for the first time, to calculate the reflecting properties of an absorbing crystal of finite thickness in situations where the Bragg planes make an arbitrary angle with the surface of the crystal.

We have recently performed extensive numerical calculations for a number of common neutron monochromator crystals: Al, Cu, Ge, Si, Be, and pyrolytic graphite (PG). In particular, we have calculated the following quantities:

- reflectivity
- figure of merit
- reflected flux
- optimum thickness
- order contamination
- Fankuchen gain

The incident flux was taken to be Maxwellian with an epithermal tail, and effective neutron temperatures were chosen to simulate both a thermal source and a cold source. The attenuation coefficient included contributions from true absorption (e.g. radiative capture), incoherent scattering, and coherent inelastic scattering. The quantities listed above were calculated for the most commonly used Bragg planes (*hkl*), to demonstrate how they depend on the neutron wavelength λ, the crystal thickness d, the mosaic spread $\Delta\theta$, and the angle α which the Bragg planes make with the surface of the crystal. For the non-symmetric reflections ($0° < \alpha < 90°$) we studied both compression and expansion geometries.

Table 1 lists the values of the optimum crystal thickness d_{opt} (cm) for various monochromator reflection planes, with $\lambda = 1$ Å and $\Delta\theta = 0.3°$, for both the symmetric Bragg case ($\alpha = 0°$) and the symmetric Laue case ($\alpha = 90°$). In the Bragg case, d_{opt} is taken to be the thickness at which the peak reflectivity reaches 80% of its saturation value and, in the Laue case, d_{opt} is the thickness at which the peak reflectivity is a maximum.

Figure 1 shows the Fankuchen gain Gas a function of α (in degrees) for the Si (111) reflection in compression geometry with $\lambda = 1, 2, 3,$ and 4 Å (reading from top to bottom at small α). The discontinuity in G occurs at the value of α where the reflected beam is parallel to the surface of the crystal. Below the discontinuity we have the Laue case and above it the Bragg case. It is evident that gains in flux of 25% to 50% or more can easily be achieved for a wide range of wavelengths.

Table1 Optimum crystal thickness (cm) at $\lambda = 1$ Å for selected reflection planes.

Planes	Bragg Case	Laue Case
Al (111)	1.006	5.490
Cu (111)	0.126	0.610
Ge (111)	0.242	1.895
Si (111)	0.983	7.313
Si (220)	1.458	6.462
Si (311)	2.609	9.930
Be (002)	0.115	0.458
PG (002)	0.056	0.441

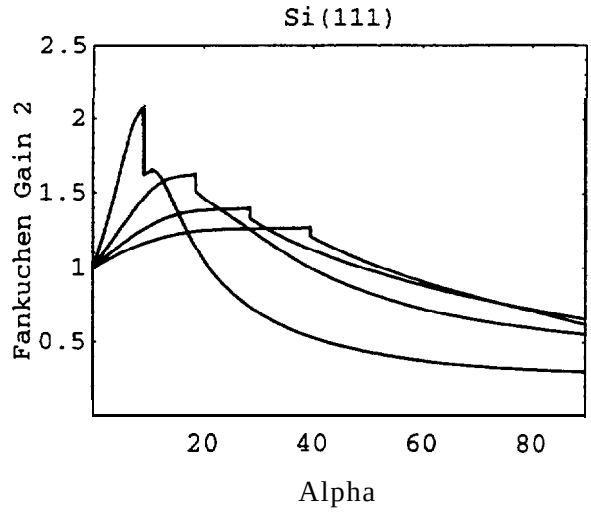

Fig. 1 Fankuchen gain G as a function of α for the Si (111) reflection with λ = 1,2,3, and 4 Å (reading from top to bottom at small α).

General Solution of the Darwin Equations

V.F. Sears *(AECL)*

The Darwin equations [1], which describe multiple Bragg reflection within a mosaic crystal, are a coupled system of two linear homogeneous first-order differential equations with constant coefficients. If the crystal takes the form of a plane slab, these equations should be exactly solvable in terms of elementary functions. Solutions have been obtained previously only for special cases: i.e. symmetrical reflections [2] (where the Bragg planes are either parallel or perpendicular to the surface), a non-absorbing crystal [3], and an infinitely thick crystal [1].

The general solution of the Darwin equations is the kind of problem that is ideally suited to a computer algebra program. We have obtained the complete and exact *analytic* solution of these equations for both the Bragg case (reflection geometry) and the Laue case (transmission geometry) by using the program Mathematica, and have shown that the resulting general formulae for both the reflectivity R and the transmissivity T can be expressed in a compact form.

The terms "anomalous absorption" or "Borrmann effect" refer to the change in the absorptivity of a crystal that occurs in the presence of a Bragg-reflected beam. We find that for a mosaic crystal such anomalous absorption occurs only in the Bragg case and not in the Laue case. In the dynamical theory of diffraction [4], which applies to an ideally perfect crystal, one finds anomalous absorption in both the Laue and Bragg cases.

The Fankuchen gain G is the ratio of the reflected flux when the Bragg planes make an angle α with the surface, to the flux when $\alpha = 0$. An often-quoted result [5] is that the maximum value of G is 2. However, this result is of limited validity. First, it only includes the effect of absorption on the reflectivity and ignores the effect of secondary extinction, which is usually not negligible for neutrons. Second, it is only valid for an infinitely thick crystal, which again is usually not a good approximation for neutrons. Using our new general expression for R, we have calculated G for a crystal of finite thickness, correctly taking into account the effects of both absorption and secondary extinction. We find that values of G larger than 2 are possible.

The optimum thickness is an important consideration in the design of neutron monochromator crystals. In the Bragg case this is the thickness at which R reaches some specified fraction of its saturation value and, in the Laue case, it is the thickness at which R reaches its maximum value. We have derived general expressions for the optimum thickness for both the Bragg and Laue cases.

There are four different ways in which a monoenergetic beam of neutrons can be reflected from a given set of Bragg planes. We have shown that these are related by parity and time reversal, and have calculated the way in which R and T transform under these symmetry operations.

The attenuation coefficient μ in the Darwin equations is the cross section per unit volume for all collision processes other than Bragg reflection. Thus μ includes contributions, not only from true absorption (e.g. radiative capture), but also from incoherent scattering and coherent inelastic scattering. At thermal-neutron wavelengths, the largest contribution to μ comes from coherent inelastic scattering in most materials at or above room temperature. We have obtained a simple expression for the contribution to μ from coherent inelastic scattering based on the assumption that the motion of different atoms is statistically independent while the distribution of vibrational frequencies is that of the actual crystal. With these assumptions, the coherent inelastic contribution to μ depends only on the root-mean-square displacement of an atom, the same parameter that determines the Debye-Waller factor.

REFERENCES

[1] C.G. Darwin, Phil. Mag. **43** (1922) 800.

[2] W.H. Zachariasen, Theory of X-Ray Diffraction in Crystals (Wiley, New York, 1945).

[3] V.F. Sears, Acts Cryst. A **33** (1977) 373.

[4] V.F. Sears, Neutron Optics (Oxford University Press, New York, 1989).

[5] R.M. Bozorth and F.E. Haworth, Phys. Rev. **53** (1938) 538.

The Condensed Phases of Carboranes

Z. Gamba *(CNEA, Buenos Aires)* and B.M. Powell *(AECL)*

Carboranes, $B_{10}C_2H_{12}$, are cage-like molecules in which the C and B atoms form an inner cage, a slightly distorted icosahedron. Each of these atoms is bonded to a H pointing outwards. The three possible atomic arrangements are para- carborane, meta-carborane and ortho-carborane. In the *para* isomer the two C atoms are at opposite sides of the icosahedron, in the *meta* isomer there is one B atom between them and in the *ortho* isomer they are adjacent.

Carboranes are molecular solids in which the molecules interact via weak van der Waals forces. An atom-atom Lennard-Jones (LJ) model for the intermolecular potential of these molecules has been developed and applied in a series of classical constant-pressure molecular dynamics simulations of p-, m- and o-carborane crystals, at several temperatures and O kbar pressure. The LJ parameters for C and H are taken from studies on hydrocarbons [1]. The parameters for B were adjusted to give reasonable agreement with the unit cell volume and configurational energy at O K. A simple charge distribution was chosen to reproduce the dipole moments of m- and o-carboranes.

Our simplified potential model for the intermolecular interactions in carboranes reproduces qualitatively several of the structural and dynamical properties of these crystals. Figure 1 shows the calculated unit cell volume and configurational energy *vs.* temperature, for the three isomers. The high-temperature phase is orientationally disordered with an fcc structure for all three isomers. For p-carborane, two solid-solid phase transitions and an intermediate phase with uniaxial rotation are found. For m- and o-carborane, the results in the intermediate range of temperatures are less certain. In m-carborane a temperature range was found in which the reorientations are anisotropic, but not uniaxial. In o-carborane crystals, the intermediate phase is not found. The calculated vibrational density of states, for all crystals at all temperatures, is in the range of the measured lattice Raman frequencies.

Molecular orbital calculations of the molecular charge distribution would be very useful in improving the electrostatic interaction term of the intermolecular potential. This term has a significant contribution to the total interaction potential and is oversimplified in the present model. Our calculations suggest, from the lack of the intermediate uniaxial rotational phase, that the present intermolecular potential is too isotropic for m- and o-carboranes.

The present work emphasizes the need for further experimental measurements, particularly of the crystalline structures and lattice frequencies at low temperatures. These data are necessary for further improvements in the intermolecular potential model.

REFERENCES

[1] D.E. Williams, J. Chem. Phys. 47 (1967) 4680.

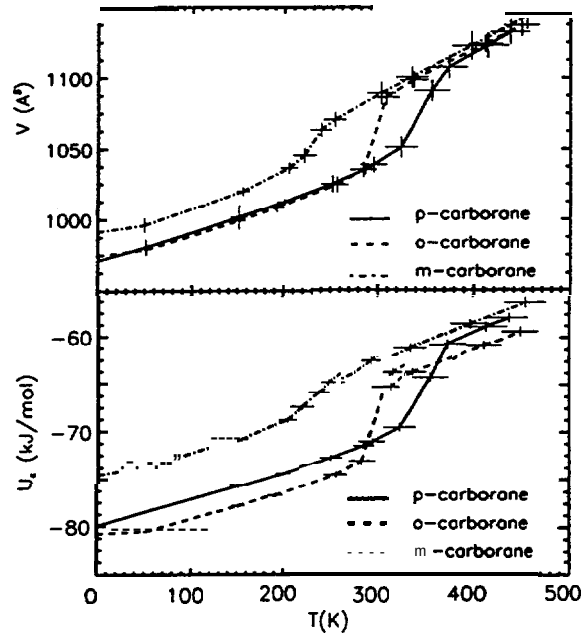

Fig. 1 Unit cell volume (Z = 4) and configurational energy *vs.* temperature, for the three compounds. The lines are a guide to the eye.

Phonon Density of States in Vanadium

V.F. Sears, E.C. Svensson and B.M. Powell *(AECL)*

In recent years, a number of neutron inelastic scattering experiments have been performed at NRU to determine the phonon density of states in various hydrogenous materials. To obtain a benchmark for this work, and to test the method used for making multiphonon corrections, we have carried out similar experiments on vanadium. A preliminary account of this work was given previously [1].

Vanadium is the prototype material for these studies because (1) it is an almost totally incoherent scatterer and (2) the atoms occupy the sites of a cubic Bravais lattice so that, to the extent that multiphonon scattering is negligible, the observed inelastic scattering is directly proportional to the phonon density of states $g(\nu)$. In all other real materials, the effective density of states obtained from such experiments is weighted by the phonon polarization vectors.

The vanadium sample was a slab, 0.457 cm thick, and the experiment was performed in symmetric transmission geometry at room temperature. We used the N5 triple-axis spectrometer at NRU with a Si (331) monochromator and a Ge (1 1 3) analyzer. The experiment was carried out with a constant momentum transfer $Q = 6.5$ Å^{-1} and a constant scattered neutron energy of 8.0 THz. The energy resolution (FWHM) was 0.35 THz at the elastic position.

The intensity in the inelastic region (typically 700 to 1300 counts) enables us to determine $g(\nu)$ with an average statistical precision of 3%. The corresponding background, was about 150 counts. Corrections were made for multiple scattering, multiphonon scattering, absorption and self-shielding, and for the spatial inhomogeneity of the incident beam.

The resulting $g(\nu)$ distribution is shown by the dots in figure 1 and is characterized by peaks at 4.9 and 6.9 THz, which we attribute to transverse and longitudinal phonons respectively, and by a cut-off at about 8.1 THz. The peaks in our $g(\nu)$ distribution are much more clearly resolved than in previous work on vanadium. We also see a small shoulder in the region 2 to 3 THz, but it is far less pronounced than in some of the earlier experiments on vanadium. Below 2 THz we find that $g(\nu)$ is proportional to ν^2, and the observed proportionality constant leads to a Debye temperature in excellent agreement with that obtained from the measured elastic constants of vanadium at room temperature. The mean-square displacements u^2 calculated from our $g(\nu)$ distribution, agree well with similar calculations by Kamal et al. from their neutron results [2]. Our calculated values of u^2 also agree with those from available x-ray Debye-Waller factor measurements [3].

Figure 1 shows a comparison of our $g(\nu)$ results (dots) with the theoretical distribution calculated by Clark [4] (solid curve). Clark's distribution is in general qualitative agreement with our experimental results. The main difference lies in the relative intensities of the two peaks in the distribution. Clark's model is certainly oversimplified in its assumption of only nearest and next-nearest neighbor central forces. Thus, the fact that Clark's results are in only qualitative agreement with our experimental distribution is not surprising.

REFERENCES

[1] Physics Division Progress Report, PR-PHY-8, AECL–1 1234, 1995.

[2] M. Kamal, S.S. Malik, and D. Rorer, Phys. Rev. B 18 (1978) 1609.

[3] M.V. Linkoaho, Phil. Mag. 23 (1971) 191.

[4] C.B. Clark, J. Grad. Res. Center 29 (1961) 10.

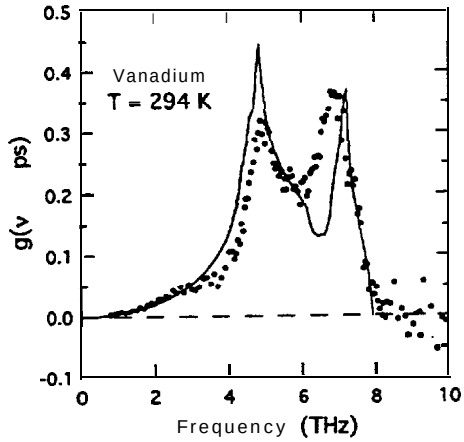

Fig. 1 Phonon density of states in vanadium: theory versus experiment.

Theoretical Modelling of Vacancies in NiAl Alloys

S.M. Kim *(AECL)*

For many years, the nearest-neighbour atom-pair bond energy model has been extensively used in understanding the observed vacancy properties in various ordered binary and ternary alloys, such as B2 FeAl, B2 NiGa, B2 CoGa, $L1_2$ Cu_3Au, $L1_2$ Ni_3Al, $L1_2$ Al_3TiX (X = Cr, etc.), LI_0 CuAu and B_{32} LiAl [1,2]. Most of the observed vacancy properties in these alloys could be well understood within this model with the bond energies either estimated from the pure metals or obtained by fitting to the observed vacancy and antistructure atom (atoms on the wrong sublattice) concentrations. In this model, it was generally assumed that the atom-pair bond energies do not change with the alloy composition or temperature.

The atom-pair bond energy model has recently been applied to B2 NiAl alloys [3], where the observed vacancy properties available at that time appeared to be well described with this model with bond energies determined by fitting to the experimentally observed vacancy and antistructure atom concentrations. In B2 NiAl, however, the atomic spacing changes appreciably with alloy composition as well as temperature, and thus the assumption of constant bond energies may not be valid if the bond energies are also sensitive functions of atomic spacings. Indeed, the most recent *in situ* neutron powder diffraction measurements carried out here at Chalk River [4] could not be well described with this model.

Recently, Cottrell [5] deduced various bond energies in NiAl alloys from electronic structure calculations and showed that the observed vacancy and antistructure atom concentrations at room temperature could be well described with a modified bonding model. In his calculation, however, it was also assumed that the Ni-Ni, Al-Al and Ni-Al bond energies in NiAl do not depend on the alloy composition. When these bond energies are recalculated following his prescription, and taking into account the experimentally observed atomic spacings for different compositions, it can be shown that his model predicts an appreciable Al vacancy formation in the Ni-rich NiAl alloys even at low temperatures, in serious disagreement with the experimental observations.

In the absence of any other viable model, we have determined the various atom-pair bond energies in NiAl alloys for different compositions and temperatures by fitting to the experimentally observed [4] vacancy and antistructure atom concentrations. The results show that both the Ni-Ni and Al-Al bond energies are largest in the most Ni-rich composition, and smallest in the most Al-rich composition. Moreover, while the Al-Al bond energy and the ordering energy increase with temperature, the Ni-Ni bond energy first increases with temperature and then decreases with temperature at higher temperatures. These results indicate that the bond energies in NiAl alloys are sensitive functions, not only of the atomic spacing but also of the electronic structure.

REFERENCES

[1] S.M. Kim, J. Mater. Res. **6** (1991) 1455, and references therein.

[2] S.M. Kim, M. Kogachi, A. Kameyama and D.G. Morris, Acts Met. Mater. **43** (1995) 3139.

[3] S.M. Kim, Acts Met. Mater. **40** (1992) 2793.

[4] S.M. Kim, Y. Takeda and M. Kogachi, Scripts Mater. (1996), to be published.

[5] A.H. Cottrell, Intermetallics **3** (1995) 341.

Instrumenting

The T3 Bioscience Diffractometer

J. Katsaras, J.H. Fox, M.D. Gauthier, L.E. McEwan, M.W. Montaigne,
M.M. Potter, J.A. Rollings and D.C. Tennant *(AECL)*

The T3 Bioscience Diffractometer, shown schematically in figure 1, was commissioned in May after a prolonged period of reconstruction. It is one of only two such instruments in North America, dedicated to the study of soft condensed matter, in particular biological materials.

The diffractometer is equipped with a 60 cm linear, position-sensitive proportional counter and uses resistance-capacitance position encoding, resulting in a linear resolution of ≈ 0.5 cm. This method of position encoding is known for its extended lifetime, reliability and simplicity of operation. The wavelength is fixed at 1.43 Å using graphite [002] as the monochromator. The sample-to-detector distance is variable (2.3 - 4.5 m). To reduce background, the incident neutron beam path is under vacuum while the diffracted beam path is filled with helium. The size of the beam can be varied up to a maximum of 4 mm × 60 mm.

Since biological samples come in a variety of forms (e.g. cells, dry powders, fibers, liquids etc.) two different sample holders have been fabricated. The simplest one designed for "powder" samples. The sample is placed in a quartz capillary, which is flame sealed in order to keep the water present in these systems from evaporating. The sample holder is temperature controlled in the range (-20 - 80°C). However, many present studies are interested in model systems of biological membranes that can be easily manipulated. An advantage of such systems is that two-dimensional crystals can be formed easily on a glass or silicon crystal substrate in the presence of water. The sample holder for these samples was designed to control both temperature (-20 - 80°C) and humidity (0 - 100% RH) to minimize the temperature gradients that can drastically affect the apparent humidity. Since its inception, the instrument has been used by a number of scientists and most recently, we have shown the bimodal distribution of the phosphoylcholine headgroup along with new insight into the so-called "hydration force".

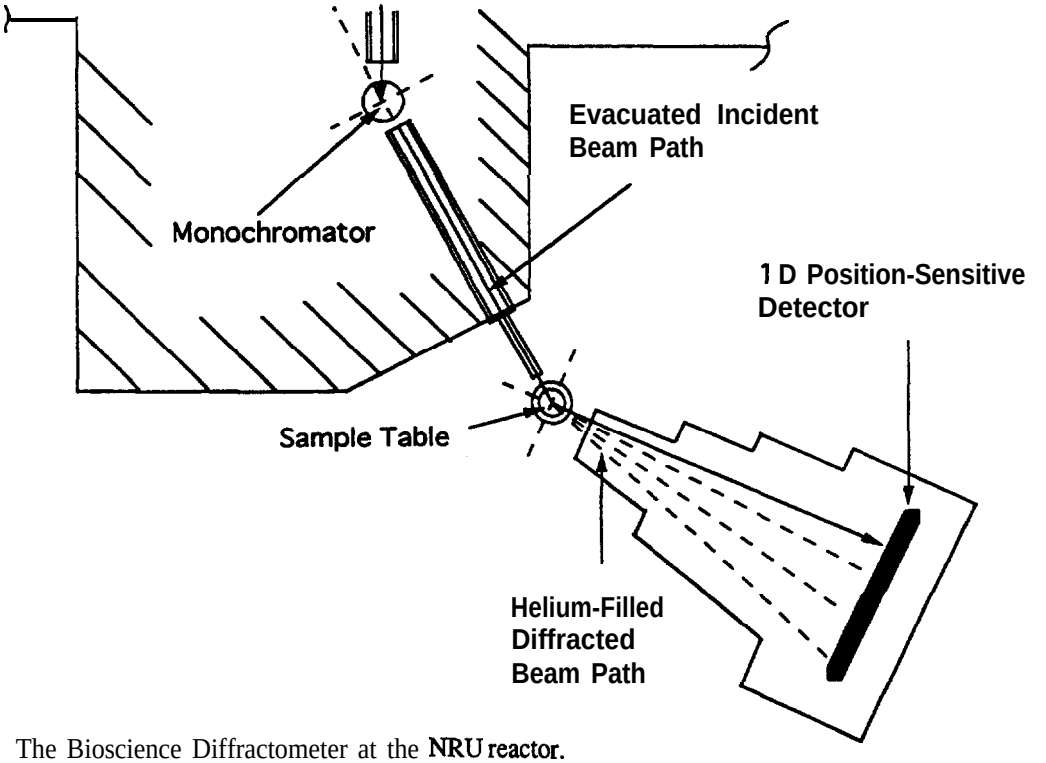

Fig. 1 The Bioscience Diffractometer at the NRU reactor.

Benchmark Tests of the DUALSPEC Neutron Powder Diffractometer

I.P. Swainson *(AECL)*

In 1994, the Commission on Powder Diffraction of the International Union of Crystallography (IUCr) published a benchmarking report of powder diffractometers in the *Journal of Applied Crystallography* [1]. *The* exercise took the form of a Rietveld Round Robin where participants were asked to measure the powder diffraction spectrum of a standard sample of monoclinic ZrO_2. Both x-ray and neutron powder diffractometers were used, of greatly varying resolution. Unfortunately, the exercise predated the commissioning of the DUALSPEC powder diffractometer, C2. However, the published results still provide a very useful database for comparison. A sample of the standard monoclinic ZrO_2 was obtained from the IUCr and run on C2 in several configurations. The test provides a validation of the calibration procedure, the effective wire-spacing and comparison of the performance of C2 to other diffractometers around the world. The survey suggests that some 30% of all variation in refined crystal structure is due to different software and refinement strategies, and the remaining 70% to instrumentational differences, such as geometry of scattering and calibration. The data in Table 1 represent results from the participants themselves (labelled IUCr(p)), IUCr re-refinements (labelled IUCr), and the preliminary results for the C2 DUALSPEC diffractometer. The IUCr refinements were performed used their standard in-house package (LHPM). The C2 refinements were performed using the GSAS software package. Direct comparison of the quoted errors is not possible, since the errors quoted from the IUCr are defined over esds of all data sets, whereas the esds given for the C2 data are for a single data set.

Table 1 Results from Rietveld refinement of standard IUCr ZrO_2. The three rows in each section represent results from three different data sets. IUCr represents the IUCr re-refined data, IUCr(p) represents the Round Robin participants' refinements, and C2 the preliminary results from the C2 DUALSPEC diffractometer.

	a	b	c	beta
IUCr	5.1463(8)	5.2116(8)	5.3134(8)	92.222(1)
IUCr(p)	5.1454(6)	5.2102(9)	5.3121(6)	99.222(1)
C2	5.1463(2)	5.2118(2)	5.3136(2)	99.226(2)
	Zr atom			
	x	y	z	B
IUCr	0.2759(1)	0.0399(1)	0.2086(1)	0.24(2)
IUCr(p)	0.2762(2)	0.0401(1)	0.2086(1)	0.27(4)
C2	0.2759(2)	0.0398(2)	0.2085(2)	0.26(5)
	O1 atom			
	x	y	z	B
IUCr	0.0706(1)	0.3335(1)	0.3440(1)	0.43(2)
IUCr(p)	0.0704(2)	0.3333(1)	0.3437(1)	0.54(5)
C2	0.0697(3)	0.3326(3)	0.3440(1)	0.40(4)
	O2 atom			
	x	y	z	B
IUCr	0.4493(2)	0.7573(1)	0.4791(1)	0.27(2)
IUCr(p)	0.4489(8)	0.7570(2)	0.4796(1)	0.33(5)
C2	0.4483(3)	0.7575(2)	0.4795(3)	0.24(5)

REFERENCES

[1] R.J. Hill and L.M.D. Cranswick, J. Appl. Cryst. 27 (1994) 802.

Near-Surface Stress Mapping

R.B. Rogge and T.M. Holden *(AECL)*,
P.J. Webster, G. Mills and X.D. Wang *(University of Salford)*

The accurate determination of residual strain by diffraction has traditionally fallen into two spatial regimes:

- surface measurements, using highly attenuated x-rays (typically 1-100 μm)
- measurements at depth, using highly penetrating neutrons (typically 1-30 mm)

The NCMS branch continues to develop the technique to probe, non-destructively, the sub-millimetre range between these regimes. Measurements in this range are necessary to fully understand the stresses introduced by surface treatments such as shot-peening and laser ablation. Previously measurements in this intermediate range required the systematic removal of surface layers followed by x-ray measurements of surface strains — a destructive process that is very labour intensive.

Most strain/stress mapping experiments performed by ANDI take advantage of the significant reduction in time achieved by using a 32-element detector that is capable of collecting a full diffraction profile at a single setting. Unfortunately, when the sample begins to occupy less than half of the gauge volume (see figure 1), various instrumental aberrations become significant, causing errors in determining strain.

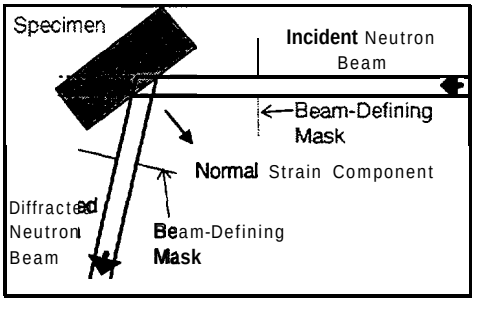

Fig. 1 A typical experimental configuration for near-surface stress mapping (NSSM) measurements.

In our previous report [1] the sources of these instrumental aberrations were identified and a new data collection method was developed to efficiently collect data while keeping these sources of error comparable with the standard precision of diffraction strain measurements. Near-surface measurements of a stress-free Ni powder cell were used to validate the technique, and proof-of-principle data was collected on a series of Waspoloy test samples.

The technique has been utilized for measurements on shot-peened steels. Results very near the surface (<0.2 mm) led to a re-evaluation of the technique for the one or two data points collected very near the surface (data at depths >0.2 mm are known to be correct). A specially designed Ni powder cell, with a thin Al foil wall was used to allow measurements to be performed very close to the surface that better match the conditions under which the measurements are made on typical samples. The test results indicate that in a stress-free sample, there are no significant instrumental effects for these data points. The unusual data that we have observed are therefore due either to the instrumental effects that appear only for a stressed or plastically deformed sample, or represent the real stress state. X-ray measurements (using the more traditional surface removal technique) on the same specimens have been performed to validate the neutron results.

We also have plans to design another test specimen to examine other sources of instrumental effects not observable with a stress-free powder sample. A form of resolution convolution will also be examined to evaluate the effect of steep strain gradients on the results.

REFERENCES

[1] Physics Division Progress Report, PR-PHY-8:2.3.1.44, AECL–1 1234, 1995.

ANDI Instrument Development

R.B. Rogge and J. Katsaras *(AECL)*

The ANDI (Applied Neutron Diffraction for Industry) group carries out residual strain/stress scanning for industrial clients. A limiting factor to the available spatial resolution is the size of the gauge volume. High resolution requires a small volume and thus weak intensity and long times. Several approaches have been considered that have the potential to increase the number of neutrons delivered to the volume of interest in the specimen. Currently two components between the monochromating crystal and specimen define the incident beam. Near the monochromator there is an aperture 50 mm high and 6 mm wide, whereas near the sample, neutron absorbing masks with slits of various dimensions are used to define the gauge volume. This aperture-pair define the horizontal and vertical angular divergence incident on the sample.

Beam Compression

Neutrons are scattered specularly from the crystallographic planes in a material. For a crystal in which the planes scattering neutrons are oriented such that their normals make a large angle with respect to the normal of the crystal surface, it is possible to "compress" a broad beam incident on the crystal into a narrow beam (see figure 1) scattered from it. This can result in more neutrons delivered down the 6 mm wide channel before the sample. An experiment was performed to confirm this effect and indicated that gains of a factor of two for the intensity delivered to a small sample are possible.

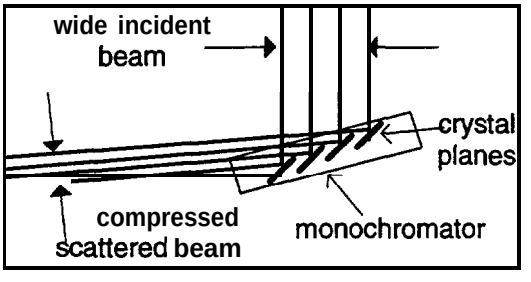

Fig. 1 Beam Compression **Geometry.**

Focusing Monochromators

Focusing monochromators consist of individual crystal segments that are aligned so that each segment directs neutrons of the selected wavelength to a focal point at the sample. The segments must be aligned using neutrons, a time-consuming procedure that usually requires the experimenter spend time in the vicinity of the neutron beam. The motor drives on focusing monochromators provide an opportunity to use the normal spectrometer control system to perform much of the alignment process, thereby automating the procedure and minimizing the risk of radiation exposure. This procedure has been tested on a first-generation vertically focusing monochromator. Alignment within the error has been realized, usually with a *single statistical* iteration of the process. Focusing improved the neutron intensity at the sample position by a factor 2.7 over the "flat" orientation of the vertically focusing monochromator. Significant gains (possibly a factor of five) can be realized by using a vertically focusing monochromator in beam compression geometry.

Polycapillary Optics

Polycapillary optic devices consist of micron-sized glass capillaries assembled into fibres that channel neutrons total external reflection. The fibres are, in turn, assembled into components to focus or to bend neutron beams. Transmission losses are significant in these devices, but when focused onto a very small spot, the net effect can be a gain in intensity delivered to the small sampling volume. Currently available data indicate a factor of two is the best gain achievable with thermal neutrons.

Neutron Detectors

D.C. Tennant and J.J-P. Bolduc *(AECL)*

Multiwire neutron detectors having 32 grounded anode wires with 2 mm anode-to-anode spacing have been successfully designed and fabricated by NCMS branch. These detectors were developed for the ANDI program and permit data from one entire Bragg reflection to be collected at a single setting of the detector. The data throughput for strain measurements has been increased by more than a factor of 10 for both the L3 and E3 spectrometers.

The detector system is a complete turnkey system that includes not only the detector but also the complete electronics for each anode wire. The detector is filled with eight atmospheres of ^{3}He and two atmospheres of stopping gas to achieve a neutron detecting efficiency of 75% for neutrons of wavelength 1.4 Å. The unwanted background noise is typically less than 1.5 counts per hour for each anode. The anode wires operate at ground potential, while -2900 volts is applied to the cathode. The overall dimensions of the detector are approximately 300 mm high by 150 mm wide by 90 mm deep, with an aluminum neutron window that is 125 mm high and 64 mm wide. Included within the body is a second compartment for the preamplifiers.

The electronic circuits are designed to match the characteristics of the detector to give minimum deadtime, excellent positional stability, and a low noise background. Each anode is equipped with a preamplifier, amplifier and discriminator. When a neutron is captured in the ^{3}He gas the distance the charged particles travel may be greater than 2 mm and therefore more than one anode wire may be activated simultaneously by a neutron. An innovative decoding module has been developed that enhances the positional accuracy and also reduces unwanted noise in each counting chain. The decoder is based on EPROMS and operates on-line as data is accumulated. Each data channel is connected to an EPROM address line and the EPROMS are programmed such that the output binary address corresponds to the position of the detected neutron. Decoding occurs within the shaping time of each amplifier pulse and therefore does not add additional deadtime counting loss to the system. However, since the decoder processes the data from all wires, the practical integrated count summed over all channels is typically 40 KHz (12% deadtime losses).

The detectors have exceeded their original specifications and are now installed on both the L3 and E3 spectrometers at the NRU reactor.

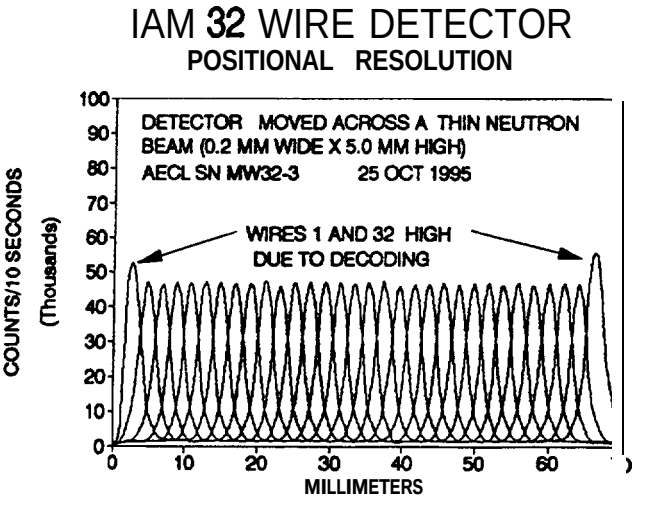

Fig. 1 The positional resolution of the 32-wire grounded-anode detector.

NCMS Computer Bulletin Boards

R.B. Rogge *(AECL)*

Electronic communication has made a significant impact on the day-to-day operations of the neutron scattering community around the world and here in Canada. The Canadian community is served by two communication netports, ANDInet, and CINSnet. The Neutron list server and World Wide Web (WWW) pages operate from Argonne National Laboratory (ANL) and various Web sites from other neutron labs have been created. The NCMS branch, in conjunction with the Canadian Institute of Neutron Scattering (CINS), is currently producing a contribution to the official AECL WWW pages.

CINSnet

The current incarnation of CINSnet consists of four components, a CINS electronic mail (email) list server, a NFNBR (Neutron Facility for Neutron Beam Research) committee list server, an email-alias database, and a shared anonymous *ftp* (file transfer protocol) site. The list server provides a central email communication channel. Anyone wishing to send a message of general interest to the CINS community can simply send their email to the address CINSnet@crl.aecl.ca. The message is then automatically relayed to the private email boxes of *all CINSnet members.*

The list of aliases provides stable email addresses for members of the CINS executive, these email addresses appear on the bottom of CINS letterhead. In addition, the CINSnet operator can be reached at CINSop@crl.aecl.ca. A second list server groups together all the members of the NFNBR committee at the address CINSnfnbr@crl.aecl.ca. Note, that there also exists an NCMS address for general enquires, mail to NCMS@crl.aecl.ca. The message will go to our branch secretary (Judy Hill), who will take appropriate action.

The last component of CINSnet is the anonymous *ftp* site where anyone is able to place or retrieve files that may be of general interest to the CINS community. There are also sub-directories in which members are encouraged to place abstracts of their recent neutron research activities. Another sub-directory contains Postscript® versions of the CINS experiment proposal and report forms, and a CINS application form. These files can be downloaded and sent to any Postscript printer.

About 66% of the CINS membership are CINSnet members. Effective use has been made of these new channels of communication that allow for more timely release of important and urgent information to the CINS community than can be achieved through the CINS newsletter, CINEWS. This channel has been used primarily by the executive, but is open to *all* members and has been used by non-executive members.

ANDInet

ANDInet is a communications network similar in structure to CINSnet, but less complex. It is intended to service the smaller, but international community of researchers who perform applied neutron diffraction. ANDInet provides a mailing list server and shares the anonymous *ftp* site with CINSnet. The intent of ANDInet is to provide researchers a means of communicating within the community and freely discussing the particular challenges, techniques and problems associated with applied neutron diffraction. For example, a recent *thread* discussed the problem of avoiding collisions between the sample (or supporting structures) and spectrometer collimating devices. Such collisions can be very costly in the form of lost time and the associated potential for cost overrun. During this thread, the anonymous ftp site provided a convenient venue for communicating graphical images.

ANDInet has grown to over 50 members from all over the world (e.g. Belgium, Indonesia, Germany, the Netherlands, the UK, France, South Africa, the US, in addition to Canada). This is a significant membership, and clearly indicates the need and interest in this type of communication. ANDInet continues to receive applications for membership.

Spectrometer Control System

M. Potter and M. Montaigne *(AECL)*

The control system for the T3 Bioscience Diffractometer was commissioned in May. The digital stabilizer for the linear detector was upgraded and the ADCs calibrated to improve the detector resolution.

Many changes have been made to the DUALSPEC control program. New features have been added, improvements have been made to the operating reliability, and several problems have been resolved.

(a) Support for an Integrated Count option was added to the SIGNAL command. It can be used in conjunction with the ROCK mode scan in sample alignment.
(b) The operating reliability was improved by adding code to cycle through a "re-try" loop when a write-to-disk error occurs.
(c) The option to run up to six scan data files at different monitor settings been added.
(d) A constant Q mode with fixed E′ has been added.
(e) The PLOT command has been modified to handle data from all detectors, including the new, multiwire detectors.
(f) The following commands are now available:

PRINT - co remand to turn the hard copy printout ON and OFF.
GO - command to drive the spectrometer to the configuration calculated from the ζ, η and ν values entered by the user.
COMMENT - command to prompt for a comment to be included in the scan title.
NAME - command to prompt for the names of the experimenters to be included in the scan title.
DETECTOR - command to test the monitors and single wire detectors.
MULTIWIRE- command to test the multiwire detectors.

A configuration to centralize data storage from all spectrometers on the node CP7 (AlphaStation) has been tested using the C2 and N5 spectrometers. This configuration will be expanded to include all spectrometers. The main advantages are

(a) CP7 is a very fast system therefore data access time is reduced;
(b) Data analysis programs can be centralized on CP7; and
(c) Single-node access makes the system more friendly for outside users.

L3 Spectrometer Hardware Design and Upgrades

J.H. FOX *(AECL)*

A column mounted jib crane with a capacity of one ton (900 kg) was designed, purchased and has been installed at the M-face of the NRU reactor. The new crane will greatly facilite handling and support of the large and heavy samples frequently investigated by the ANDI (Applied Neutron Diffraction for Industry) Group on the L3, Strain Scanning Diffractometer. The crane will also assist in the maintenance of the instrument.

Several new and/or improved accessories have been designed and manufactured for the ANDI program. Linear encoders with a resolution of 5 micrometres (0.0002") were adapted to all the translating stages, including the new 120 mm lift elevating stage. Spindles were designed and manufactured to allow the grips of the tensile stress rig to be rotated under load. A nickel powder cell with a .025 mm thick aluminum foil window was designed and fabricated to assist near surface diffraction calibration.

The design of a new detector shield to house the 32-wire grounded anode neutron detector is in progress. The new shield will be moveable on precision linear bearings so that the sample to detector distance may be varied thus changing the effective resolution of the instrument. The integrity of the shielding will be optimized by eliminating the analyzer components that are included in the current triple axis design.

3.2 Neutrino Physics

Sudbury Neutrino Observatory (SNO) Acrylic Vessel

E.D. Earle, B. Sur, R.J.E. Deal and E. Gaudette *(AECL)*

The SNO detector vessel is a sphere approx. 236″ in radius with a 2.1″ thick acrylic shell. It will contain 1000 tonnes of heavy water. Monenco-Agra has been hired by SNO to design and oversee the construction of the vessel and SNO and Monenco-Agra hired Reynolds Polymer Technology (RPT) to fabricate the vessel from 121 acrylic panels purchased from Polycast Corp. There is also a chimney extending above the vessel for access, which is formed from eight acrylic panels. The size of the panels is constrained by the capacity of the mine elevator used to lower the panels into the mine.

Quality control was monitored on the radioactive content, optical properties and the strength of the acrylic panels as they were supplied by Polycast Corp. The procedures used by RPT to thermoform and machine the panels to the required shape were observed and a test assembly of eight spare panels was made at the RPT plant. The lessons learned from this allowed a second test assembly to be made successfully and procedures concerning fabrication and possible repair of the vessel were written. In 1995 May, the formed panels were delivered to the SNO site at Sudbury for assembly into the spherical detector. This has necessitated extensive effort by SNO scientists in general and the Chalk River SNO group in particular.

The vessel is being constructed in rings of 11, 13 and 20 panels. The panels forming a ring are accurately positioned, bonded together vertically and then post-cured to maximize the strength of the bond. After a ring of panels is completed, it is bonded to the ring below. To date the seven chimney panels have been bonded into two sections, the equatorial ring is complete and the ring above has been completed and bonded to the equatorial one. Three more rings in the upper hemisphere must be formed before the chimney can be attached. Construction will then proceed on the lower hemisphere.

The post-cure equipment initially used for the chimney sections was found to be inadequate. The Chalk River SNO group identified the cause of the inadequacies and played a major role in developing equipment and procedures to resolve the problems. Each batch of bonding syrup is tested at CRL for strength before it is used. To date, one batch of 22 has been rejected. The radioactivity in the syrup has been tested at CRL and, although within specifications, is higher than SNO would like. More than twelve SNO scientists are working on various aspects of the vessel construction and the organization of these people is partially the responsibility of the CRL SNO group. Two of the CRL scientists are activity leaders for two of the four stages of vessel construction; accurately positioning panels, bonding, post-curing the bond and sanding the finished bond.

The acrylic vessel construction will remain on the critical path of the SNO project for much of 1996. Efforts to speed the progress on this activity by significantly increasing the effort, primarily by bringing in physicists from the SNO institutions, have been initiated.

MnO_2 Bead Production Facility

E. Gaudette, R.J.E. Deal, E.D. Earle and M. Choi *(AECL)*

The laboratory of the Sudbury Neutrino Observatory (SNO) will require up to 10 kg/wk of MnO_2 coated acrylic beads as part of the purification and assaying of the light and heavy water. In late 1994 and the first quarter of 1995 approximately 80 kg of coated XAD7-type beads were produced in the prototype Chalk River fluidized bed MnO_2 coating facility. These beads were used in several experiments and calibration tests for SNO at CRPP, Ottawa.

As a result of problems with bead fragmentation during usage, the SNO water group requested that we attempt to coat Diakon acrylic beads, a product that is much more robust than XAD7 beads.

In 1995 March the frost batch of coated Diakon beads were produced at Chalk River with a prototype procedure. These beads are less porous than XAD7, and thus have a tendency to float on top of the coating solution. This property renders the fluidization method of sieving and coating inadequate. A new vessel capable of holding more than 150 litres of liquid was built and tested for the new bead production system. These beads are coated in a stirring mode by a motor and propeller mounted from the top.

The first full-scale run (8 kg) was completed at the end of March. The beads had to be pre-washed and sieved at CRPP as the CRL fluidization method would not work with beads that tend to float. There were six batches of approximately 8 kg each produced using this method.

Following a sequence of tests, CRPP were dissatisfied with the efficiency of this type of bead coating and requested a change in our procedure to include sulphuric acid in the solution.

A cone-shaped sieve insert was developed for use in the pre-wash and sieving of Diakon beads in the vessel. To date two 8 kg batches have been produced using this improved method. These batches have been found to be satisfactory by the SNO water group.

This facility is presently located in the Chemical Engineering Building 250 at CRL. We are currently designing the production facility that will fit into a $6' \times 10'$ area with a mezzanine deck. A schematic diagram of this new facility is shown in figure 1. The facility is scheduled to be fully operational in 1996.

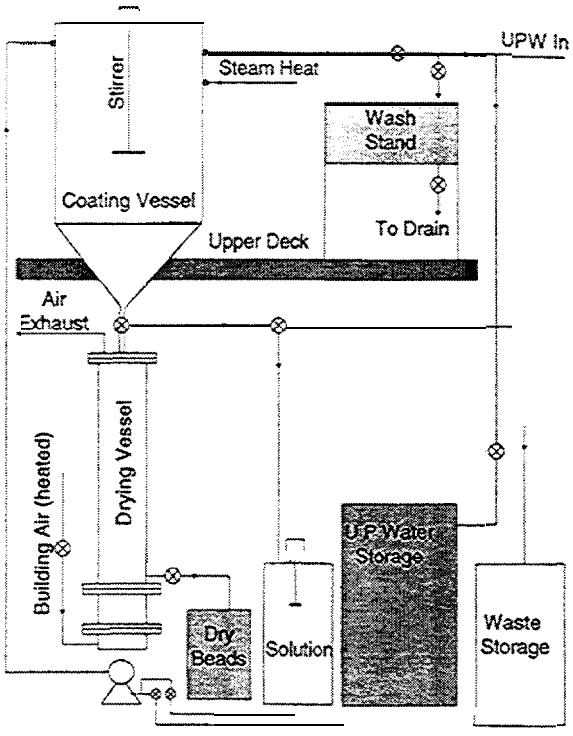

Fig. 1 Schematic diagram of CRL Bead Production Facility.

A Gas Transport Calibration System for the Sudbury Neutrino Observatory (SNO) Detector

B. Sur, E.D. Earle, E. Gaudette, R.J.E. Deal and J.H. Fox *(AECL)*, G. Jonkmans *(Queen's University)*, E.B. Norman, M. Moorhead, Y.D. Chan and M. Isaac *(Lawrence Berkeley Laboratory)*

A system to produce and deliver short-lived radioactivities for calibrating the SNO detector has been developed. Radioactivities will be produced by 14-MeV neutrons in a gas-filled target chamber surrounding a small D-T generator. This neutron source will be located inside a shielded "neutron pit" about 50 m away from the detector. The activities will be transported rapidly to a decay chamber inside the detector by a laminar gas stream flowing through a capillary tube. The following calibration sources have been tested:

(a) ^{16}N ($t_{1/2} = 7.13$ s, 613 MeV γ-ray source), made by $^{16}O(n,p)$ and using O_2 gas as both target and gas stream. This source will be used for absolute energy or gain calibration.

(b) ^{8}Li ($t_{1/2} = 0.84$ s, β's with a 13 MeV endpoint), made as recoils from $^{11}B(n,\alpha)$ and transported by aerosol particles in a He stream. The β-spectrum spans the same energy range as the ^{8}B neutrino signal and thus is useful for electron differential energy or spectral shape calibration.

(c) ^{17}N ($t_{1/2} = 0.44$ s, β-delayed neutron source) made by $^{17}O(n,p)$ using $^{17}O_2$ gas in a recirculation loop. Tagging the neutrons by the β's will allow the determination of the absolute neutron detection efficiency.

In the last year, we have completed a safety analysis of the proposed system. Based on this analysis, SNO has received a licence for construction of the facility from the Atomic Energy Control Board. A Model A-320L sealed tube neutron generator, made by MF Physics Corporation of Colorado Springs, Co. has been purchased, and operator training has been completed.

The shielding design for the neutron pit has been done at the SNO site office, and after reviews a contract for this work has been awarded. Engineering design of the neutron generator housing, target chambers, and positioning apparatus has been completed at Chalk River and machining of parts has begun. Procurement of other components for monitoring and gas handling is continuing at Chalk River. The closed loop gas recirculation and recovery system for the separated $^{17}O_2$ system is being designed at Lawrence Berkeley National Laboratory, as is the tagged decay chamber for the ^{16}N and ^{17}N sources.

Extensive Monte-Carlo simulations have been carried out over the last year at Chalk River to optimize the design of the ^{8}Li decay chamber. The result of such a calculation is shown if figure 1. The ^{8}Li spectrum from a cylindrical target chamber made of 3 mm thick *W* transparent acrylic is compared with the charged current spectrum of solar neutrinos generated in the same volume. Calibration of the SNO detector by the electrons with the well-defined β-spectral shape of ^{8}Li will thus lend confidence to conclusions that are drawn from SNO data about possible spectral distortions in the solar neutrino spectrum caused by neutrino masses in the MSW scenario.

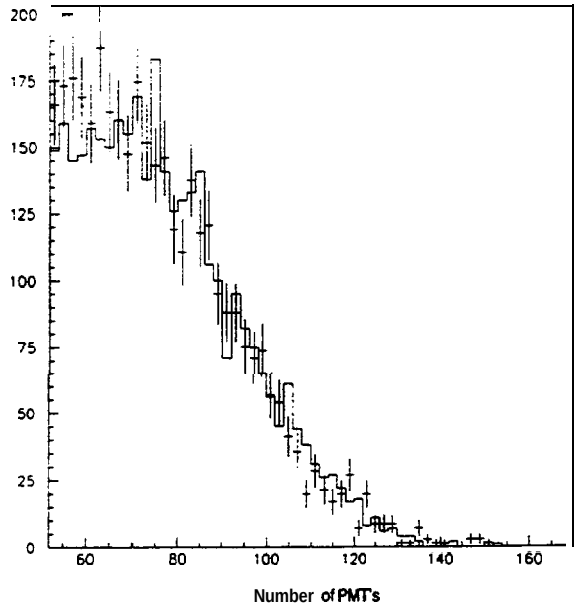

Fig. 1 Comparison between ^{8}B neutrino spectrum (continuous line) and ^{8}Li calibration source spectrum (crosses) in SNO.

SNOMAN Code Development

G. Jonkmans *(Queen's University)*, D.F. Cowen *(University of Pennsylvania)*
and R. Komar *(University of British Columbia)*

SNOMAN and CERNLIB

SNOMAN is the name of the Monte Carlo and analysis software being developed for the Sudbury Neutrino Observatory (SNO). This program has the capability to generate, by Monte Carlo simulation, hit patterns in the SNO detector, for various classes of signal and background events. It also will serve as an analysis tool and as such it will read the actual data from the SNO detector and reconstruct the event data structure.

The installation of SNO MAN necessitates the prior installation of the CERN Program Library. This is a large collection of general-purpose programs maintained and offered as both source code and object code form on the CERN central computers.

SNOdb

SNOdb, the SNO database, is being developed intensively at Chalk River Laboratories (CRL). The main functions of the SNO database is to provide a repository for constants associated with the SNO dataset and for status logs with time-dependent information on components and processes. The repository of constants will be read from and written to, principally by SNOMAN, and the data acquisition system (DAQ). SNOdb is constructed around one of the CERNLIB package, HEPDB. Together they meet the requirements of the SNO experiment for constant management; fast access to the database content; low rate of transactions between directly addressable storage medium and the computer memory; robustness and safety. In a multi-user, multi-computer environment, such as the large SNO collaboration, keeping up to date a centralized database and optimizing the data flow is not a trivial matter. It will be achieved through dedicated "service" machines under the control of a database "server". Database updates will be disseminated to the entire collaboration as frequently as necessary.

The integration of HEPDB and SNOMAN in a way such that the data structure is preserved (and harmonizes with the code) has been achieved and a release of the first version of SNOdb is scheduled in 1996 January. In that year, CRL will play central role in providing support for SNOdb to the collaboration. It is anticipated that the next version of SNOdb will contain a monitoring package (written at CRL) to assess the behaviour of various database objects as a function of time and will serve as an essential diagnostics *tool* of the SNO detector and laboratory.

High-Loading Bubble Detectors for Environmental Testing and Dark Matter Detection

B. Sur, R.J.E. Deal and E. Gaudette *(AECL)*, G. Jonkmans *(Queen's University)*,
V. Zacek, L. Lessard and L. Hamel *(Université de Montréal)*

AECL holds the patents for bubble detector technology. The present bubble detectors marketed by BTI use a dispersion of Freon droplets in a water-based gel. The detectors are composed of approximately 98% water, 2% polyacrylamide (gel) and < 0.5% Freon. The liquid Freon droplets are superheated by operating at low (atmospheric) pressure or elevated (0 to 55°C) temperature or both. Bubble formation is triggered by energy deposition by ionizing radiation such as nuclear recoils (following neutron scattering interactions), α-particles or β and γ radiation. The dE/dx threshold for bubble formation, hence the *type of detected radiation*, *can* be controlled by the superheat applied to the Freon. Thus detectors can be operated in a mode where they are insensitive to β's and γ's, or to α's from either internal contamination or external sources. The detector sensitivity to external radiation should scale with the loading fraction of the Freon, whereas the sensitivity to internal contamination will also depend on the surface to volume ratio, hence the droplet size for a given loading.

It should be possible to use the bubble detector technique for extracting and α-counting actinides from environmental soil samples. The advantages are (a) the discrimination against a large β or γ activity, and (b) the relatively large source mass for low-activity α-counting. However, high loading (i.e. greater than 1%) is required for reasonable efficiency. A new technique for monitoring environmental radioactivity would be of interest to AECL.

A collaboration headed by V. Zacek (Université de Montréal) is proposing an experiment to search for Cold Dark Matter particles by detecting their nuclear recoils using a bubble detector. Although there are many experiments being mounted worldwide for this purpose, this technique appears to require the least extrapolation to reach adequate sensitivity, i.e. 0.01 to 0.1 counts per day per Kg of detector mass, for a meaningful search. The proposed method requires ultra-pure water an underground location, and expertise in ultra-low level radioactivity, all available at the Sudbury Neutrino Observatory (SNO).

In the last year, our group has commissioned BTI to develop several types of high-loading bubble detectors. We have tested detectors with Freon loadings from 1% to 25% all manufactured using ultra-pure water from the SNO water systems. Ambient count rates (presumably fast neutrons) are approximately 1 per day per percent loading for normal (25 μm diameter) size droplets. This rate drops by a factor of 20 in the underground SNO laboratory and by another factor of 3 inside a 30 cm H_2O neutron shield. The count rate is limited by internal trace radioactive contaminants, as shown by γ-assays of the detectors and their constituents in the SNO laboratory 4600 ft down and at the Gran Sasso Laboratory. This demonstrates the need for elimination of these constituents.

A novel acoustic system for real-time detection and localization of bubble formation has been perfected at Université de Montréal. At CRL, we have also developed an inexpensive system to maintain individual detectors at a fixed superheat and to acoustically detect bubbles. To elucidiate the sensitivity to internal radioactivity, BTI has manufactured 20 detectors of varying Freon loading, droplet size and ^{241}Am spikes. Experiments with these detectors have demonstrated the sharp onset of a-particle sensitivity at 40°C, the monotonic increase in β, γ sensitivity with temperature and very good agreement with the expecting scaling of count rates with loading, droplet size and radioactivity.

The feasibility of using high-loading detectors for counting internal sources has thus been demonstrated. Our goal is to construct and operate a 1 Kg prototype Dark Matter Detector in the SNO laboratory in 1996.

3.3 Accelerator **Physics and Applications**

Laser Plasma Generation of Hydrogen-Free Diamond-Like Carbon Thin Films with a Pulsed High-Power CO_2 Laser

N.A. Ebrahim, J.F. Mouris, C.R.J. Hoffmann, R.W. Davis and D.A. Guzonas

Recently there has been a great deal of interest in amorphous carbon thin films with diamond-like properties. A material is amorphous if it has no detectable long-range order. Amorphous material with diamond-like characteristics results from random alternations between cubic and hexagonal geometries of carbon atoms. Although graphite, soot and carbon black all have the same chemical composition as diamond (i.e. all are forms of carbon), x-ray diffraction shows they have very different crystal structures. Graphite consists of layers of condensed, six-membered two-dimensional aromatic rings of sp^2-hybridized carbon atoms. It absorbs visible light and appears greyish-black. In the plane parallel to the aromatic network, graphite is a good electrical conductor. The lengths of the aromatic bonds in the ring system are 1.415 Å. The spacing between the layers, however is 3.354 Å because these atoms are held together by weaker van der Waals bonds. The layers can slide over each other, which makes graphite a soft material, suitable as a lubricant. Soot and carbon black are *microcrystalline* forms of graphite. Diamond has a different, but related, structure. Its crystallographic network consists exclusively of covalently bonded, three-dimensional aliphatic sp^3-hybridized carbon atoms arranged tetrahedrally with a uniform distance of 1.545 Å between atoms. The tetrahedrons connect to one another at their tips to form the crystal lattice. It is this structure of diamond that accounts for many of its extreme properties of hardness, resistance to wear, low-friction coefficient, electrical insulation, chemical resistance and optical trans-parency in the infrared. Single-crystal, impurity-free diamond is transparent in wavelength from the extreme ultraviolet through the visible spectrum to the near infrared (220 to 2500 nm) and from mid-infrared and beyond (wavelengths greater than 6000 nm). Amorphous or partly-crystalline carbon films also display the properties of diamond such as extreme hardness, high electrical resistivity, optical transparency in the infrared and chemical resistance. These macroscopic properties have been explained on the assumption that three-dimensional sp^3 diamond-like bonds exist in the carbon films. The high hardness of and the strong bonding to substrates make these films particularly attractive for improving wear-resistance of components.

The first experiments on the laser plasma deposition of hydrogen-free diamond-like carbon (DLC) films on Zr-2.5Nb CANDU pressure tube materials and silicon substrates, using the short-pulse, high-power, CO_2 laser have been carried out in the High Power Laser Laboratory at Chalk River [1]. The films were characterized using Raman spectroscopy, Vickers microhardness testing, and Atomic Force Micro-scopy (AFM). The thin films show the characteristic signature of diamond-like carbon films in the Raman spectra obtained using a krypton-ion (Kr^+) laser. The Vickers ultra-low-load microhardness tests show hardness of the coated surface of approximately 7000 kg force mm^{-2}, which is consistent with the hardness associated with diamond-like carbon films. Atomic Force Microscope (AFM) examination of the film morphology shows diamond-like crystals distributed throughout the film, with film thicknesses of up to 0.5 µm generated with 50 laser pulses. With significantly more laser pulses, it is expected that very uniform diamond-like films would be produced. These experiments suggest that it should be possible to deposit hydrogen-free, diamond-like films, of relevance to nuclear reactor components, with a high-power and high-repetition-rate laser facility.

REFERENCES

[1] N.A. Ebrahim, J.F. Mouris, C.R.J. Hoffmann, R.W. Davis and D.A. Guzonas, AECL Report AECL-1 1346 (1995 June), "Laser Plasma Generation of Hydrogen-free Diamond-like Carbon Thin Films on Zr-2.5Nb CANDU Pressure Tube Materials and Silicon Wafers with a Pulsed High-Power CO_2 Laser".

A Far-Infrared Free-Electron Laser Facility for Applications in Basic and Applied Research

N.A. Ebrahim and C.R.J. Hoffmann

Free-electron lasers (FELs) are coherent sources of electromagnetic radiation that can cover the electromagnetic spectrum from the far-infrared to the vacuum-ultraviolet. The first sources of powerful coherent radiation were the radar and microwave electron tubes invented in the earlier part of this century. To this day, these tubes remain the most successful and useful sources of coherent radiation, with wavelengths ranging from several metres down to approximately a millimetre. Electron tubes are generally inexpensive, compact, reliable, efficient and powerful. A microwave tube called the Ubitron, developed in 1960 by Phillips, was the forerunner of the FEL, with similarities in the design and operation.

AECL has developed the IMPELA family of high-power electron accelerators that are intended for use as industrial irradiators, but have characteristics that appear favourable for the generation of far-inbred radiation in a FEL configuration. These characteristics include an electron energy range from 5 to 15 MeV, with average beam power $\geq$ 50 kW. The success of FELs combined with the potential of the IMPELA technology leads to the question of whether this technology can make a useful near-term contribution to FELs, as well as promote applications that could benefit CANDU reactor technology and development. A small group was formed in Accelerator Physics Branch to assess the potential of the IMPELA technology as a basis for a far-infrared FEL, and to survey potential applications, particularly in CANDU reactor research and development. In this study the basic principles of FELs were identified, potential applications were discussed, a proposal for a far-infrared facility was outlined, and recommendations were offered for future action [1].

The study concluded that with relatively modest modifications to the IMPELA prototype accelerator, it would be possible to build an internationally competitive far-infrared FEL user facility. For instance, calculations based on a conceptual design show that such an FEL could produce radiated peak power in a 12.2 ps micropulse of 14 MW at 20.7 μm wavelength and 1.7 MW at 57.5 μm. The corresponding radiated power during a 200 μs macropulse is 10.7 kW at 20.7 μm wavelength and 1.25 kW at 57.5 μm. By comparison, the Advanced Free-Electron Laser at Los Alamos operates in the region 4 to 6 μm, and has an estimated peak power of 4 MW in a 19 ps micropulse, and radiated output power of 9 kW during an 11 μs macropulse.

The IMPELA prototype at Chalk River has high-power capabilities and a useful range of beam energies that are suitable for an FEL. However, modifications would be required to improve the beam quality (decrease the transverse emittance and axial energy spread) and appropriately bunch the charge in the beam into a small time-window to generate a high peak current. These requirements could be addressed in a new structure that incorporates an appropriate electron source in the first accelerating cell, which has a large accelerating gradient and focusing elements to control beam blowup from the action of space charge forces at nonrelativistic beam energies. Photocathode sources have been used for this application and thermionic triode guns may be of interest also. The rest of the structure would be similar to existing commercial versions of IMPELA structures.

The study also concluded that since CANDU-related R&D activities tend to be multidisciplinary, a far-infrared FEL facility could not be targeted at a specific application, but must be capable of enhancing a whole range of CANDU-related R&D activities, as a versatile laboratory instrument An IMPELA-based FEL facility could meet the needs of basic and applied research over a wide area within AECL and create new scientific opportunities for university-based researchers in Canada.

REFERENCES

[1] N.A. Ebrahim and C.R.J. Hoffmann, AECL Report AECL-11499 (1995 December).

Safe Discharge of the Superconducting Cyclotron Magnet

C.R.J. Hoffmann

A study was undertaken to identify some of the consequences of mechanical failure of the dump switch in the network of resistors and diodes that connects the magnet power supplies to the magnet coils. The probability of the switch failing to break contact in at least two of its three legs is low; however, the results from the study show that the consequences of such a failure might threaten magnet integrity, with a resulting lengthy shutdown for repairs.

The magnet has two independently driven, magnetically-coupled coils, each divided symmetrically about the cyclotron midplane. They are wound as double pancakes, which are stacked vertically and held in place by axial precompression forces that Belleville washer springs generate. At operating currents the magnet iron poles are saturated, but are not saturated at lower currents, which occur during charging and discharging. Then, radial magnetic field components may develop that result in axial forces on the coils directed away from the midplane. In some conditions these forces can overcome the axial precompression that holds the coil pancakes within the required position tolerances. To avoid this situation during charging a protocol is followed to ensure that the inner coil current is at least 600 A before the outer coil current exceeds 50 A. During discharge, resistors in the network control the coil discharge rates, and thereby the dangerous current combinations that can cause removal of the precompression. They occur when the inner coil current is between roughly 200 and 500 A, and the current of the outer coil is comparable to or exceeds that of the inner coil.

A computer code, DISCHRGE, was modified to model discharging of the magnet when any one of the three legs of the dump switch does not open when required. Then, the diodes from at least one of the driving power supplies remain connected to the network and as a result modify the coil discharge.

Figure 1 and 2 give examples of results for emergency discharge from the maximum operating currents when the dump switch operates correctly (figure 1) and when it disconnects the power supply from the inner coil only (figure 2). In the latter case, the axial precompression forces will be removed from the coils. Failure of each of the other legs of the dump switch also generates dangerous current combinations.

The risk to the magnet cannot be completely eliminated, but it can be further reduced through careful maintenance and perhaps reconfiguration of some elements of the network.

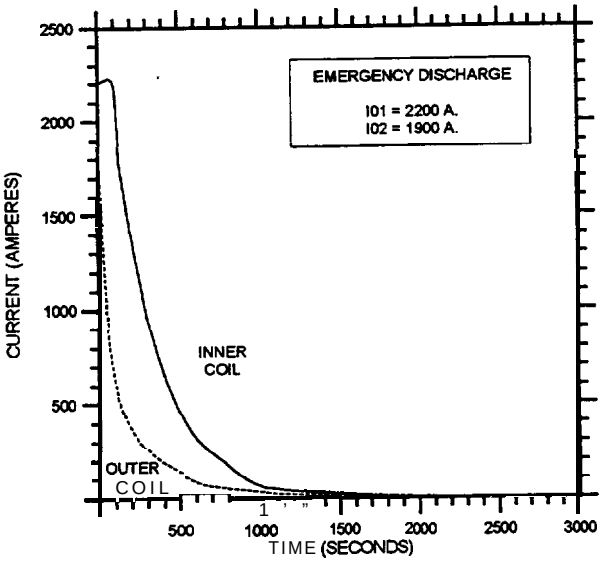

Fig. 1 Emergency discharge without dump switch failure.

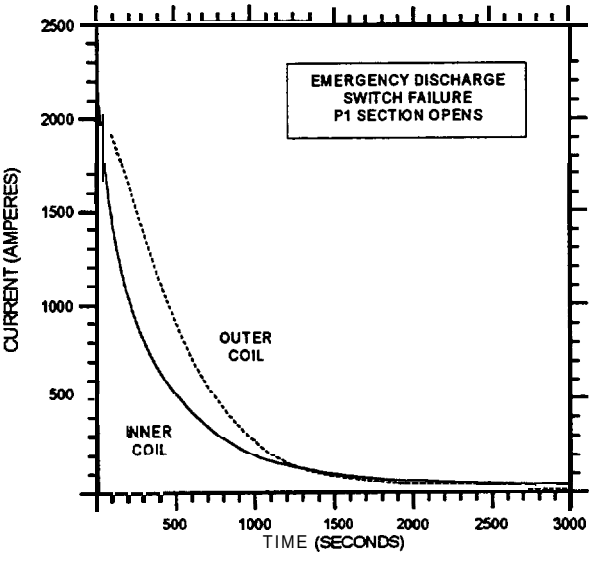

Fig. 2 Emergency discharge with the dump switch disconnecting the inner coil only.

High-Temperature Dielectric Properties Measurement System

R.M. Hutcheon

During the last seven years, a simple but unique system was developed for measuring high-temperature (up to 1500°C) dielectric properties, based on the resonant cavity perturbation technique. A small sample in a high-purity amorphous silica tube is heated in a conventional furnace and then rapidly (<0.5 sec) moved by a linear translator into a large, well-cooled multimode cavity. A high speed network analyzer measures the frequency and "Q" factor of up to eight modes, taking =1.3 seconds per mode. The sample is rapidly returned to the furnace for further heating. The long sample tube allows one to use any desired process gas flow, and the minimal cooling during the measurement period allows one to simulate the temperature-versus-time curve for a specific process, such as ceramic sintering.

For measurements above 400°C, which constitute most of the ceramics work, the system has been automated using the Labview control software and a 1700°C Lindberg furnace. Both in-house system development work and collaborative projects with outside groups have continued. The results of in-house dielectric properties research were published [1,2,3].

Collaborations with M. Mathis (Pennsylvania State University) and Y. Carmel (University of Maryland) have demonstrated the importance of stoichiometry in the dielectric properties of some crystalline materials, and in particular have demonstrated the advantage of specific cover gases during microwave sintering and processing [4,5,6,7].

For example, the synthesis of aluminum titanate (α alumina + TiO_2) occurs at lower temperatures if defected (as opposite to undefected) rutile (TiO_2) is used in the reaction. Dielectric properties measured during this synthesis, using conventional heating, show much increased dielectric absorption at low temperatures if defected rutile is used. If undefeated rutile is used, the synthesis generally requires a higher temperature, but if it is done under a nitrogen cover gas (i.e. a reducing environment) the synthesis proceeds at a lower temperature, and the dielectric absorption is again enhanced - presumably by the defects induced in the rutile by the reducing atmosphere. A similar increase in dielectric absorption and in sintering rate of ZnO was measured when a reducing atmosphere was used.

REFERENCES

[1] R.M. Hutcheon, P. Hayward, B.H. Smith and S.B. Alexander, American Ceramic Society Microwaves: Theory and Application in Materials Processing III, Ceramics Transactions 59 (1995) 235.

[2] R.M. Hutcheon, F.P. Adams and M.S. de Jong, ibid., p.215.

[3] J. Batt, J.G.P. Binner, T.E. Cross, N.R. Greenacre, M.G. Hamlyn, R.M. Hutcheon, W.H. Sutton and C.M. Weil, ibid., p.243.

[4] M.D. Mathis, D.K. Agrawal, R. Roy, R.H. Plovnick and R.M. Hutcheon, ibid., p.557.

[5] Z. Fathi, R.S. Gerard, J. Clemons, C. Saltiel, R.M. Hutcheon and M. DeMeuse, ibid., p.441.

[6] J.P. Calame, Y. Carmel, D. Gershon, A. Birman, L.P. Martin, D. Dadon, M. Rosen and R. Hutcheon, to be published in the proceedings of the 1996 Spring meeting of the Materials Research Society.

[7] Yu.V. Bykov, A.G. Ercmeev, V.V. Holoptsev, V.E. Semenov, A. Birman, J. Calame, Y. Carmel, D. Gerson, B. Levush, D. Dadon, P. Martin, M. Rosen and R. Hutcheon, ibid.

4. PUBLICATIONS AND LECTURES

4.1 Neutron and Condensed Matter Science Branch

Publications

SMALL MOMENTS IN HEAVY FERMIONS: A MODEL HAMILTONIAN
A.E. Sikkema, W.J.L. Buyers, J. Gan and I. Affleck
Physics B: Condens. Matter 206-207 (1995) 132

THE MAGNETIC PHASE DIAGRAM AND ZERO FIELD STRUCTURE OF HOLMIUM — LUTETIUM SUPERLATTICES
P.P. Swaddling, D.F. McMorrow, R.A. Cowley, J.A. Simpson, M.R. Wells, R.C.C. Ward, K.N. Clausen, M.F. Collins and W.J.L. Buyers
J. Magn. and Magn. Materials 140-144 (1995) 783

NON-TRIVIAL MAGNETIC ORDER IN URu_2Si_2?
T.E. Mason, W.J.L. Buyers, T. Petersen, A.A. Menovsky and J.D. Garrett
J. Phys.: Condens. Matter 7 (1995) 5089

COMMENT ON "CRYSTAL FIELD MODEL OF THE MAGNETIC PROPERTIES OF URu_2Si_2"
M.B. Walker and W.J.L. Buyers
Phys. Rev. Lett. 74 (1995) 4097

MAGNETIC FLUCTUATIONS IN HEAVY-FERMION METALS
T.E. Mason, T. Petersen, G. Aeppli, W.J.L. Buyers, E. Bucher, J.D. Garrett, K.N. Clausen and A.A. Menovsky
Physics B: Condens. Matter 213-214 (1995) 11

THE APPLICATION OF NEUTRON DIFFRACTION TO MATERIALS SCIENCE PROBLEMS IN THE CANADIAN NUCLEAR INDUSTRY
T.M. Holden, J.H. Root, R.B. Rogge and A.P. Clarke
Technical Suppl. to CNS Bulletin 16 (1995) 2

DIFFRACTION MEASUREMENTS ON CPF STEEL FATIGUE SAMPLES
A.P. Clarke, T.M. Holden, J.F. Porter and R. Yee
Proceedings of the 2nd Canadian Forces/CRAD meeting on "Naval Applications of Materials Technology" 1995 May 2-5, ed. J.R. Matthews (Defence Research Establishment Atlantic: Halifax).

A Gd PROPORATIONAL COUNTER SYSTEM FOR USE AS A NEUTRAL DETECTOR IN SNO
C.K. Hargrove, I. Blevis, D. Peterson and E.D. Earle
Nuc. Inst. & Meth. in Phys. Res. A 357 (1995) 157

DIFFRACTION MEASUREMENTS OF LINEWIDTH IN PLASTICALLY DEFORMED AND FATIGUED HY-80 MATERIALS
T.M. Holden, J.H. Root, J.H. Fox, J. Porter, J.A. Pineault and M. Brauss
The American Society of Mechanical Engineers, Reprinted from NDE-Nol.13, For the Energy Industry (1995)

NEUTRON STRAIN SCANNING OF A SMALL WELDED AUSTENITIC STAINLESS STEEL PLATE
P.J. Webster, G. Mills, X.D. Wang, W.P. Kang and T.M. Holden
Journal of Strain Analysis 30 (1995) 35

CHARACTERIZATION OF TEXTURE AND RESIDUAL STRESS IN A SECTION OF 610 mm PIPELINE STEEL
L. Clapham, T.W. Krause, H. Olsen, B. Ma, D.L. Atherton, A.P. Clarke and T.M. Holden
NDT and E International 28 (1995) 73

NEUTRON-DIFFRACTION MEASUREMENTS OF STRESS
T.M. Holden, J.H. Root, R.A. Holt and M. Hayashi
Physics B: Condens. Matter 213-214 (1995) 793

NON-INVASIVE TEMPERATURE MEASUREMENTS BY NEUTRON DIFFRACTION IN AERO-ENGINE COMPONENTS
T.M. Holden, J.H. Root, D.C. Tennant and D. Leggett
Adv. in X-ray Analysis 38 (1995) 9

INVESTIGATION OF RESIDUAL STRESSES IN A SLEEVE COLD-WORKED LUG SPECIMEN BY NEUTRON AND X-RAY DIFFRACTION
R. Lin, B. Jaensson, T.M. Holden, R.B. Rogge and J.H. Root
Adv. in X-ray Analysis 38 (1995) 455

MOLECULAR CHIRALITY AND THE "RIPPLE" PHASE OF PHOSPHATIDYLCHOLINE MULTIBILAYERS
J. Katsaras and V.A. Raghunathan
Phys. Rev. Lett. 74 (1995) 2022

STRUCTURE OF THE SUBGEL ($L_{C'}$) AND GEL ($L_{\beta'}$) PHASES OF ORIENTED DIPALMITOYLPHOSPHATIDYCHOLINE MULTIBILAYERS
J. Katsaras
J. Phys. Chem. 99 (1995) 4141

EVIDENCE FOR A TWO-DIMENSIONAL MOLECULAR LATTICE IN SUBGEL PHASE DPPC BILAYERS
J. Katsaras, V.A. Raghunathan, E.J. Dufourc and J. Dufourcq
Biochemistry 34 (1995) 4684

STRUCTURE OF THE $L_{C'}$ PHASE IN A HYDRATED LIPID MULTILAMELLAR SYSTEM
V.A. Raghunathan and J. Katsaras
Phys. Rev. Lett. 74 (1995) 4456

X-RAY DIFFRACTION STUDIES OF ORIENTED LIPID BILAYERS
J. Katsaras
Biochemistry and Cell Biology 73 (1995) 209

ATOMIC ORDERING AND LATTICE SITE LOCATION IN CUBIC Al_3 Ti-BASED ALLOYS
S.M. Kim, M. Kogachi, A. Kameyama and D.G. Morns
Acts Metall. Mater. 43 (1995) 3139

ATOMIC ORDERING AND LATTICE SITE LOCATION IN CUBIC ($L1_2$) Al_3 Ti-BASED ALLOYS
S.M. Kim, M. Kogachi, A. Kameyama and D.G. Morris
Mat. Res. Soc. Symp. Proc. 364 (1995) 1209

NEUTRON YIELDS FROM PROTON-INDUCED SPALLATION REACTIONS IN THICK TARGETS OF LEAD
M.A. Lone and P.Y. Wong
Nucl. Instr. & Meth. in Phys. Res. A 362 (1995) 499

FISSION ^{99}Mo PRODUCTION WITH AQUEOUS FUEL SYSTEMS
M.A. Lone and P.Y. Wong
Proceedings of the 1995 Symposium and Applied Mathematics Centre for Mathematical Sciences
RC-1458, CMS-94-03
1995 February 24-25

SENSITIVITY OF SELF-POWERED DETECTOR (SPD) PROBE TO ELECTRON AND GAMMA RAY FIELDS
M.A. Lone and P.Y. Wong
Proceedings of the CNA/CNS Annual Meeting, Saskatchewan, Vol. 1, Session 1.4.
RC-1221, CMS-94-02
1995 June 4-7

EFFECTS OF MULTIPLE SCATTERING AND WAVELENGTH-DEPENDENT ATTENUATION ON STRAIN MEASUREMENTS BY NEUTRON SCATTERING
T.C. Hsu, F. Marsiglio, J.H. Root and T.M. Holden
Journal of Neutron Research 3 (1995) 27

PAIRING IN THE HOLSTEIN MODEL IN THE DILUTE LIMIT
F. Marsiglio
Physica C 244 (1995) 21

POLARON PROPERTIES OF THE HOLSTEIN MODEL
F. Marsiglio
VIII International Conference on Recent Progress in Many Body Theories, eds. E. Schachinger, H. Mitter and H. Sormann, Plenum Press, (1995) 423

SIGNATURES OF THE ELECTRON-PHONON INTERACTION IN THE FAR—INFRARED
F. Marsiglio and J.P. Carbotte
Phys. Rev. B 52 (1995) 16192

COMMENTS ON THE CRYSTAL STRUCTURE OF SOLID TRICHLOROFLUORMETHANE
P. Prado, R.L. Armstrong and B.M. Powell
Can. J. Phys. 73 (1995) 650

INFLUENCE OF SUBSTITUTIONAL IMPURITIES ON THE STATIC AND DYNAMICAL BEHAVIOUR OF K_2OsCl_6 IN THE VICINITY OF THE STRUCTURAL PHASE TRANSITION: A NEUTRON DIFFRACTION STUDY
P.J. Prado, R.L. Armstrong and B.M. Powell
Can. J. Phys. 73 (1995) 626

AN IRRADIATION RESEARCH FACILITY FOR CANADA
B.M. Powell
Neutron News 6 (1995) 26

THE INTERACTION OF SORBATES WITH ACID SITES IN ZEOLITE CATALYSTS: A POWDER NEUTRON DIFFRACTION AND ^2H NMR STUDY OF BENZENE IN H-SAPO-37
L.M. Bull, A.K. Cheetham, B.M. Powell, J.A. Ripmeester and C.I. Ratcliffe
J. Am. Chem. Soc. 117 (1995) 4328

PHONON DENSITY OF STATES IN VANADIUM
V.F. Sears, E.C. Svensson and B.M. Powell
Can. J. Phys. 73 (1995) 726

NEUTRON SCATTERING NEAR THE ORDER-DISORDER TRANSITION IN Cu_3Au: EVIDENCE FOR A LOWER SPINODAL TEMPERATURE
R.B. Rogge, B.D. Gaulin, E.C. Svensson, E.D. Hallman and W. Wei
Can. J. Phys. 73 (1995) 779

DIFFRACTION PLANE DEPENDENCY OF ELASTIC CONSTANTS IN FERRITIC STEEL IN NEUTRON DIFFRACTION STRESS MEASUREMENT
M. Hayashi, M. Ishiwata, N. Minakawa, S. Funahashi and J.H. Root
Journal of the Society of Materials Science 44 (1995) 1115

CHARACTERIZATION, VALIDATION AND FINITE MODELLING OF EXTRUSION
S.R. MacEwen, A. Langille, J. Savoie, J. Root, M.J. Stout, S-R. Chen and U.F. Kocks
Proceedings of the 5th International Conference on Numerical Methods in Industrial Forming Processes, 1995 June 18-21, Cornell University, Ithaca, NY

RESIDUAL STRESSES IN STEEL AND ZIRCONIUM WELDMENTS
J.H. Root, C.E. Coleman, J.W. Bowden and M. Hayashi
The American Society of Mechanical Engineers Reprinted from NDE-Vol. 13, For the Energy Industry (1995) 41

INVESTIGATION OF TEXTURE AND INTERFACES IN A Zr-2.5 Nb ALLOY WITH ZIRCONIUM HYDRIDES
P. Gangli, J.H. Root and R. Fong
CIM 33rd Annual Conference of Metallurgists 1994 August 20-24, Canadian Metals Quarterly
Canadian Metallurgical Quarterly 34 (1995) 211

MATHEMATICAL MODELLING OF HOT TANDEM ROLLING OF AA5XXX ALUMINUM ALLOYS
M.A. Wells, D.J. Lloyd, J.H. Root, I.V. Samarasekera, J.K. Brimacombe and E.B. Hawbolt
Recent Metallurgical Advances in Light Metals Industries (eds. S. MacEwen and J.P Gilardeau). Proceedings of the 34th Annual Conference of Metallurgies of CIM, Vancouver, B.C. (1995) 255

ANGULAR AND TIME RESOLUTION OF NEUTRON TIME OF FLIGHT SPECTROMETERS
R. Crevecoeur, I. de Schepper, L. de Graaf, W. Montfrooij, E.C. Svensson and C. Carlile
Nucl. Instr and Meth. in Phys. Res. A 356 (1995) 415

NEUTRON-DIFFRACTION STUDIES ON LIQUID, GLASSY, AND CRYSTALLINE $Ca_{0.4}K_{0.6}(NO_3)_{1.4}$
E. Kartini, M.F. Collins, B. Collier, F. Mezei and E.C. Svensson
Can. J. Phys. 73 (1995) 748

ON THE THERMAL EXPANSION OF β–CRISTOBALITE
I.P. Swainson and M.T. Dove
Phys. Chem. Minerals 22 (1995) 61

MOLECULAR DYNAMICS SIMULATION OF α- AND β-CRISTOBALITE
I.P. Swainson and M.T. Dove
J. Phys: Condens Matter 7 (1995) 1771

NEUTRON POWDER DIFFRACTION STUDY OF THE FERROELASTIC PHASE TRANSITION AND LATTICE MELTING IN SODIUM CARBONATE, Na_2CO_3

I.P. Swainson, M.T. Dove and M.J. Harris
J. Phys.: Condens. Matter 7 (1995) 4295

CRYSTAL STRUCTURE AND THERMAL EXPANSION OF HEXAKIS (PHENYLTHIO) BENZENE AND ITS CBr_4 CLATHRATE

D. Michalski, M.A. White, P. Bakshi, T.S. Cameron and I.P. Swainson
Can. J. Chem. 73 (1995) 513

NEUTRON DIFFRACTION STUDY OF $Ag_2MnGeTe_4$

J.C. Woolley, A.-M. Lamarche, G. Lamarche, C. Church, I.P. Swainson and T.M. Holden
J. Sol. Stat. Chem. 115 (1995) 192

A SINGLE CRYSTAL NEUTRON Scattering STUDY OF A HIGHLY FRUSTRATED PYROCHLORE
M.J. Harris, M.P. Zinkin, Z. Tun, B.M. Wanklyn and I.P. Swainson
J. Magn. and Magn. Mater. 140-144 (1995) 1763

FERROMAGNETIC ORDER IN U_2NiSi_3
A. Schröder, M.F. Collins, C.V. Stager, J.D. Garrett, J.E. Greedan and Z. Tun
J. Magn. and Magn. Materials 140-144 (1995) 1407

MAGNETIC PROPERTIES OF THE NONCOLLINEAR ANTIFERROMAGNET $KNiCl_3$
O.A. Petrenko, M.F. Collins, C.V. Stager and Z. Tun
Phys. Rev. B51 (1995) 9015

THE EFFECT OF MICROSTRUCTURE ON THE STRAIN-INDUCED TRANSFORMATION OF A Si-Mn BAINITIC STEEL
A. Di Chiro, J.H. Root and S. Yue
Phase Transformations During The Thermal/Mechanical Processing Of Steel (Proceedings Of The International Symposium), eds. E.B. Hawbolt and S. Yue, Canadian Institute of Mining, Metallurgy and Petroleum (1995) 259

Reports

DIFFRACTION MEASUREMENTS OF LINEWIDTH IN PLASTICALLY DEFORMED AND FATIGUED HY-80 MATERIALS
T.M. Holden, J.H. Fox, A.P. Clarke, J. Pineault and M. Brauss
ANDI-94
1995 October

RESIDUAL STRESSES IN AN ALUMINUM PISTON CASTING WITH A KAOWOOL REINFORCING RING
A.P. Clarke and T.M. Holden
ANDI-95
1995 January

MEASUREMENTS OF INTERPHASE CONSTRAINTS IN Al:SiC
T.M. Holden and A.P. Clarke
ANDI-98
1995 August

ROLE OF INTERNAL STRESSES IN THE TRANSIENT OFIRRADIAITON GROWTH OF ZIRCALOY-2
C.N. Tomé, N. Christodoulou, P.A. Turner, M.A. Miller, C.H. Woo, J.H. Root and T.M. Holden
AECL-11383, COG-95-352,
1995 July

HOW COULD CANADIAN INDUSTRY BENEFIT FROM A NEW NEUTRON BEAM RESEARCH FACILITY?
J.H. Root
RC-1436
1995 May

EVALUATION AND SEMI-AUTOMATIC ALIGNMENT OF A VERTICALLY FOCUSSING MONOCHROMATOR
R.B. Rogge
RC-1446
1995 June

Th CONCENTRATION IN VARIOUS ACRYLIC TUBING
E.D. Earle
SNO Scientific and Technical Report SNO-STR-95-011
1995 March

ACRYLIC PANEL DIMENSIONS AS MEASURED BY RPT
E.D. Earle
SNO Scientific and Technical Report SNO-STR-95-012
1995 March

DIARY FOR RPT VISIT FROM JAN 20 TO JAN 31, 1995 ®
E.D. Earle
SNO Scientific and Technical Report SNO-STR-95-013
1995 March

ACRYLIC VESSEL CLEANLINESS
E.D. Earle
SNO Scientific and Technical Report SNO-STR-95-014
1995 March

RPT BOND TEST IN RAMP
E.D. Earle
SNO Scientific and Technical Report SNO-STR-95-015
1995 March

Th IN KEVLAR ROPE BY NAA
E.D. Earle
SNO Scientific and Technical Report SNO-STR-95-029
1995 April

SAFETY REPORT FOR A NONMEDICAL ACCELERATOR FACILITY AT THE SUDBURY NEUTRINO OBSERVATORY
B. Sur and E.D. Earle
SNO Scientific and Technical Report SNO-STR-95-031
1995 June

GAS TRANSPORT CALIBRATION SYSTEM FOR SNO: A PRELIMINARY DESIGN DOCUMENT
B. Sur and E.D. Earle
SNO Scientific and Technical Report SNO-STR-95-053
1995 January

^{8}Li: A BETA CALIBRATION SOURCE FOR SNO
B. Sur, E.D. Earle, R. Deal and E. Gaudette
SNO Scientific and Technical Report SNO-STR-95-054
1995 June

NAA ACRYLIC CONTAMINATION TEST IN THE CAVITY
B. Sur, E.D. Earle, E. Gaudette, R. Deal and G. Jonkmans
SNO Scientific and Technical Report SNO-STR-95-055
1995 October

Invited Talks

EXACT CALCULATIONS FOR THE PAIR-HOPPING MODEL
F. Marsiglio
Seminar given at the CIAR Meeting, McGill University
1995 January 27

DISORDER-ORDER TRANSFORMATIONS IN A 2D LIPID BILAYER/WATER SYSTEM
J. Katsaras
Concordia University, Department of Physics, Quebec
1995 March 6

STRUCTURE AND DYNAMICS OF AMORPHOUS AND CRYSTALLINE ICE
E.C. Svensson
Physics Department, Brookhaven National Laboratory, Upton, New York
1995 March 17

NEUTRON SCATTERING STUDIES OF FRUSTRATED PYROCHLORE ANTIFERROMAGNETS $Tb_2Mo_2O_7$ AND $CsNiCrF_6$
Z. Tun
Meeting of the American Physical Society, San Jose, California
1995 M-arch 20-24

FROM CRADLE TO GRAVE: THE LIFE-STORY OF A NEUTRON
W.J.L. Buyers
University of Montreal
1995 April 7

STRUCTURE AND DYNAMICS OF AMORPHOUS AND CRYSTALLINE ICE
E.C. Svensson
Symposium in Honour of Dr. B.N. Brockhouse, 1994 Nobel Laureate in Physics, McMaster University, Hamilton, Ontario
1995 April 24

THE MOST FAMOUS PHONON OF ALL
E.C. Svensson
Symposium in Honour of Drs. B.N. Blockhouse and C.G. Shull, 1994 Nobel Laureates in Physics, at CAM 95/50th Anniversary CAP Congress, Laval University, Quebec
1995 June 11-16

NEAR-SURFACE AND NEAR-INTERFACE STRAIN MEASUREMENT BY NEUTRON DIFFRACTION
R.B. Rogge, T.M. Holden, X.D. Wang, G. Mills and P.J. Webster
Canadian Materials Science Conference; University of Western Ontario, London, ON
1995 June 13-16

NEUTRON POWDER DIFFRACTION TECHNIQUES FOR MATERIALS SCIENCE
R.B. Rogge and J.H. Root
Canadian Materials Science Conference, University of Western Ontario, London, Ontario
1995 June 13-16

C-STATISTICAL TRANSFORMS OF THE HEISENBERG SPIN CHAIN AND BRAIDED SYMMETRY
M. Couture
Nankai Institute of Mathematics, Theoretical Physics Division, Tianjin, China
1995 July

C-STATISTICAL TRANSFORMS OF THE HEISENBERG SPIN CHAIN AND BRAIDED SYMMETRY
M. Couture
Satellite meeting of STATPHY 19, Nankai University, Tianjin, China
1995 August

LOW MOMENTS IN HEAVY-FERMION SYSTEMS
W.J.L. Buyers
International Conference on Strongly Correlated Electron Systems, Goa, India
1995 September 27-30

NEUTRON SCATTERING FOR BIOLOGY, CHEMISTRY, PHYSICS AND MATERIALS SCIENCE
W.J.L. Buyers
Chulalong Rein University, Bangkok, Thailand
1995 October 2

NEUTRON DIFFRACTION IN THE MATERIALS-SCIENCE TOOLBOX
J.H. Root
Presented at McMaster University, Department of Materials Science and Engineering
1995 October 2

NEUTRON SCATTERING FOR MATERIALS RESEARCH
W.J.L. Buyers
Office of Atomic Energy for Peace, Bangkok, Thailand
1995 October 3

NEUTRON DIFFRACTION IN THE MATERIALS-SCIENCE TOOLBOX
J.H. Root
Presented at University of Guelph, Physics Department
1995 October 3

NEUTRON SCATTERING AT CHALK RIVER
W.J.L. Buyers
Bhabha Atomic Research Centre, Bombay, India
1995 October 6

THE ROLE OF NEUTRONS IN MATERIALS SCIENCE AND INDUSTRY
T.M. Holden
ICANS XIII Conference, Wurenlingen, Switzerland
1995 October 12

INDUSTRIAL APPLICATIONS OF NEUTRON DIFFRACTION
T.M. Holden
Institut Laue-Laugevin, Grenoble, France
1995 October 16

RECENT NEUTRON REFLECTIVITY EXPERIMENTS AT CHALK RIVER
Z. Tun
Queen's University, Kingston
1995 November 1

Contributions

EVIDENCE FOR HEADGROUP SUPER-LATTICE IN SUBGEL PHASE DPPC BILAYERS
J. Katsaras
Biophysical Society, San Francisco, CA USA
1995 February 12-16

CREEP OF SiC-PLATELET REINFORCED ALUMINA
R. Ham-Su, D.S. Wilkinson and J.H. Root
Conference of the American Ceramic Society 97th Annual Meeting, Cincinnati, Ohio
1995 April 30 - May 4

BROKEN SYMMETRY AND HEAVY FERMIONS: ARE SMALL MOMENTS REAL?
W.J.L. Buyers, L. Taillefer, B. Lussier, T.E. Mason and T. Petersen
Physical Phenomena at High Magnetic Fields Conference
Florida State University, Tallahassee, Florida
1995 May 5-9

BROKEN SYMMETRY AND HEAVY-FERMIONS: ARE SMALL MOMENTS REAL?
W.J.L. Buyers, L. Taillefer, B. Lussier, T.E. Mason and T. Petersen
Physical Phenomena at High Magnetic Fields Conference
CAP Congress 95, Laval University, Quebec
1995 June 11-16

STRUCTURE OF ICE GROWN ON HIGH VOLTAGE CONDUCTORS
M. Farzaneh, J. Bouillot, Y. Teisseyre, E.C. Svensson and R.L. Donaberger
International Offshore and Polar Engineering Conference (ISOPE-95), The Hague, The Netherlands
1995 June 11-16

NEUTRON POWDER DIFFRACTION TECHNIQUES FOR MATERIALS SCIENCE
R.B. Rogge and J.H. Root
Canadian Materials Science Conference, University of Western Ontario, London, Ontario
1995 June 13-16

ULTRASONIC PREDICTIONS OF PLASTIC STRAIN RATIOS IN STEEL SHEET
K. Forouraghi, R.B. Thompson, N. Izworski, M. Shi, F. Reis and J.H. Root
1995 TMS/ASM Materials Week, Cleveland
1995 October 29-November 2

4.2 Accelerator Physics Branch

Publications

HIGH TEMPERATURE DIELECTRIC CONSTANT MEASUREMENT — ANOTHER ANALYTICAL TOOL FOR CERAMIC STUDIES?
R.M. Hutcheon, P. Hayward, B.H. Smith and S.B. Alexander
American Ceramic Society, Ceramic Transactions 59 (1995) 235

WHAT IS THE BEST MICROWAVE ABSORBER?
R.M. Hutcheon, F.P. Adams and M.S. de Jong
ibid., p. 215

A PARALLEL MEASUREMENT PROGRAM IN HIGH TEMPERATURE DIELECTRIC PROPERTY MEASUREMENTS: AN UPDATE
J. Batt, J.G.P. Binner, T.E. Cross, N.R. Greenacre, M.G. Hamlyn, R.M. Hutcheon, W.H. Sutton and C.M. Weil
ibid., p. 243

MICROWAVE SYNTHESIS OF ALUMINUM TITANATE IN AIR AND NITROGEN
M.D. Mathis, D.K. Agrawal, R. Roy, R.H. Plovnick and R.M. Hutcheon
ibid., p. 557

ACCELERATION OF PARTICLES BY RELATIVISTIC ELECTRON PLASMA WAVES DRIVEN BY THE OPTICAL MIXING OF LASER LIGHT IN A PLASMA
N.A. Ebrahim and S.R. Douglas
Laser and Particle Beams 13 (1995) 147

A SHORT-PULSE ELECTRON LINEAR ACCELERATOR FOR LASER DRIVEN PARTICLE ACCELERATOR RESEARCH
N.A. Ebrahim, R.W. Davis and J.F. Mouris
Nucl. Instr. & Meth. in Phys. Res. A 366 (1995) 207

Reports

LASER PLASMA GENERATION OF HYDROGEN-FREE DIAMOND-LIKE CARBON THIN FILMS ON Zr-2.5Nb CANDU PRESSURE TUBE MATERIALS AND SILICON WAFERS WITH A PULSED HIGH-POWER CO_2 LASER
N.A. Ebrahim, J.F. Mouris, C.R.J. Hoffmann, R.W. Davis and D.A. Guzonas
AECL Report AECL-11346 (1995)

A SHORT-PULSE HIGH ENERGY ELECTRON LINEAR ACCELERATOR FOR LASER ACCELERATION EXPERIMENTS
R.W. Davis, N.A. Ebrahim and J.F. Mouris
AECL Report, RC-1526 (1995)

A PROPOSED LASER WAKEFIELD ACCELERATION EXPERIMENT
N.A. Ebrahim
AECL Report, AECL-11241 (1995)

A FAR—INFRARED FREE-ELECTRON LASER FACILITY FOR APPLICATIONS IN BASIC AND APPLIED RESEARCH
N.A. Ebrahim and C.R.J. Hoffmann
AECL Report, AECL-11499

Contributions

DEVELOPMENT OF A FUEL THERMAL DIFFUSIVITY MEASUREMENT TECHNIQUE USING PULSED ELECTRON BEAMS
M.S. de Jong, F.P. Adams, R.M. Hutcheon, P.G. Lucuta, and R.A. Verrall
Proceedings of the Canadian Nuclear Society Fourth International Conference on CANDU Fuel, Pembroke, Ontario (1995).

FUEL THERMAL DIFFUSIVITY MEASUREMENTS USING PULSED ELECRON BEAMS
M.S. de Jong, F.P. Adams, R.M. Hutcheon, P.G. Lucuta and R.A. Verrall
ibid.